ISAS - INTERNATIONAL SCHOOL
FOR ADVANCED STUDIES

Kinetic Studies of Intracellular Magnesium Blockage of Sodium Currents

Thesis submitted for the degree of
"Doctor Philosophiae"

CANDIDATE
Fan Lin

SUPERVISOR
Prof. Oscar Moran
CO-SUPERVISOR
Prof. Antonio Borsellino

September 1990

TRIESTE

SISSA - SCUOLA
INTERNAZIONALE
SUPERIORE
DI STUDI AVANZATI
TRIESTE
Strada Costiera 11

International School for Advanced Studies
Trieste

Kinetic Studies of Intracellular Magnesium Blockage of Sodium Currents

Thesis submitted for the degree of
"Doctor Philosophiae"

CANDIDATE
Fan Lin

SUPERVISOR
Prof. Oscar Moran
CO-SUPERVISOR
Prof. Antonio Borsellino

September 1990

All the experimental part of this thesis
is done in
Biophysics Laboratory of SISSA, Trieste

In Memory of My Dear Grandmother

Acknowledgements

On the occasion of completing this thesis, I wish to express my gratitude to: Prof. Antonio Borsellino for his continuous encourage in the last four years' studies and works; Dr. Oscar Moran for his helpful discussions and suggestions during the whole work of this thesis, from teaching the experimental technique to the present writing; Prof. Franco Conti from *Instituto di Cibernetica e Biofisica, CNR, Genova, Italy* for his important discussions and advices during part of the experiment designs and the establishment of the Mg^{2+} blockage model; Dr. Michael Pusch from *Instituto di Cibernetica e Biofisica, CNR, Genova, Italy* for his thoughtful criticisms, suggestions and language improvement on Chapters 4, 5 and 6 of this thesis. Finally, I would like to thank all the members in our Biophysics Laboratory for their collaboration in the daily works and Department of BBCM of University of Trieste for their continuously providing rats. All of their contributions are essential for the finishing of the whole thesis. As finishing, I would also like to thank Mr. Gadi Geiger for his kindly improving the English of the first chapter of this thesis.

Notes

Part of this thesis has been submitted or accepted for publishing:

1. *Voltage-dependent sodium current on cultured rat cerebellar granule cell,*
   F. Lin and O. Moran,
   Bioscience Report (in press, 1990).
2. *Development of Voltage Dependent Ionic Currents in Rat Cerebellar Granule Cells Grown in Primary Culture*
   Z. Galdzicki, F. Lin, O. Moran, A. Novelli, G. Puia and M. Sciancalepore
   Int. J. of Neurosci. (in press, 1990)
3. *Competitive blockage of the sodium channel by intracellular magnesium ions in central mammalian neurons*
   F. Lin, F. Conti and O. Moran,
   submitted.
4. *The influence of intracellular Mg^{2+} on the sodium channel gating*
   F. Lin and O. Moran,
   submitted.

and congresse communication:

1. *Sodium currents in long-term cerebellar granule cell cultures*
   F. Lin, and O. Moran,
   12th Annual Meeting of the Europen Neuroscience Association, Torino, Italy. Europ. J. Neurosc. **supp 2**:154, 1989.
2. *Sodium channel is blocked by intracellular magnesium ions,*
   F. Lin and O. Moran,
   9th Regional meeting of Biochemists, Biophysicists, Biotechnologists, Opatija, Yugoslavia 1990

3. *The influence of intracellular Mg^{2+} on the sodium channel gating*
   F. Lin and O. Moran,
   IX Congresso Societá Italiana di Biofisica Pura ed Applicata, Isola d'Elba, Italy, 1990

4. *Intracellular magnesium binds competitively to a site inside the sodium channel,*
   F. Lin and O. Moran,
   10th International Biophysics Congress, Vancouver, Canada 1990

Abbreviations

All abbreviations which are often used the text are listed below.

a_h: the steepness of the voltage dependence of the steady–state inactivation process of sodium currents.

DIC: days in culture

F: the Faraday's constant. $F = 9.648X10^{-4}Cmol^{-1}$.

GHK equation: The Goldman–Hodgkin–Katz equation (current or voltage).

HH model: Hodgkin–Huxley model

I_p: Peak sodium current

I_p^{max}: Maximum inward peak sodium current

I_n: Normalized peak current (peak current measured in the presence of Mg^{2+} divided by that in the absence of Mg_i^{2+}).

k: Boltzmann's Constant. $k = 1.381X10^{-23}VCK^{-1}$

K_i: Dissociation constant of the intracellular Na^+ with Na channel.

K_o: Dissociation constant of the extracellular Na^+ with Na channel.

K_{Mg}: Dissociation constant of the intracellular Mg^{2+} with Na channel.

K_{Nai}: Michaelis constant of the intracellular Na^+ with Na channel.

K_{Nao}: Michaelis constant of the extracellular Na^+ with Na channel.

Mg_i^{2+}: intracellular magnesium ions.

$[Mg^{2+}]_i$: The intracellular Mg^{2+} concentrations.

Na_i^+ and Na_o^+: intracellular and extracellular sodium ions. respectively

$[Na^+]_i$ and $[Na^+]_o$: the intracellular and the extracellular Na^+ concentrations.

R: the ideal gas constant. $R = 8.314 VCK^{-1}mol^{-1}$.

T: Absolute temperature

V_m: Applied membrane potential.

V_{pp}: Applied prepulse membrane potential (double–pulse experiment).

$V_{1/2}^h$: Half–inactivation potential of the sodium channel, at which the probability of the inactivation gate *not* inactivated is 0.5.

$V_{1/2}^m$: Half–activation potential of sodium channels, at which the open probability of each activation gate is 0.5.

V_{rev}: Equalibrium ionic potential (reversal potential).

z_m: The apparent valence of a single steady–state activation process of sodium currents (m–gate).

z_s: The charge valence of the ion.

Contents

Chapter 1

Introduction

A nervous system is a part of an animal which is concerned with the rapid transfer of information through the body in forms of electrical and chemical signals. The action potential is a rapid propagated, all–or–none electrical message that travels along axons of the nervous system and over the surface of some muscle and glandular cells. The action potential may further directly or indirectly trigger a series of physiological or chemical changes of cells, such as the release of neurotransmitters, secretion of glandular cell and muscle contraction etc. Like all electrical messages of the nervous systems, the action potential is a membrane potential change caused by the flow of ions trough ionic channels in the membrane.

The interior of a neuron, as well as most of other cells, has a high concentration of K^+ and low concentration of Na^+. This ionic gradient is maintained by energy consuming mechanisms, such as the Na^+,K^+–ATP*ase* pumps (figure 1.1). In the resting state, the cell membrane is much more permeable to K^+ than to Na^+. Hence, the resting membrane potential is largely determined by the K^+ equilibrium potential, which can be calculated by the Nernst equation (Nernst, 1888):

$$E_{eq} = E_i - E_o = \frac{RT}{Z_s F} \ln \frac{[S]_o}{[S]_i} \tag{1.1}$$

where, $E_i - E_o$ is the membrane potential difference. $[S]_i$ and $[S]_o$ represent the concentrations of a permeable ion S on both sides of the

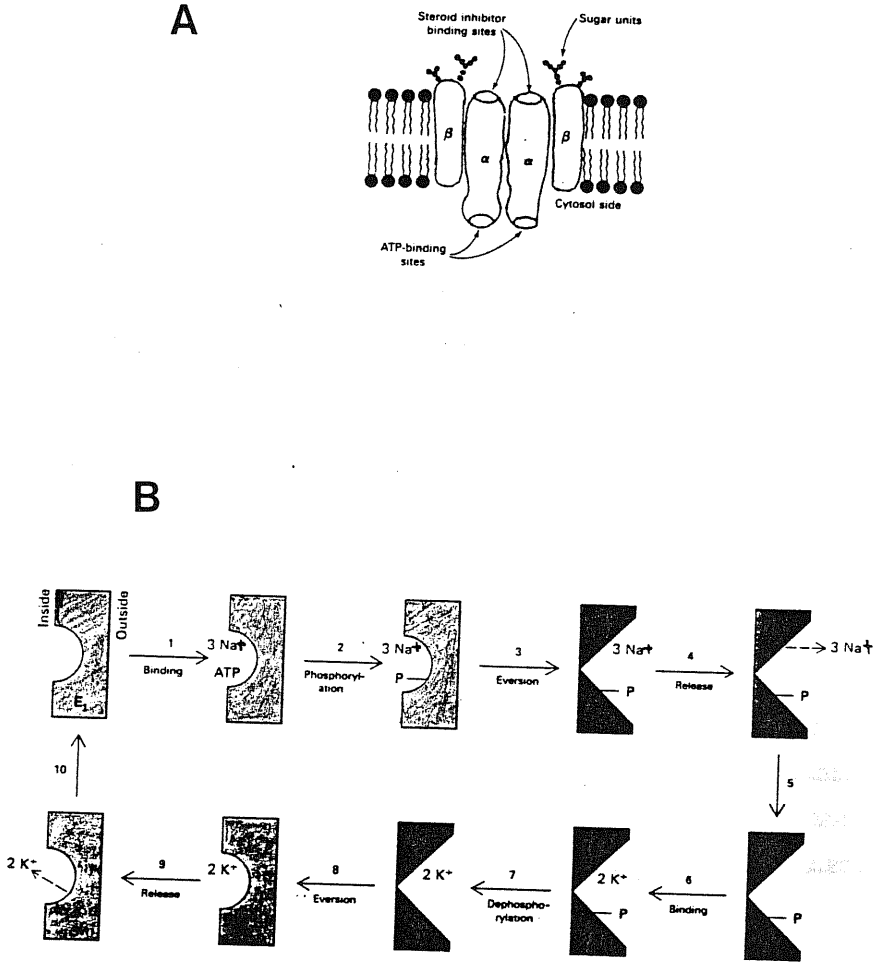

Figure 1.1:

A. A Na^+,K^+–ATP*ase* pump consists of two kinds of subunits α and β, most likely associated in the membrane as an $\alpha_2\beta_2$ tetramer. The activity of the pump can be inhibited by cardiotonic steroids. **B** Schematic diagram of a proposed mechanism for the Na^+–K^+–ATP*ase* pump. The upper sequence of reactions depicts the extrusion of three Na^+ ions, whereas the lower reactions show the entry of two K^+ ions. The E_1 and E_2 forms are shown here as having very different conformations. The actual conformational differences may be quite small (Stryer 1988).

membrane. R is the gas constant, T absolute temperature. F is the Faraday's constant and z_s is the charge valence of ion S. However, in the presence of more than one type of membrane permeable ions on the both sides of the membrane, the resting equilibrium potential should be calculated according to the Goldman–Hodgkin–Katz voltage equation (GHK equation, Goldman 1943, Hodgkin and Katz 1949). In the presence of monovalent permeable ions such as K^+, Na^+ and Cl^-, the resting potential is calculated as:

$$E_{eq} = \frac{RT}{F} \ln \frac{P_K[K]_o + P_{Na}[Na]_o + P_{Cl}[Cl]_o}{P_K[K]_i + P_{Na}[Na]_i + P_{Cl}[Cl]_i} \tag{1.2}$$

where P is the ionic permeability.

1.1 Action Potential and Ionic Channels

An action potential is generated when the membrane potential is depolarized beyond a critical threshold value. Depolarization of the membrane over the threshold level leads to an increase of cation permeability: large and fast influx of Na^+ through the voltage–gated sodium channel gives out an increase of membrane potential, slower outward flux of K^+ through voltage–gated K channel lead to the decline phase of the action potential, as well as to the recovery of the resting potential (figure 1.2).

There are mainly two kinds of stimuli which may lead to suprathreshold membrane depolarization. One kind of stimuli is nonelectrical, such as a specific chemical neurotransmitter, mechanical touch, light etc. This is an *"indirect generator"* of action potentials. Generally, nonelectrical stimuli are first detected by their specific receptors. The interaction between the receptor and the stimulus opens cation channels (receptor–gated channel) and leads to the ionic permeability change of the membrane (mainly Na^+ due to its large electrochemical gradient, but also has K^+, Ca^{2+} fluxes etc), which may further trigger an action potential in the neighboring region of the cell membrane. The other type of stimulus is an electrical stimulus, which can be generated due to several reasons. For example, it can be endogenously originated by the

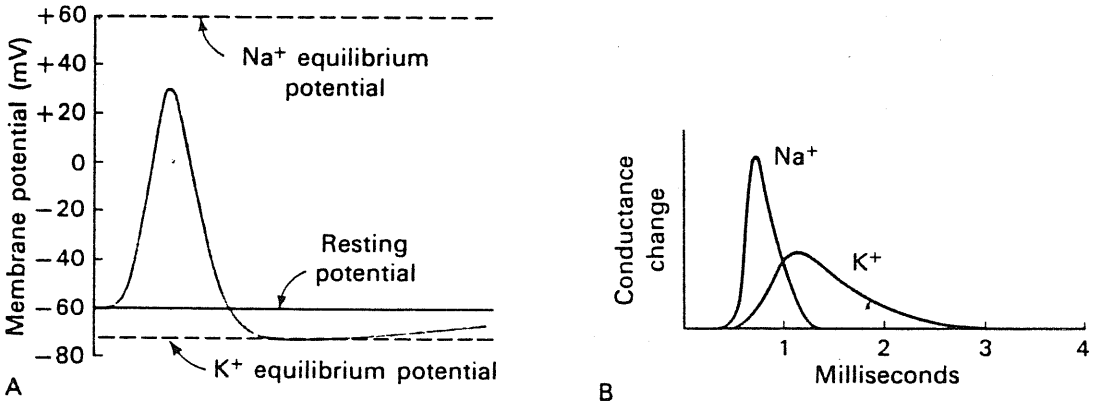

Figure 1.2:
Depolarization of an axon membrane results in an action potential. Time course of (A) the change in membrane potential and (B) the change in Na^+ and K^+ conductance (after Stryer, 1988).

local membrane depolarization caused by nonelectrical stimuli or an action potential that occurs in the neighbor membrane. It may also results from extracellular electrical stimuli, or intercellular electrical communication (through gap junction channel). This type of stimuli is directly detected by voltage–gated ionic channels and leads to the generation of action potential.

1.1.1 Receptor–Gated Ionic Channels

One kind of most commonly studied nonelectrical stimuli is chemical neurotransmission. Nerve cells interact with other neurons at junctions called synapses (figure 1.3). Nerve impulses are mostly communicated across synapses by chemical neurotransmitters, which are small and diffusible molecules. The transmitter molecules are packaged into small vesicles in the end of the presynaptic axon. The arrival of the electrical impulse at the presynaptic membrane leads to the entry of the

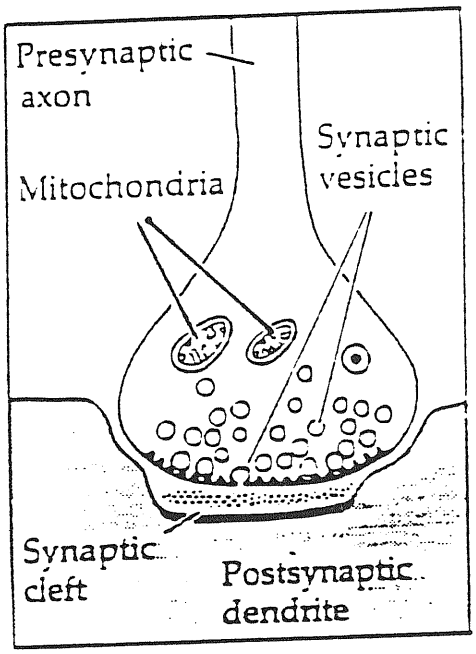

Figure 1.3:
Schematic diagram of a synapse (Kuffler et al. 1984).

extracellular Ca^{2+} through voltage–gated calcium channels. The elevated level of Ca^{2+} in the cytosol promotes the fusion of the synaptic vesicle membrane with the presynaptic membrane and releases the neurotransmitters into the gap between the presynatic membrane and the postsynatic membrane (synaptic cleft).

The transmitter molecules diffuse to the postsynaptic membrane, where they combine with specific receptor molecules and lead to the opening of the ionic channels, which in turn causes a potential change of the postsynaptic membrane. Figure 1.4 illustrates the working mechanism of the receptor–gated ionic channel. If the membrane is depolarized over the threshold value, an action potential may be further triggered. With the hydrolysis of transmitter molecules by their specific enzymes, the polarization of the postsynatic membrane is restored. There are two different kinds of neurotransmitters: excitatory and inhibitory. The excitatory transmitter, such as acetylcholine, increases the permeability of postsynaptic membrane to Na^+ and K^+, which leads to the depolar-

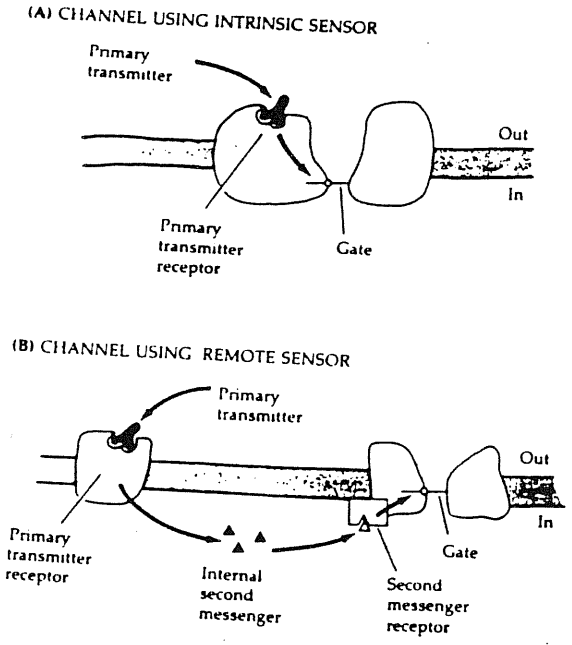

Figure 1.4:

Intrinsic versus remote sensing mechanism of receptor–gated channels. **A.** In some channels, the physiological stimulus acts directly on the channel macromolecule to affect the gating function, e.g. nicotinic acetylcholine receptor. **B.** In other channels, the receptor is a spatiablly separated molecule which communicates with the channel macromolecule through a diffusible, intracellular second–messenger molecule. The muscarinic acetylcholine receptor belongs to this class (Hille 1984).

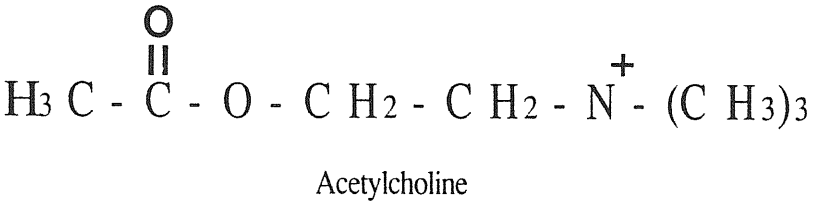

Acetylcholine

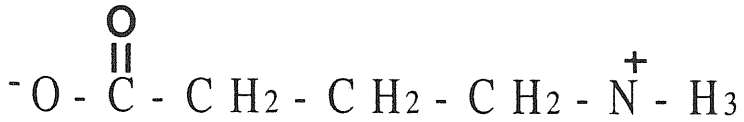

γ- Aminobutyrate (GABA)

Figure 1.5:
Molecular structure of two different kinds of neurotransmitters. Acetylcholine is an excitable transmitter. on the other hand, GABA serves as inhibitory transmitter.

ization of postsynatic membrane. The inhibitory transmitter, such as $\gamma-$Aminobutyrate (GABA), increases the permeability of the postsynatic membrane to Cl^-, which leads to the membrane hyperpolarization and therefore, increases the threshold value for triggering an action potential. Figure 1.5 shows the molecular structures of an excitatory and an inhibitory transmitters.

1.1.2 Voltage–Gated Ionic Channels

As mentioned above, although the initial stimuli could be electrical or nonelectrical ones, the action potentials, however, are always created when the membrane is depolarized over a certain threshold value. In other words, the action potential is created only after sensing the membrane potential change. The membrane potential change can be sensed by sensed by the voltage–gated ionic channels (figure 1.6A). Among the voltage gated channels, the sodium channel is remarkable due to its prin-

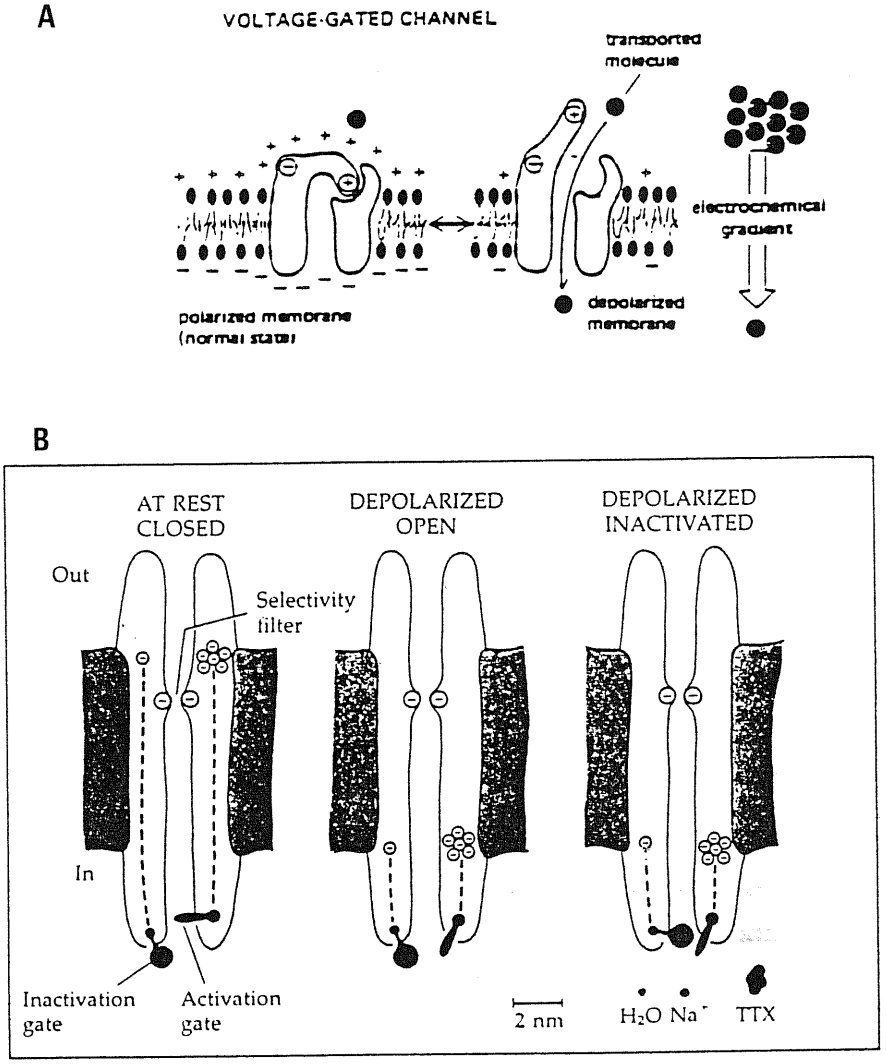

Figure 1.6:

A Voltage–gated ionic channels. In this type of ionic channel, there is an intrinsic voltage sensitive gate which controls the opening of the channel (From Alberts et al. 1983). Sodium, potassium, and calcium channels are all belonging to this type of channels. **B** Voltage–gated sodium channel, drawn schematically to scale according to biochemical, electron microscopic, and electrophysiological information. Ionic selectivity is provided by a constriction lined with negative charges near the outer surface of the membrane. The activation gate near the inner surface opens in association with the translocation of negative charges across the membrane from the outside to inside. The inactivation gate blocks the inner mouth of the channel and prevents the closing of the activation gate. A water molecule, an hydrated sodium ion, and a tetrodotoxin molecule are drawn to scale for comparison (From Kuffler et al. 1984).

cipal role in the generation of action potential. Sensing a suprathreshold depolarization, voltage–gated sodium channels (figure 1.6B) are first opened. Na^+ begins to flow into the cell due to its electrochemical gradient across the membrane. The entry of Na^+ further depolarize the membrane, which leads to more sodium channels opened. This positive feedback between depolarization and Na^+ entry leads to a rapid and large change of the membrane potential in a very short time (i.e. action potential). Voltage–gated potassium channels open after the closing of the sodium channel and serves to remove the depolarization and stabilize the membrane (figure 1.2).

1.2 Voltage–Gated Sodium Channels

Since its essential role for the generation of action potentials in many excitable cells, the voltage–gated sodium channel has attracted major attention of biophysicists. As early as the end of 1940's, the development of the voltage–clamp technique made it possible to control the membrane potential and study ionic currents through the membrane (Marmont 1949, Cole 1949, Hodgkin et al. 1949, 1952). Hodgkin and Huxley have performed a series of excellent voltage clamp experiments. From their experimental results, they have proposed a model to quantitatively describe the kinetic process of Na^+, as well as K^+ permeations (Hodgkin and Huxley 1952a, b, c, d), which have been widely applied to explain the voltage dependent behavior of the voltage gated sodium and potassium channel in the last decades.

1.2.1 Sodium Channels Kinetic Model

According to the Hodgkin and Huxley model (HH model), there are two opposing gating processes during Na^+ permeation: activation and inactivation processes, which are controlled by two kinds of gating particles. Sodium channels are first controlled by a rapid activation process which opens the channel during a depolarization. Then they are controlled by a slower inactivation process, which closes the sodium channels dur-

ing a depolarization. Once sodium channels have been inactivated, the membrane must be repolarized or hyperpolarized for some milliseconds to "remove" the inactivation. In their model, they further indicated that since the opening is favored by depolarization, the opening event must consist of an inward movement of a negative gating charge, or an outward movement of a positive charge, or both. These necessary movements of charged gating particles within the membrane should also be detectable in a voltage clamp experiment as a small electric current that would precede the ionic currents, whis is now called the "gating current". In the beginning of 1970's, gating currents (see figure 1.7) were successfully detected experimentally (Schneider and Chandler 1973, Armstrong and Bezanilla 1973, 1974, Keynes and Rojas 1974), which strongly supported the hypothesis of Hodgkin and Huxley. The gating current recording provides a method to obtain the direct information about the molecular rearrangement of the channel protein as it opens and closes. Beginning from 1970's, two modern developments have made it possible to explore, in detail, the single ionic channels. A breakthrough in this field was the development of the patch clamp technique (Neher and Sakmann 1976. for details, see Section 2.2). This technique has been further improved (Sigworth and Neher, 1980, Hamill et al. 1981), and is widely used today to measure the single channel events (figure 1.8) and the macroscopic ionic currents on the small cells. In addition, the analysis of current fluctuation caused by the ionic flow through the membrane has fundamentally broadened the range of current recording methods, which allowed to indirectly detect the behavior of single events by measuring the stationary fluctuation (Katz and Miledi 1970, 1971; Anderson and Stevens 1973, Conti et al 1976a,b), and nonstationary fluctuations of voltage dependent sodium channels (Sigworth 1980). Today, the gating current, together with microscopic and macroscopic currents, have become important tools in the studying of channel.

Beyond the great sucess of the HH model, it has been observed that there are some new kinetic phenomena which disagree significantly with specific predictions of the HH model. For example, it was found both in gating current behavior (Armstrong and Bezanilla, 1977) and

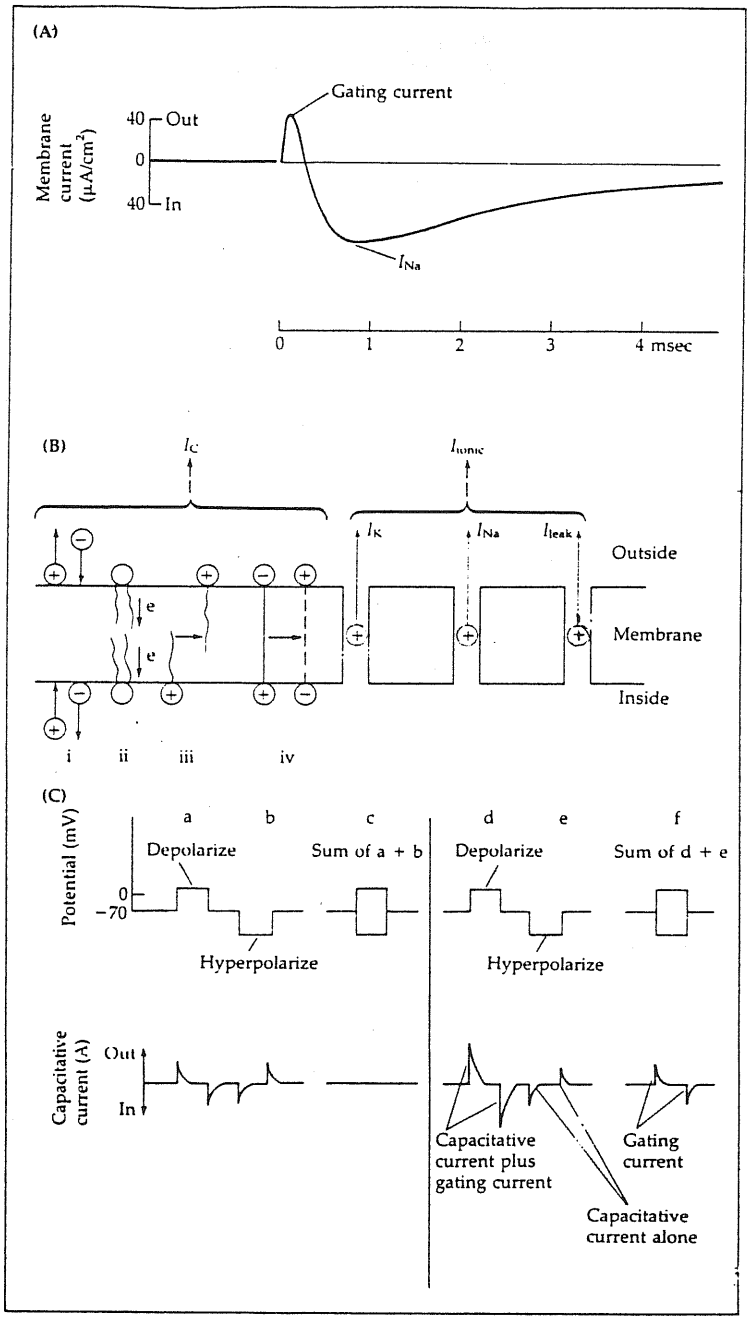

Figure 1.7:

Gating current in squid axon. (A) Brief outward gating current precedes inward sodium current. Gating current is a small component of the total capacitive current produced by depolarizing the axon. (B) In response to a depolarizing step, a charge is displaced from the surface of the membrane (i); within the membrane, electrons are redistributed (ii); and charged (iii) or bipolar (iv) molecules become reoriented. To separate the charge movements, which is associated with the gating from the rest of the capacitive currents, the procedure shown in (C) is used. Symmetrically depolarizing (a) and hyperpolarizing (b) pulses are applied. For a perfect capacitance, the sum of the resulting currents should be zero (c). If, however, a gating current is produced by depolarization (d) but not by hyperpolarization (e), then such a current should appear when the currents produced by the two pulses are summed (f). (After Armstrong and Bezanilla, 1974).

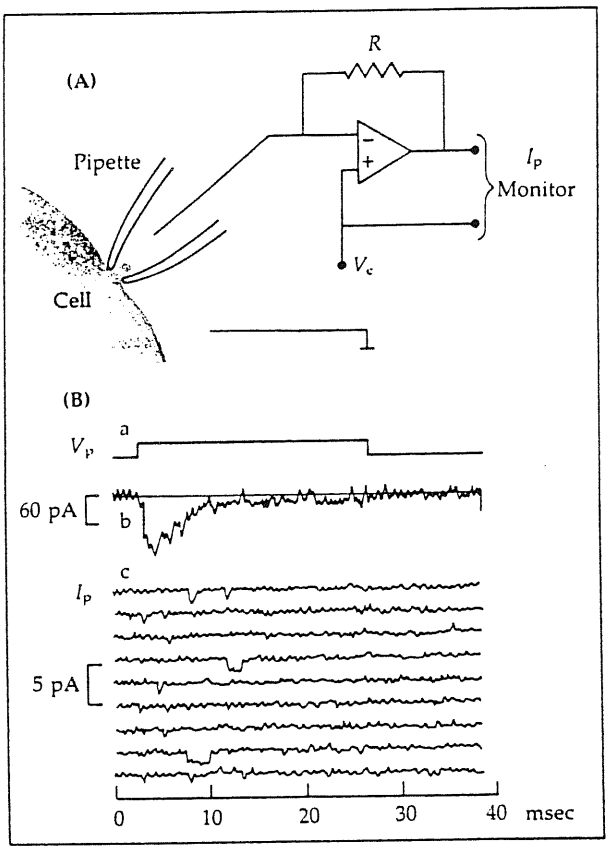

Figure 1.8:

Single sodium channel currents recorded with a patch clamp. (**A**) Recording arrangement. A patch clamp amplifier enables recording of small currents from the cell–attached patch and provides a method of supplying depolarizing pulses. (**B**) Successive voltage pulses applied to the patch with the waveform shown in (a) result in current pulses from individual channels (downward deflections) in the nine successive records shown in (c). The sum of 300 such records (b) shows that most channels open in the initial 1–2 msec, after which the probability of channel openings decays with the time constant of inactivation. (From Sigworth and Neher 1980).

in single current recording (Aldrich et al. 1983) that Na activation and inactivation processes are coupled, which contradictes the Hodgkin and Huxley idea of independence of activation and inactivation (Hodgkin and Huxley 1952a). Nevertheless, even if its kinetic details cannot be taken literally, the HH model has many important general properties with the implications which are still valid. Such as the ionic current reverses at their equilibrium potentials, Na channels activate in a S–shaped time course with several components controlling open events (i.e m in the HH model) and the voltage–dependent time constants τ_m and τ_h etc. The HH model has been widely used as a standard tool to characterize sodium channels found in new biological tissues (reviewed by Meves 1984).

1.2.2 Pharmacological studies of sodium channels

Until the mid–1960s, there were few clues as to how ions actually move across the membranes of excitable cells. A variety of mechanisms were considered possible. They included permeation in a homogenous membrane, binding and migration along charged sites, passage on carriers and flow through pores. It is pharmacological studies that finally provided the evidence needed for understanding ionic permeations. Among the drugs which can modify the ionic channels found now, tetrodotoxin (TTX) (figure 1.9A) has played an extraordinary role in the finding that different ions pass the membrane through their own ionic channels. TTX is a paralytic poison of some puffer fishes and of other fishes of the order *Tetraodontiformes* (Halstead, 1978). It blocks sodium channels selectively, leaving potassium channels untouched (Narahashi et al. 1964). TTX's receptor faces the extracellular medium and is not accessible to TTX molecules placed in the intracellular space, i.e it is membrane impermeable. TTX blocks sodium channels in nanomolar concentrations by binding with a site inside the sodium channels with a high affinity. From fluctuation measurements, it was found that TTX reduces the number of functioning sodium channels without changing gating or single channel permeability of those remaining channels (Sigworth 1980).

Another natural sodium channels blocker which bears similar properties to TTX is saxitoxin (STX) (Narahashi et al. 1967). Its structure is also shown in figure 1.9A. The finding of TTX and other sodium channel specific blockers has played an importent role in the understanding the working mechanism of sodium channels and the isolation of the sodium channel protein. Figure 1.9B illustrates hypothetical binding sites on the sodium channel molecular for TTX, STX, as well as some other kinds of sodium channel modifiers (see Chapter 5).

1.2.3 The Structure and Function of Sodium Channels

Our understanding of the sodium channels is tightly related with the development of new techniques for the measurement and manipulation of the channels. Such as the voltage–clamp, the gating currents, the single–channel recording and the specific pharmacology agents. More recently, the clone of cDNA of sodium channel genes provided a new way to directly study the relationship between the channel structure and function: site–directed mutagenesis combined with electrophysiological studies.

In the 1970s, with the development of protein chemistry and pharmacology, it was clear that many channels and receptors are transmembrane proteins. Shosaku Numa and coworkers have cloned and sequenced the cDNAs of several sodium channels – from electric organ of eel (Noda et al. 1984) and from rat brain (Noda et al. 1986). Their studies have shown that the amino acid sequence of the sodium channel has been conserved over a long evolutionary period. Most interesting, they revealed that a channel contains four internal repeats having similar amino acid sequences (Figure 1.10). Hydrophobicity profiles indicate that each homology unit contains five hydrophobic segments (S1, S2, S3, S5 and S6). Each unit also contains a highly positive charged S4 segment: arginine or lysine residues are present at nearly every third residue. Numa further proposed that segments S1–S6 are membrane–spaning α helices and that the pore is formed by the walls of four S2

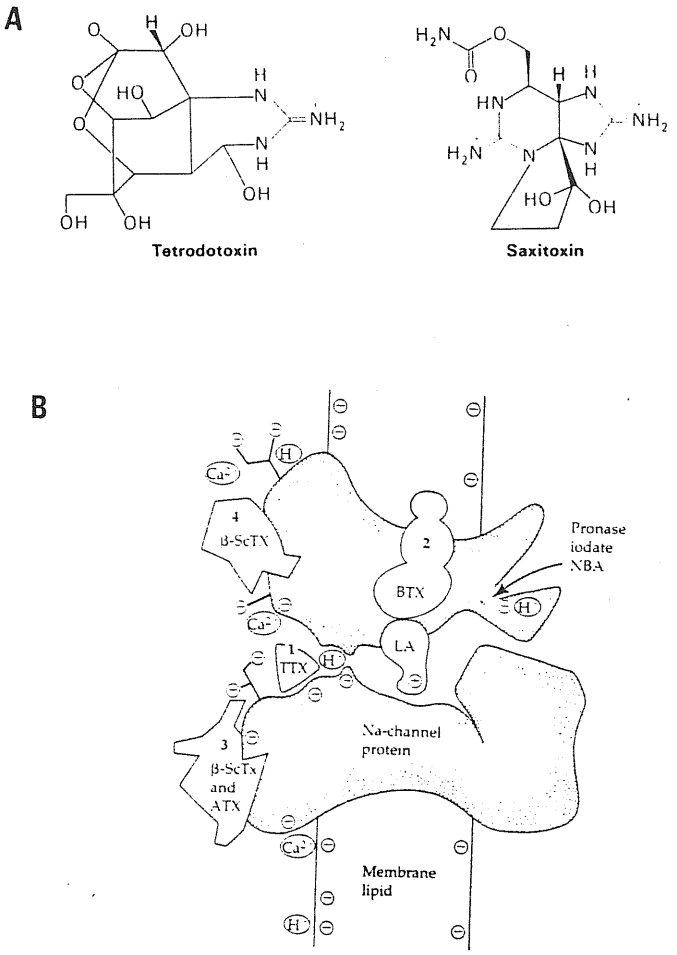

Figure 1.9:

A Poison of sodium channels. TTX has one guanido group, whereas Saxitoxin has two. This positively charged group of the toxin interacts with a negatively charged carboxylate at the mouth of the channel on the extracellular side of the membrane. **B** Hypothetical view of a sodium channel macromolecule in the membrane. Three receptors are numbered according to a scheme of Catterall (1980): (1) TTX and STX (2) lipid–soluble gating modifiers and (3) inactivation–modifying scorpion and anemone pipette toxins. Site 4 (Jover et al. 1980; Darbon et al. 1983) binds activation–modifying "β–scorpion toxin" (β–Sctx). In addition, there are intracellular points of attack of chemical modifiers of inactivation, a binding site within the pore from local anesthetic analogs, and external negative charges that attract divalent ions (and Na^+ ions) to the channel (Hille, 1984).

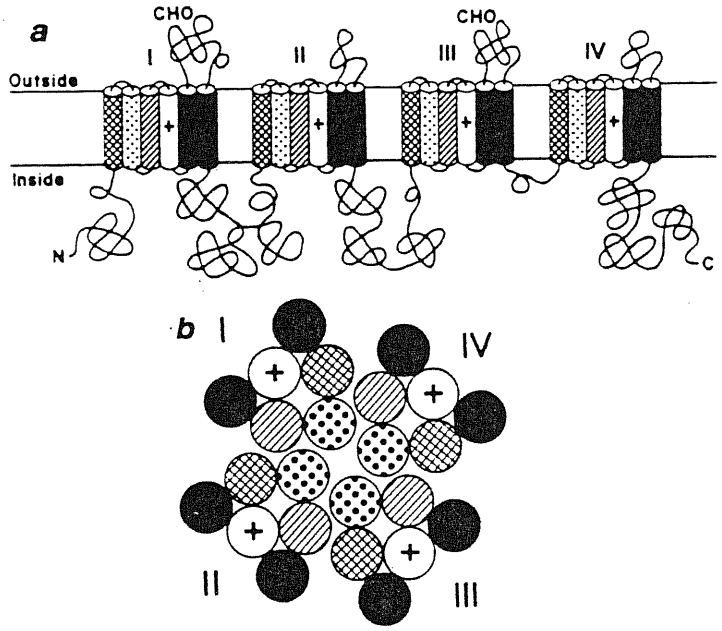

Figure 1.10:

a, proposed transmembrane topology of the sodium channels; b, proposed arrangment of the transmembrane segments viewed in the direction perpendicular to the membrane. In a, the four units of homology spanning the membrane are displayed linearly. Segments S1–S6 in each repeat (I–IV) are indicated by cylinders as follows: S1, cross–hatched; S2, stippled; S3, hatched; S4, indicated by a plus sign; S5 and S6, solid. Putative sites of N–glycosylation (CHO) are indicated. In b, the ionic channel is represented as a central pore surrounded by the four units of homology. Segments S1–S6 in each repeat (I–IV) are represented homology. Segments S1–S6 in each repeat (I–IV) are represented by circle indicated as in a. (From Noda et al. 1986)

helices. The S4 segments probably participate in making the channel responsive to the membrane voltage (Noda et al. 1986).

The relationship between the gating kinetics of the sodium channel and its structure has been first tested by Stühmer and coworkers. They analysed the mechanisms of voltage–dependent gating through a combination of *in vitro* mutagenesis and electrophysiological experiments on altered channels in heterogenous expression: *Xenopus* oocyte (Stühmer et al. 1989). Their work (shown and explained in figure 1.11) show that: (1) An intact cytoplasmic domain which links the third and fourth repeats is necessary for the normal sodium channel inactivation. (2) The positive charged amino acids in S4 of the first homologous repeat response to the steepness of the relationship between the probability of channel opening and voltage. The role of the S4 segments in sodium channel activation process has also been found in other mutation: the activation range of sodium channels can be shifted if a neutral leucine is mutated to phenylalanine in S4 of repeat II (Auld et al. 1990). On the other hand, the measurements of gating current fluctuations in sodium channels expressed in *Xenopus* oocytes reveal that the gating charge movements occur abruptly in "shot", whereby an equivalent of 2.3 electronic charges cross the membrane (Conti and Stühmer 1989). Three such shots are needed to open sodium channels. Combining all these observations from mutation and gating experiments, Guy and Conti (1990) proposed a model to describe the function of S4 segment in the activation gating processes, which is illustrated in figure 1.12.

Although many questions are still remained to be answered, it can be expected that our knowledge about ionic channels may be greatly enriched with the latest, and probably most powerful, breakthrough of site–directed mutagenesis combined with electrophysiological studies of ionic channels.

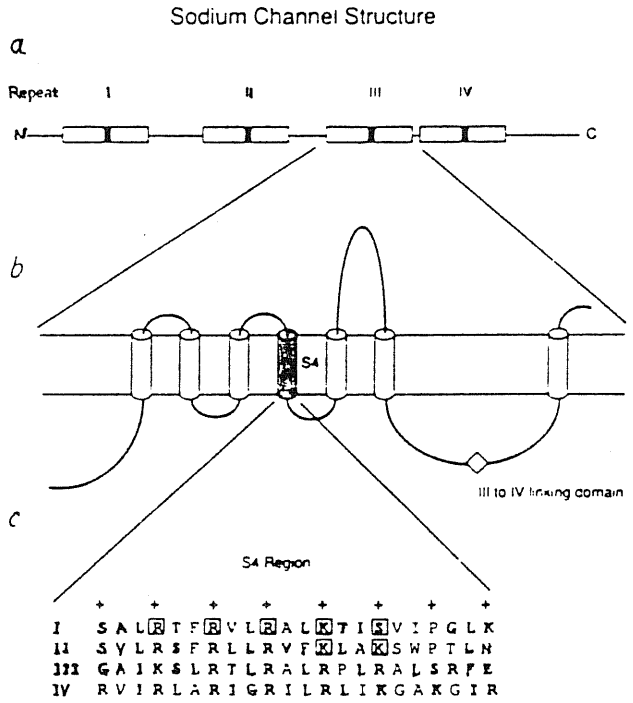

Figure 1.11:

Structure of sodium channels. *a*, The sodium channel α–subunit consists of a string of four internally homologous repeats, indicated by the boxes labelled I–IV, linked together by cytoplasmic linkages. The black bars in each box indicate the S4 regions. *b*, Each of the repeats has a proposed structure consisting of six membrane–spanning regions, shown here for repeat III. The S4 regions, thought to act as a voltage sensor, is shaded. *c*, The amino–acid sequences of the four S4 regions. They have a conserved structure motif of basic amino acids (arginine or lysine, R or K), indicated in bold. The amino acids which have been mutated by Stühmer and collaborators are enclosed by the squares. The mutations in the III–to–IV linking domain are indicated by a diamond point (From Aldrich 1989).

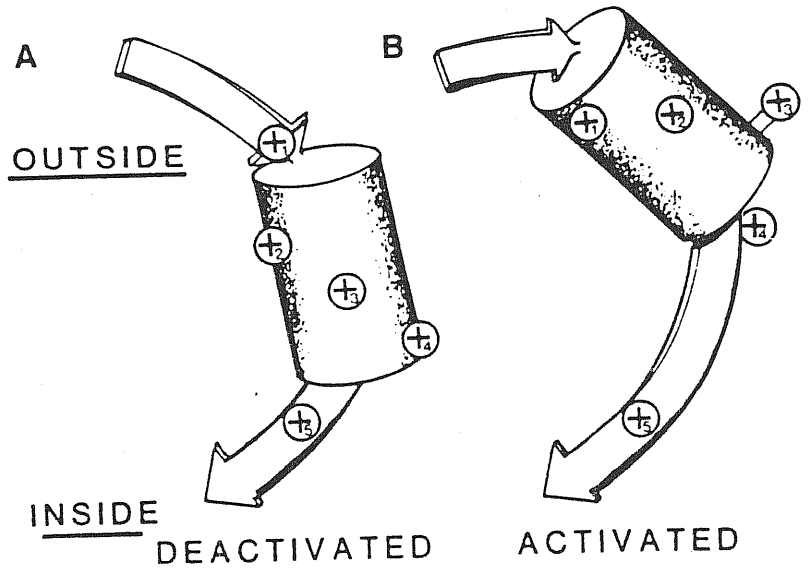

Figure 1.12:

Postulated conformation of the S4 segment (A) in the deactivated conformation of closed channels and (B) in the activated conformation of open channels. The secondary structure of at least two residues on each end of the helix changes (β to α at the N terminus and α to β at the C terminus) during the transition from the deactivated to the activated conformation. The large movement through the transmembrane region of $^{+}2$, $^{+}3$ and $^{+}4$ residues may produce a sufficiently large gating movement (from Guy and Conti 1990).

1.3 A special problem about sodium channels modification: intracellular Mg^{2+} interferes with the permeation through the sodium channel

More than 40 years ago, Bernard Katz discovered in Skeletal muscle an "anomalous inward rectification". This name was originated from his observation that K^+ conductance increases with the hyperpolarization but reduced with the depolarization, which is a phenonmenon opposite to the changes in K^+ conductance involved in the repolarization of action potentials (Katz 1949). Inward rectification is also opposite to what is expected from a greater concentration of K^+ inside cells than in the outside. To study this phenomenon, three possibilities were considered: (1) that channels themselves were rectifiers, as a result of the arrangement of energy barriers and wells that K^+ traverses as it permeats the channels (Woodbury 1971). (2) that channels were gated by voltage and were close under depolarization, and that this process was in some way influenced by extracellular K^+. (3) that there were some intracellular blocking particles that prevented K^+ outward flux by moving into the inner mouth of the K^+ channel. This blocking particle was driven out again at negative voltage partly by the inrush of K^+ (Armstrong 1966). In heart muscle, the idea that a blocking ion is at least partly responsible for inward rectification turns out to be correct (Vanderberg 1987, Matsuda et al. 1987, Matsuda 1988). In the late of 1980's, it begins to be clear that the blocking ion is Mg^{2+}. Mg^{2+} is known to act as a cofactor and regulator in the function of many enzymes, special kinases (Vidair 1981, Strata and Benedetti 1988, Stryer 1988), it is now found to be also a modifier in the function of many types of channel proteins such as ATP–sensitive potassium channel (Horie et al. 1987), muscarinic potassium channel (Horie and Irisawa 1987) and calcium channels (White 1988). Furthermore, Mg^{2+} may interfere with the ionic currents through the N–methyl–D–Aspartate ($NMDA$) activated ionic

channels from both the extracellular (Mayer et al. 1984, Nowak et al. 1984) and the intracellular cell sides (Johnson and Ascher 1990). In the case of K^+ inward rectification, the blockage by internal Mg^{2+} is found to increase both with depolarization of the membrane and with concentration of Mg^{2+}. The blocking effects occurs with great rapidity, Mg^{2+} entering and leaving the channel, i.e. to block and unblock it at rates approaching that at which K^+ ions permeated the channel (Vanderberg 1987, Matsuda et al. 1987, Matsuda 1988).

The rectification of outward currents through the sodium channel has also been studied in the sodium channels, which are expressed in *Xenopus* oocytes injected with cDNA–derived mRNA coding for the rat brain type II sodium channel (Pusch et al. 1989 and Pusch 1990a). Pusch and his collaborators first described the Mg_i^{2+} blockage of the "macroscopic" sodium currents as voltage and $[Mg^{2+}]_i$ dependent (1989). In his very recent paper Pusch (1990a), using a new type of sodium channel mutant ('cZ–2', which has long single–channel open time), observed that the blockage caused by the low concentration Mg^{2+} is due to Mg_i^{2+} flickering through the sodium channels. In order to explain the Mg^{2+} blocking effect, Pusch and his colaborators proposed that the reduction of conductance above the sodium reversal potential, which deviates from the prediction of Goldman–Hodgkin–Katz current equation, has mostly been attributed to the non–validity of the GHK equation at high potentials (Pusch et al. 1989). Since the GHK equation is based on the assumption of a constant electric field along the permeation pathway and on the independence principle, which states that the ion permeation is independent of the presence or concentration of other ions. Therefore, the GHK current equation was modified with a "Boltzmann factor" (Pusch 1990a):

$$p = \frac{1}{1 + \frac{[Mg^{2+}]}{K_d(0)} \exp\left(\frac{\delta F V}{RT}\right)} \tag{1.3}$$

in which $K_d(0)$ is the apparent dissociation constant of Mg_i^{2+} from the sodium channel. δ is the location of the Mg^{2+} binding site inside the sodium channel. With this modification, it was proposed that deviations from GHK current equation at high membrane depolarization but at

physiological Na^+ concentrations can be accounted for by a voltage– and dose–dependent blocking action of intracellular Mg^{2+} ions.

Although the modified GHK current equation can fit the instantaneous sodium current voltage relationships, many questions still remained. The most serious one is the inability to explain the dependence of Mg_i^{2+} on the intracellular $[Na^+]_i$, which also can not be explained well by assuming multi–ionic of sodium channels (Pusch 1990a). Furthermore, the aim of Pusch's work was emphasized on using Mg_i^{2+} blocking effect in the different sodium channel mutants as a probe to study the structure of the sodium channel, instead of attempting to explain the possible Mg^{2+} blocking mechanism. The aim of this thesis is therefore to determine, from macroscopic current analysis, how intracellular Mg^{2+} ion, interferes with sodium channels of mammalian neurons. In order to explain more accurately the possible mechanism of the reductance of outward sodium currents by intracellular Mg^{2+}, a series of experiments have been performed and theoretical explanation has been attempted in this thesis. A kinetic model was proposed for the explanation of Mg^{2+} blocking effect and a simple quantitative analysis method has been developed to solve the model. All the characterizations of Mg^{2+} effect observed in our experiments can be well explained with this model, such as voltage–, $[Na^+]_i$– and $[Na^+]_o$–dependence of Mg_i^{2+} blockage. Furthermore, this model has wide generalization and may be applied to explain some other divalent ionic effect, such as Ca_o^{2+} effect on the inward sodium currents (Nilius 1988) or "Mg^{2+}"–like ionic effect (Co^{2+}) on the $NMDA$-activated ionic channel (Ascher and Nowak 1988).

Due to the large population of cerebellar granule cells in the brain, the study of its function has received the attention in the middle of 1980s. Levi and his colleagues (1984) first described a method to culture rat cerebellar granule cells. With this culture method, granule cells can be easily identified morphologically under the differential interference contrast optics up to the 30th days in culture (DIC) (Levi et al. 1984, Galdzicki et al 1990). They are characterized by their small size (diameter 5–10 μm), their spherical shape and their greatly outnumber other larger cell types present. Cytological identification of granule cells

as neurons has been confirmed with the neurofilament–selective monoclonal antibody RT97 (Wood and Anderton, 1981) by Cull–Candy et al (1985, 1986, 1989). In their works, neurofilament has been detectable in granule cell processes within 6–8 hrs of plating, and fine neurites contained large amounts of neurofilaments by 20 hr. But outgrowth was sparse even after several days in culture, and the extent of arborization was clearly much less than that in a mature granule cell *in situ* (Cull–Candy et al. 1989).

Until now, the rat cerebellar granule cell in culture has been recognized as an excellent model for studying electrophysiological properities (Cull–Candy et al. 1986, 1988, 1989; Hockberger et al. 1987; Lin 1988; Zheng 1989; Sciancalepore et al. 1990), the cell development such as studying the ionic channel conductance change with the days in culture (Sciancalepore et al. 1989; Galdzicki et al. 1990) and biochemical properties (Levi et al. 1984; Levi and Gallo 1986; Nicoletti et al. 1987) of neurons, due to its maintained morphological and functional properties as native neurons (Levi et al. 1984). In order to obtain an overall picture of how the granule cells function, the activation and inactivation kinetics and the steady–state gating processes of the sodium currents of rat cerebellar granule cells were characterized, in the first part of this thesis, in terms of the Hodgkin–Huxley model. It was found that sodium channels in this type of neurons bear all the common features as sodium channels characterized in the other preparations (Carbone and Lux 1986; Moolenar and Spector 1977; Moran and Conti 1990). Based on its common features as the other neurons, a series of experiments therefore were further performed on granule cells to study the blocking effect of Mg^{2+} on sodium channels.

The organization of this thesis is as follows. After describing experimental methods in Chapter 2, the research results will be described in the following four chapters. In Chapter 3, the characterization of the voltage–dependent sodium channel gating process in cerebellar granule cells is described in terms of the HH model. Sodium channel properties are compared with those in other preparations. In the Chapter 4, Mg_i^{2+} blocking effect of sodium currents is demonstrated. Furthermore,

Mg^{2+} blockage was further characterized by its dependence on voltage, $[Mg^{2+}]_i$, as well as on $[Na^+]_i$ and $[Na^+]_o$. The Mg^{2+} blockage on mammanlian neurons has been further compared with the Mg^{2+} blockage observed on sodium channels expressed in oocytes. In Chapter 5, the possible influence of Mg_i^{2+} on voltage dependent gating processes of sodium channels is studied. This chapter illustrates that Mg^{2+} modification on the voltage dependent gating process of sodium channels is not the essential factor of Mg^{2+} blockage. In Chapter 6, a kinetic model, in which Mg_i^{2+} and Na^+ compete for occupying the sodium channel, is proposed. The sodium permeation in the presence of Mg^{2+} is described as ionic binding–unbinding process with the sodium channel. This description is similar to that of Michaelis–Menten kinetics for enzymatic reaction. Ionic binding sites of Mg_i^{2+} and Na^+ may be different inside the channel, but in one binding site, only one ion can be bound at a time. In this chapter, the voltage dependent rate constants of Mg_i^{2+} and Na^+ binding process are further expressed in terms of reaction free energy with an additive Eyring rate factor for considering the applied electrical field effect. With these expressions, Mg^{2+} and Na^+ binding sites inside the channel are located and ionic binding affinities are calculated. It will demonstrated that high Mg^{2+} affinity with sodium channels can account for the Mg^{2+}. The different potential drops detected by Mg^{2+} and Na^+ inside the sodium channel explain the voltage dependence of Mg^{2+} blockage. Finally, a general discussion on the experimental results were given in Chapter 7. In this chapter, the kinetic model and data analysis used in this thesis are evaluted. Right after Chapter 7, the general conclusions of this thesis will be given.

Chapter 2

Material and Methods

2.1 Cell Preparation

The Primary culture of rat cerebellar granule cells was prepared from 8-day-old postnatal rat pups following the procedure described by Levi et al. (1984). The main procedure is as follows: Cerebella were removed from a group of rat pups under sterilizing condition. Meninges and blood vessels on the surface of cerebellum were peeled off and minced in the sterilized Krebs solution. Connective tissues between the cells were digested with 0.5 mg/ml trypsin (Sigma, USA). Cells were further mechanically separated as much as possible with a series of Pasteur pipettes with different tip sizes. Separated cells were washed and purified with a series of centrifugations. Finally obtained cell pallet was diluted to the density of 0.75 $million/ml$ with the culture medium and plated on freshly poly-L-lysine (Sigma) covered 35 mm Petri dishes (covered with 5 $\mu g/ml$ poly-L-Lysine for at least 20 minutes before plating). The ideal quantity of cells is 1.5 *million* per dish. Culture chambers with plated neurons were maintained at 37°C, 5% CO_2, saturated humidity incubator (Heraeus FRG). 10 μM cytosine arabinoside furanoside (Sigma), as a mitotic inhibitor, was added into each dish after about 19 hours *in vitro* to inhibit the replication of non-neuronal cells. A detailed procedure for the cell culture and the composition of solutions can be found

in the previous thesis (Lin 1988).

Rat cerebellar granule cells cultured with this method can be easily identified morphologically under the differential interference contrast optics (Zeiss, FRG) until the 30th days in culture (DIC), characterized by their small size (diameter 5–10 μm), their spherical shape and their greatly outnumber other larger cell types present. Although the granule cells in culture undergo less development than that *in vivo* (Cull–Candy et al. 1989), the neuritic growth process still leads to very complicated cell shape (figure 2.1) after several days in culture, which makes it diffult to control the applied voltage over the patch cell membrane (space–clamp problem). Furthermore, the ionic channels themselves also undergo the similar differentiation *in vitro* as *in vivo*, which may reflect as the ionic conductance increase with days in culture. This increase has been observed in the single–channel recording of the $NMDA$–activated ionic currents (Sciancalepore et al. 1989), the whole–cell calcium currents (Marchetti et al. 1990), the whole–cell potassium currents (Galdzicki et al. 1990), as well as the whole–cell sodium currents (Lin and Moran 1989), which may be caused by the higher channel density (more ionic channels expressed) or the higher probability of channels to be activated. Therefore, in the experiments described in this thesis, the cells used for characterizing sodium currents, as well as for studying Mg_i^{2+} blocking effect were limited in $3 \sim 5$ DIC, since the current density is more homogenous and less dendrites developed in this period (see Section 3.1).

2.2 Patch clamp

The emergence of the patch–clamp technique has revolutionized the study of ionic channels. It was originally developed to directly measure the current through the single ionic channel. In 1976, Erwin Neher and Bert Sakmann reported the first single–channel current recording recorded from a biological membrane (Neher and Sakmann 1976). In brief, this method consists of placing a microelectrode on the membrane

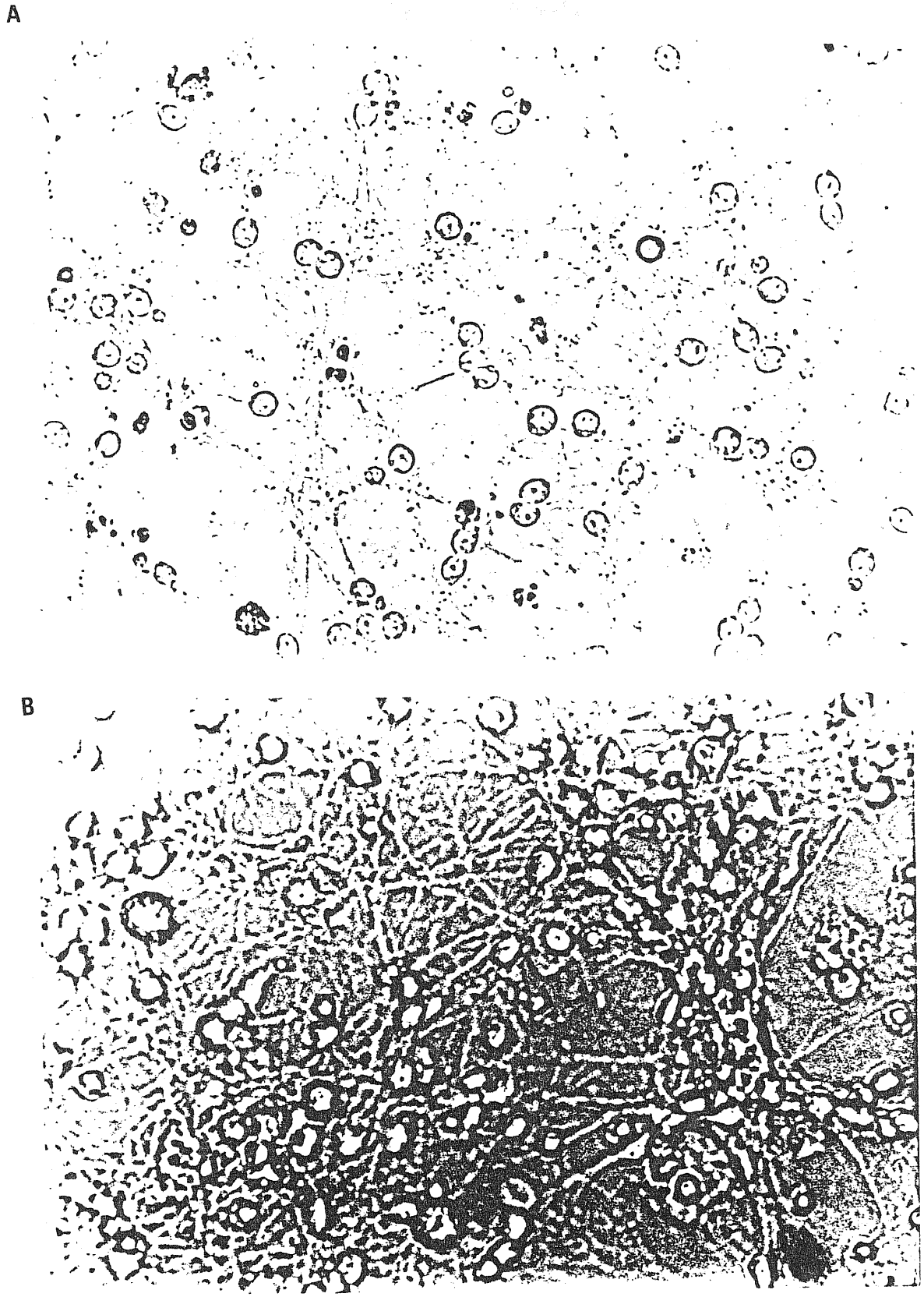

Figure 2.1:
The primary cultured rat cerebellar granule cells. A The granule cell is characterized by its spherical shape. B The neuronal dentrites and axons are clearly shown.

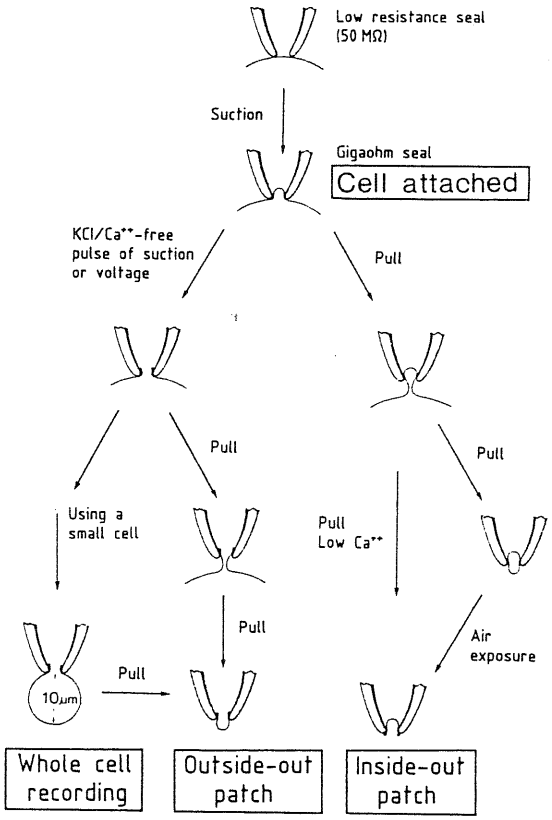

Figure 2.2:

Four patch–recording methods. All methods start with a clean pipette pressed against an intact cell to form a gigaohm seal between the pipette and the membrane it touches. Channels can be recorded in this on–cell mode. Additional manipulations permit the same pipette to be used to clamp a whole cell or excise a patch of membrane in inside–out or outside–out configurations. (After Hamill et al. 1981).

to be investigated, with an especially tight contact between the special fire polished electrode tip and the membrane (the resistance of the contact is in the order of $10^{12}\Omega$. This tight contact prevents currents leaking from the ectoplasm to the inside of electrode. Therefore, using a command circuit to control the membrane potential, the currents flowing between the pipette electrode and an external electrode will be the ionic currents passing through the ionic channels of the patched membrane. Different manipulations after achieving the tight seal between the pipette and the membrane allow to get several patch–clamp configurations for specifically required current recordings, such as the single channel or the whole–cell current recordings (figure 2.2; Hamill et al. 1981). Among all the configurations, the cell–attached configuration is directly obtained by the formation of the seal between the pipette and the membrane. With this method, the cell content is kept intact. The intact cell content is important for studying ionic channels which are sensitive to the metabolic process of the cell such as the calcium channels. The other two recording configurations, i.e. so called "inside–out" and "outside–out", are obtained by pulling up the recording pipette before or after disrupting the patched cell membrane (see figure 2.2). In these two cases, the ionic current recorded is those flowing through this small piece of membrane. If the tip of the pipette is small enough, it is possible to have only one channel under the patched membrane and gives the single channel recording. These two configurations also open the possibility to easily control the "intracellular" or "extracelular" compositions of the patched membrane. The whole–cell configuration, used in the experiments of this thesis, was achieved by applying a negative pressure or voltage pulses to break the membrane after the cell–attached configuration is formed. Since the direct communication is established between the pipette and the intracellular compartment in the whole–cell configuration, the intracellular solution is rapidly dialyzied to the pipette solution, giving a control of intracellular composition of the patched cell.

Borosilicate glass pipettes (Hilgenberg, FRG) were used to prepare the recording electrode pipettes with a two–step puller (List Medical Electronics, FRG). Tips of recording pipettes were fire polished with a

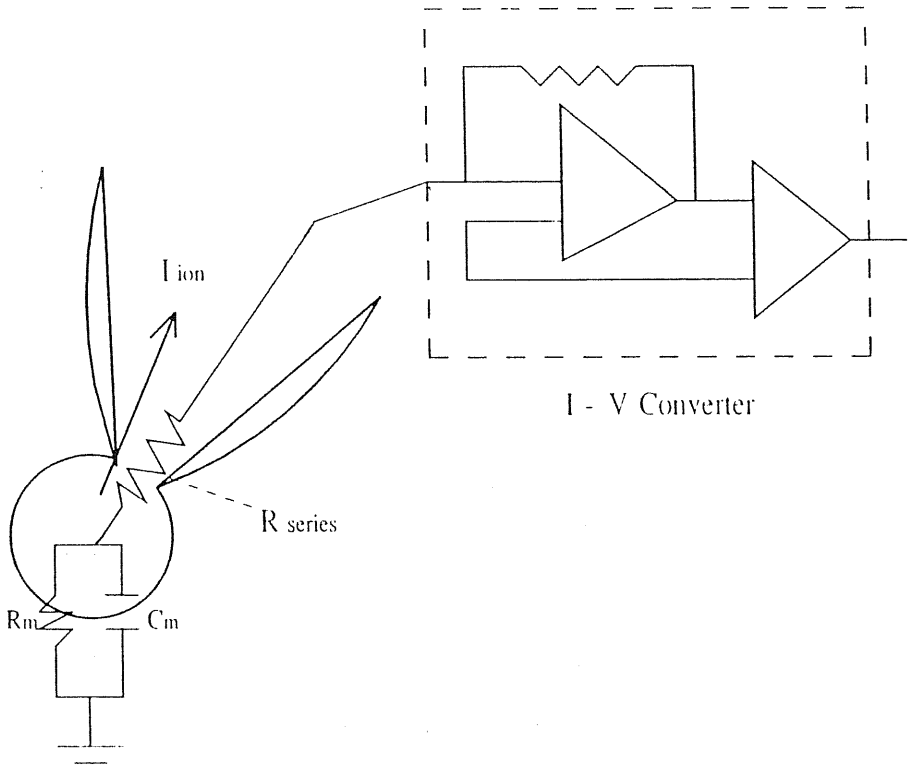

Figure 2.3:
The electrical pathway of ionic currents through the patch cell membrane.

hot platinum under a microscope with the magnification of 20×. Pipette resistance was in the range of 2.5 to 4 MΩ, measured in the working solutions described in Section 2.5. Sodium currents were recorded with the standard whole–cell configuration (Hamill et al. 1981). The Seals of 30 to 70 $G\Omega$ were routinely obtained between the pipettes and the patched cells.

With the whole–cell configuration, the series resistance may seriously influence in the correct voltage controlling over the patched cell membrane. The series resistance problem was first described in the squid axon preparation (Hodgkin and Katz 1949). The series resistance (R_{series}) is introduced in the electrical pathway between the output of the patch clamp amplifier and the patched cell (Figure 2.3). The presence of the series resistance will cause two problems on the voltage controlling of the patched membrane: 1) the time delay of the onset

and the offset of the voltage pulse. The time delay τ can be calculated as: $\tau = R_{series}C_{membrane}$; 2) an unexpected drop of the applied membrane potential: $\Delta V = I_{ionic}R_{series}$. The series resistance problems mainly result from three reasons. The first one is the area of the cell surface: $C_{membrane} \propto$ membrane area. Hence, the smaller cell is used, the smaller membrane capacity is. The second factor is the ionic current itself. If the patched cell has the high amplitude currents (for example, due to its high channel density, its high probability of channels in the activated states, etc), the large current will increase the membrane potential drop caused by the electrical pathway (Δ in the second point mentioned above). If this is the case, the series resistance effect can be diminished by adding a low concentrated TTX to the cell bath for blocking some sodium channels, or by using lower external sodium concentration for decreasing the current amplitude. But this was not a series problem in the current recording with the granule cells in my experiments, since the maximum inward peak sodium current is generally less than 100 pA. The other factor which may influence the magnitude of the series resistance is the dimension of the pipette tip, since the size of the tip limits the maximum size of the opening of the membrane under the patch. The opening of the membrane patched, on the other hand, directly relates with the magnitude of the resistance between the cell interior and the recording electrode (R_{series}, figure 2.3). Therefore, the recording pipettes used should be as big as possible, taking into consideration the small dimensions of granule cells ($5 - 10\mu m$). The series resistance measured from 63 patches is 16.8±4.8 MΩ. With this range of series resistance, the maximum possible potential error ΔV is always less than 2 mV at the potential that the inward sodium current reaches its maximum.

The ionic currents were recorded using a standard patch-clamp amplifier (EPC-7, List Medical Electronics, FRG), with a 50 $M\Omega$ feedback resistor in headstage. The patch–clamp instruments used in our experiments were organized as in figure 2.4 (the recording part) and 2.5 (the support part).

The cell dish was mounted on a movable support on a microscope

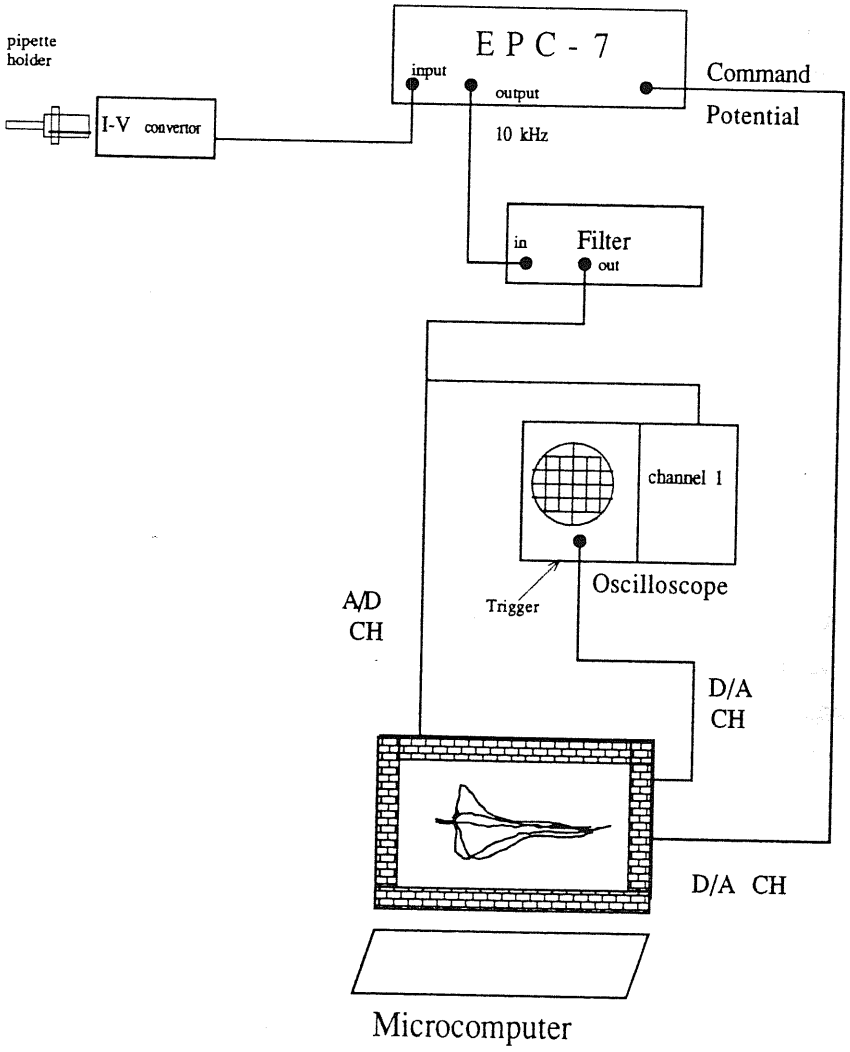

Figure 2.4:

Electronic part of the patch–clamp equipments

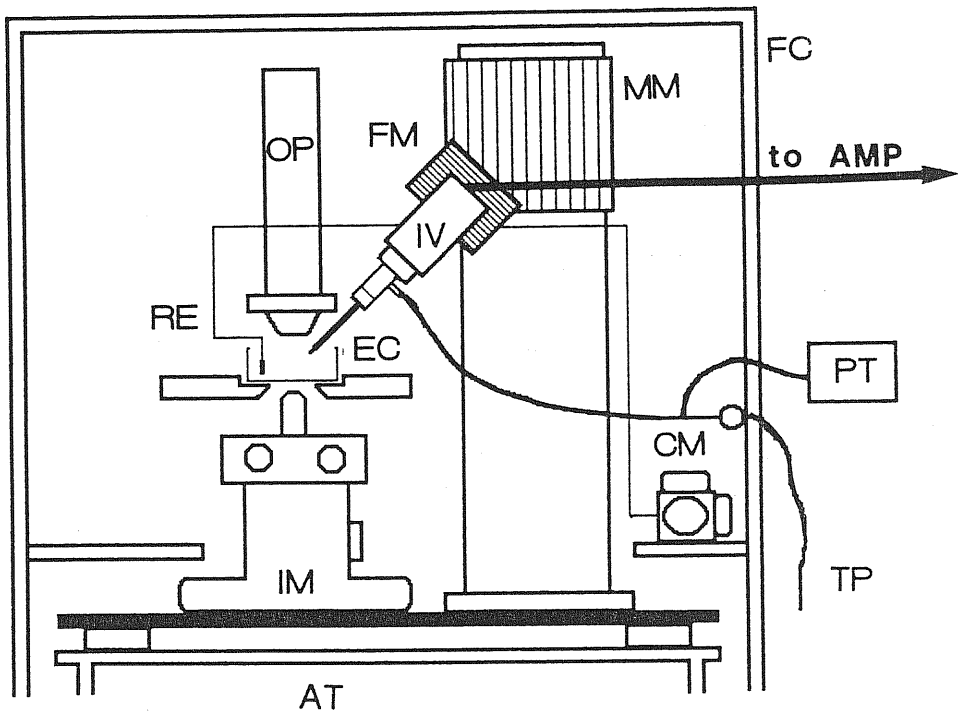

Figure 2.5:

Mechanical part of the patch–clamp equipments

AMP: Patch–clamp amplifier AT: Antivibratory table. CM: Coarse micromanipulators. EC: Experimental chamber. FC: Faraday cage. FM: Fine micromanipulators. IM: Inverted microscope. IV: Current to voltage converter. MC: Three–dimensional micro movement controller. OP: Microscope optics. PT: Pressure transducer for pipette pressure measurement. RE: Reference electrode. TP: Tube for applying pressure (kindly provided by Dr. O. Moran).

(IM35, Zeiss, FRG) with a Nomanski optics (Figure 2.5). The $I - V$ converter of EPC-7 was mounted on a three-dimensional micro movement manipulator (Micro–Control, France). The finally fine movement of recording pipette was controlled by a piezoelectric micromanipulator (Physik Instrumentes, FRG).

The stimulation and data acquisition were controlled by a microcomputer (Atari 1040ST, HongKong) with "Patch Program" written in Modula–2 by H. Affolter (Instrutech, USA), using a 12 bits A/D - D/A converter (M2–Lab, Instrutech, USA). The acquisition program contains several functions such as real time operations, data displaying, designs of several sets of voltage pulses and subtraction of linear components of ionic currents with P/4 procedure (see below) and some simple measurements as peak values. The experimental data was directly saved into the hard-disk of the computer during the experiment. The membrane current was sampled at frequence of 50 kHz. Before digital acquisition, the output of patch-clamp amplifier was filtered by a low–pass 4–pole Bessel filter (Ithaco 4302, USA), set at a cut–off frequency of 5 kHz or 10 kHz.

2.3 Experimental Protocols

The standard pulse protocols were used to study the macroscopic properties of the sodium currents. Sodium currents are quickly inactivated when the cell membrane is depolarized, with a half inactivation potential lower than –40 mV measured in many cell preparations, such as in the rat myelinated nerve fibres (Neumcke and Stämpfli 1982), the rat and human skeletal muscle (Almers et al. 1984) and the sodium channels expressed from rat brain cDNA (Stühmer et al. 1986). A low holding potential, therefore, was chosen in order to remove the inactivation resulting from the holding state as much as possible. The holding potential was maintained at –90 mV in all of the experiments. In all cases, most of the capacitive components of the membrane currents in response to a voltage–step stimulation was compensated analogically,

i.e. by zeroing the capacity transient induced by a voltage pulse with the patch–clamp capacitive compensation circuit. All the stimulations for the sodium current measurements were followed by a similar pulse protocol in which pulse amplitudes were reduced to 1/4 and the holding potential was brought to –110 mV (P/4 procedure, Bezanilla and Armstrong 1977). The P/4 responses were used to make a further digital correction of the linear capacitive and the leakage membrane responses from the measured currents.

2.3.1 One–pulse experiment

To yield the voltage dependence of the steady–state activation process and those of the activation and the inactivation kinetics, a series of voltage pulses to various depolarization levels between –40 and 130 mV in every 10 mV step were applied. All the voltage pulses were preceded by a –100 mV amplitude prepulse with a 5 msec duration (to futher remove the inactivation). In order to observe better the sodium current behavior at high potentials, the applied potential pulses are increased in every 5 mV steps at $V_m > 50$ mV.

2.3.2 Double–pulse experiment

The steady–state inactivation parameters were elicited from the traditional double–pulse protocol (Hodgkin and Huxley, 1952c). The first long duration voltage step, with variable amplitudes called conditional prepulse, is intended to be long enough to permit the inactivation process to reach its steady–state level at the prepulse potential. The second voltage step to a fixed level, which is called the test pulse, elicits the usual transient I_{Na}. The relative peak current amplitude I_p/I_p^{max} is used to determined the fraction of sodium channels which were not inactivated by the conditional prepulse. In our experiments, the test pulse is fixed at –10 mV, preceded by conditional prepulses with 40 msec duration to various potentials between –80 to –5 mV in the step of every 5 mV.

2.4 Data Analysis

Raw experimental data were directly saved into the computer hardisk during the experiment. The experimental data were later transferred to the Microvax station. All the data analysis were performed on Microvax station. The analysis programs were written in Fortran-77. All the fitting procedures were based on the Standard least–chi–square method (Press 1989).

2.4.1 Peak current I_p *vs.* membrane potential V_m relationship

The most obvious way to demonstrate the voltage dependence of the ionic currents is to construct the relationship between the peak current I_p and the membrane potential V_m. I_p was estimated by fitting the experimental current record in a short interval around the peak with a third order polynomial. From the I_p *vs* V_m relationship, some parameters can be further obtained: One is the experimental reversal potential of sodium current V_{rev}, i.e. at which the sodium current changes the sign. V_{rev} was obtained by fitting the linear part of I_p *vs.* V_m relationship with a linear equation. The measured reversal potential usually deviates from the reversal potential predicted from Nernst equation (eq. 1.1). The difference may originated from several aspects. First of all, the quality of the experiments can directly influence the reversal potential, even the accuracy of the applied potentials. For example, the quality of the compensation of the zero–current potential before the seal formation may seriously influence the applied membrane potentials. The zero–current potential is mainly created by the liquid junction potential due to the unequilibrium ionic exchange between the pipette and the bath solutions (Marty and Neher 1983). The junction potential may be significant with the presence of large ions, such as Cs^+, due to its slow speed of diffusion. In my intracellular solutions, the intracellular Cs^+ concentration can be as high as 110 mM and the junction potential can reach +30 mV. Therefore, the careful compensation of the zero–current potential

is critically important to ensure the reality of the applied membrane potential. The quality of this compensation, on the other hand, can be directly reflected on the reversal potential measured.

The difference between the experimental and the theoretical reversal potential may be also due to the presence of ions which has low permeability through sodium channels, such as Cs^+, Mg^{2+}, Ca^{2+} etc. Therefore, the accurate reversal potential should be calculated according to GHK voltage equation (eq 1.2), taking into account of the presence of other permeable ions.

Another useful parameter which can be directly obtained from the $I_p - V_m$ relationships is the maximum inward peak current I_p^{max}. I_p^{max} is obtained by further fitting the inward peak current part of the $I_p - V_m$ relationship with a third order polynomial, similar to that used to estimate the peak current I_p from the total current trace. The amplitude of the inward peak macroscopic sodium current is the combined result of two opposite effects: the decreasing driving force and the increasing open probability of sodium channels with the increase of membrane potentials. The formation of maximum inward peak currents could be considered as the equilibrium of these two opposite effects and used as a characterizing value of sodium channels. In fact, this maximum inward sodium peak current scaled by the corresponding cell membrane area can be approximately used as the current density of patched cells and compared with those measured in the other cell preparations (see Section 3.3).

2.4.2 The voltage dependent gating parameters

The voltage dependent sodium current is characterized in terms of the HH model (1952a). The study of the voltage dependent gating process composed of characterizing the voltage dependence of the steady–state activation and inactivation parameters, as well as the time constants of the activation and the inactivation kinetics processes. The data necessary for characterizing the voltage dependence of the kinetics processes and steady–state activation process were directly obtained from the one–

pulse experiment (Section 2.3.1). The voltage dependence of the steady–state inactivation parameters was obtained according to the classical analysis of the double–pulse experimental results (Section 2.3.2).

To study the voltage dependence of the steady–state activation (m_∞) and the kinetics time constants (τ_m and τ_h), each trace of sodium currents, elicited from different potential pulses, was fitted with equation 2.1:

$$I(t) = I'(1 - \exp(-\frac{t - \delta t}{\tau_m}))^3 \exp(-\frac{t - \delta t}{\tau_h}) \qquad (2.1)$$

where,

$$I' = g_{max}(V_m - V_{rev})m_\infty^3 h_0 \qquad (2.2)$$

Since the inactivation process can be removed under the hyperpolarization condition, it is assumed that the inactivation process at the initial pulse is almost absent, i.e. $h_0 \simeq 1$, in the presence of strongly negative holding potential and hyperpolarized prepulse as described in Section 2.3.1. δt is an empirical delay at the onset of the classical m^3h kinetics observed in the HH model (Keynes and Rojas 1976). The initial delay δt is found to be a function of the holding potential (figure 2.6). It is found that δt is noticeable when the holding potential is more negative than –60 mV (Keynes and Rojas 1976, Keynes and Kimura 1983, Taylor and Bezanilla 1983).

In order to make it easy, the four–parameter problem as describing by equation 2.1 was solved by several steps. Considering the declining phase of sodium currents mainly contributed from the inactivation kinetics of sodium currents and the rising phase from the activation kinetics, the declining phase of the current was fitted with a single exponential function: $I_i(t) = I_0' \exp(t/\tau_{h0})$, which decays to a stationary level which is significant only for the responses to the moderate depolarization($V < -40$ mV). This fitting step allowed us to get the approximate values of I' and τ_h: I_0' and τ_{h0}. Since the activation process is much more faster than the inactivation process as indicated in equation 2.1, the activation process may be assumed to approximately reach its steady state when the sodium current reaches to its maximum, i.e. I_p. The inactivation process begins to be dominant after reaching

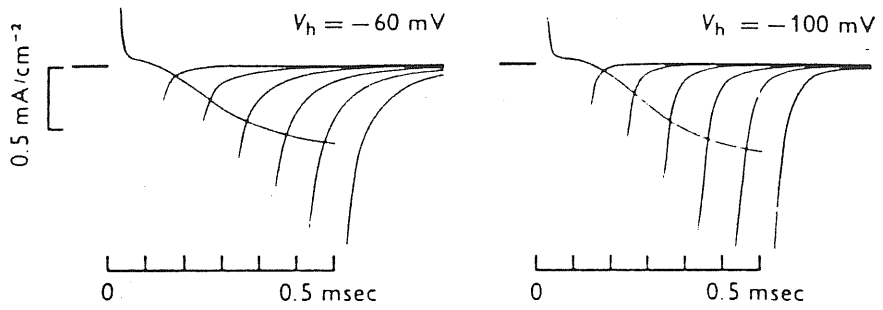

Figure 2.6:

Sodium currents associated with depolarization pulses of different duration at two different holding potentials. Conditions: perfused axon in seawater with 107.5 mM Na^+ and 10 mM Ca^{2+}; perfusion fluid 300 mM Cs^+; holding potential V_h is indicated above records; pulse potential 20 mV; temperature, $7°C$. The turning-on of I_{Na} could be fitted by equation 2.1 with $\delta t = 0$, $\tau_m = 202\mu sec$ for $V_h = -60$ mV, and $\delta t = 30\mu sec$, $\tau_m = 210\mu sec$ for $V_h = -100$ mV. The time constants for the tail constants are 101 μsec at $V_h = -100$ mV (From Keynes and Rojas, 1976).

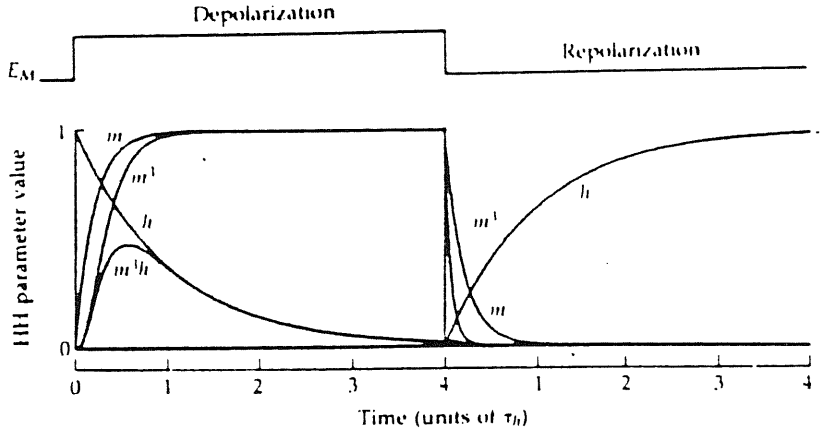

Figure 2.7:

The course of HH model parameters. A purely hypothetical example representing a depolarizing step followed by a repolarization. The time constants τ_m and τ_h are assumed to be in the ratio of 1:5 and the duration of the depolarization (to the middle vertical line) is assumed to be 4 τ_h. Unlike a real case, the time constants are taken to be the same at both potential. Curves for m on the left and h on the right are $1 - \exp(-t/\tau)$. That is, an exponential rise toward a value of 1.0. Curves for m on the right and h on the left are $\exp(-t/\tau)$, that is an exponential fall toward a value of zero. Other curves are the indicated powers and products of m and h showing how m^3h imitate the time course of g_{Na} in the HH model (Hille 1977).

the peak (see figure 2.7). Therefore, a quite close value of τ_h can be obtained by fitting declining phase beginning at a time which is the twice of time to peak (t_p). Estimated values of δt and τ_m: δt_0 and τ_{m0}, were obtained by fitting the rising phase of the current which has been scaled with the relation of $I(t)/I_i(t) = (1 - \exp(-(t - \delta t_0)/\tau_{m0}))^3$. Reintroducing these four estimated values of I_0', τ_{h0}, τ_{m0} and δt_0 into equation 2.1, we can more easily readjust them to yield the best fit with the total current. A complete fitting process generally used in this thesis is shown in figure 2.8.

The steady-state activation gating parameter m_∞ has been further obtained from the equation 2.2, i.e. $m_\infty^3 = g/g_{max}$. The steady–state activation parameter m_∞ can be expressed as a function of the membrane potential, which is characterized by the half–activation potential, $V_{1/2}^m$, at which the open–state probability for each activation gate is 0.5, and by the apparent valence z_m of a single activation process (m–gate). These parameters were obtained by fitting data obtained from equation 2.2 to:

$$m_\infty(V) = \frac{1}{1 + \exp\left(z_m e_0 \frac{V - V_{1/2}^m}{kT}\right)} \tag{2.3}$$

where, e_0 is the proton charge (1.6 x 10^{-19} Coulomb), k is Boltzmann's constant and T is the absolute temperature.

The double–pulse protocol was designed to obtain the steady–state inactivation parameter of the sodium currents, since the ratio of I_p to the maximum I_p^{max}, I_p/I_p^{max}, elicited by the test pulse reflects the fraction of sodium channels which are not inactivated by the conditional potential. Hence the voltage dependence of the steady state inactivation parameter h_∞ can be calculated from the relation of $h_\infty \simeq I_p/I_p^{max}$. Its voltage dependence can be expressed as a function of the prepulse potential V_{pp} as:

$$h_\infty = \frac{1}{1 + \exp\left(\frac{V_{pp} - V_{1/2}^h}{a_h}\right)} \tag{2.4}$$

Where, $V_{1/2}^h$ and a_h characterize the half–inactivation potential and the steepness of the voltage–dependence respectively. I_p^{max} is the mean of

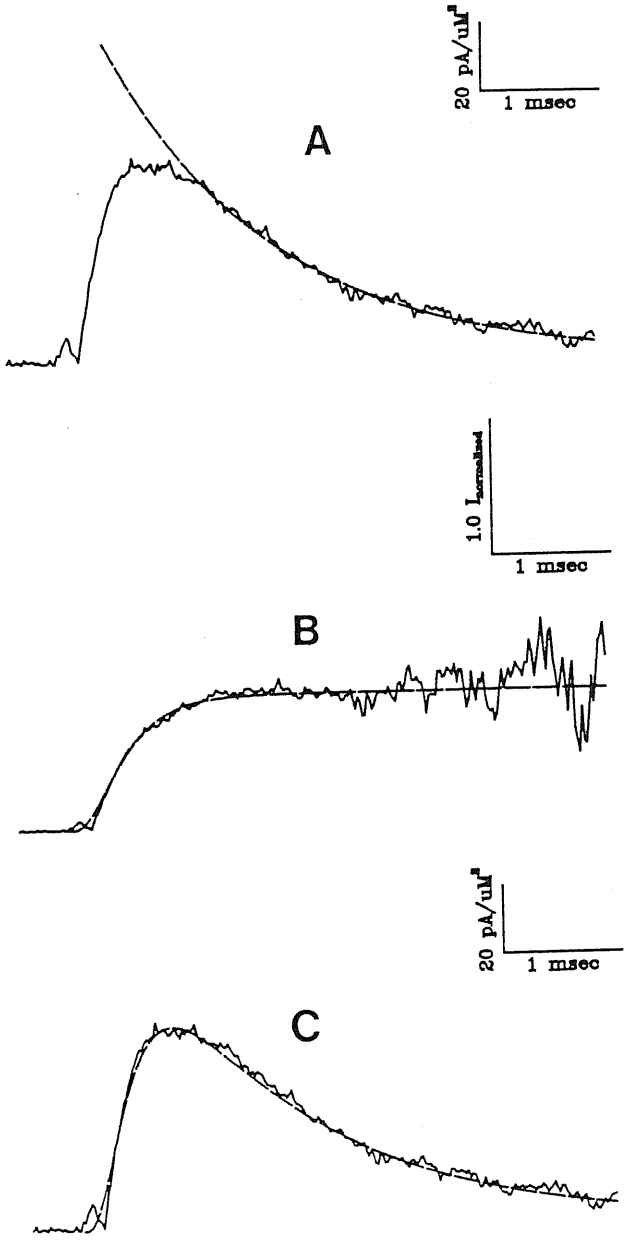

Figure 2.8:

The fitting procedure of the sodium current. **A.** The decline part of sodium current is fitted with an one-exponential function, to obtain the approximate value of I' and τ_h. Fitting from 2.0 to 4.0 msec, approximate values obtained of I' and τ_h are 169.25 pA and 1.43 msec respectively. **B.** The rising part of the normalized sodium current is fitted with $(1 - \exp((t - \delta t)/\tau_m)^3$. τ_m and δt were estimated to be 0.27 and 0.43 msec by fitting from 0.7 to 1.1 msec. Reintroducing the approximate values of I', τ_m, τ_h and δt obtained from last two steps into equation (2.1), the four parameters are readjusted and yield the best fitting of total current (**C**). The final fitting results are: I' is 123 pA, τ_m = 0.27 msec, δt = 0.44 msec and τ_h = 1.43 msec. For this current trace, V_m = 20 mV.

the maximum peak currents measured at the strongly negative conditional potentials, at which the inactivation is still insignificant.

2.5 Solutions for electrophysiological studies

With the aim of studying Mg_i^{2+} blocking effect, we have designed a series of experimental solutions by varying $[Na^+]_i$, $[Na^+]_o$ and $[Mg^{2+}]_i$, based on the standard (control) extracellular and intracellular solutions. The control solutions are those used for characterizing the sodium channel on the rat cerebellar granule cells (Chapter 3).

The control extracellular solution used in the cell bath was (in millimolar): $CaCl_2$ 2, $CoCl_2$ 5, HEPES 10, and NaCl 100. The control pipette solution, dialyzing the intracellular compartment, was NaCl 5, CsF 110, HEPES 10 and EGTA 11. The pH values of both solutions were adjusted to 7.35 with NaOH. The osmolarity of intracellular solution was corrected to 295 mOsm and that of external solution to 310 mOsm with *d*–glucose. 5% osmolarity difference makes patched membrane broken easily. In all experiments, potassium currents were absent because of intracellular substitution of K^+ with Cs^+. Calcium currents were also insignificant with these recording solutions, as demonstrated by the absence of any appreciable effect of 2.5 mM Cd^{2+} or 5 mM Co^{2+}, known to be very potent blockers of calcium channels (Brown et al. 1981; Carbone and Lux 1984).

As mentioned above, the aim of this thesis is to study the interaction between the Na^+ and Mg_i^{2+}. To approach this goal, the experimental design has been separated to two different parts. The first part of experiments is to test the interaction between the intracellular Na^+ and Mg_i^{2+}. In this part of the test, the extracellular solution is fixed as the control one shown above. The intracellular Na^+ concentrations have been changed from 15, 20 to 30 mM. With each $[Na^+]_i$, $[Mg^{2+}]_i$ was varied from 0 to 7 mM (table 2.1). $[Mg^{2+}]_i$ has also been increased up to 30 mM in order to study the possible Mg_i^{2+} influence

Composition mM	$15Na(0-7)$ mM	$20Na(0-7)$ mM	$30Na(0-7)$ mM	$30Na(30)$ mM
NaCl	5	10	20	20
$MgCl_2$	0,0.5,1,3,7	0,0.5,1,2,3,5,7	0,0.5,1,3,7	30
CsF	110	105	95	70
EGTA*	11	11	11	11
HEPES+-NaOH	10	10	10	10

Table 2.1:

Intracellular solutions

* EGTA: Ethylenglycol-*bis*-β-amino-ethylether

+ HEPES: *N*–2–Hydroxyethylpiperazine

Intracellular pipette solutions. The osmolarities of solutions are adjusted with *d*-glucose to 291 mOsm.

on the voltage dependent sodium channel gating process. The different sets of intracellular solutions used in this part of study are shown in table 2.1. When the intracellular CsF concentration is decreased to 65 mM, there is no potassium current observed by adding 10 μM TTX to cell bath. Osmolarities of intracellular solutions are hence kept to 295 mOsm by reducing intracellular CsF concentration in those solutions with high $[Na^+]_i$ and $[Mg^{2+}]_i$ (see specially columns 4 and 5 in table 2.1), in addition of varying glucose concentrations.

The second part of experiments is to test the interplay between Mg_i^{2+} and Na_o^+. To do this, two sets of extracellular solutions with lower $[Na^+]_o$ are added, see table 2.2.

In this part of experiments, the intracellular solutions are those with 30 mM Na_i^+ and various $[Mg^{2+}]_o$ (column 4 in table 2.1).

To express explicitly, the different sets of solutions will be named according to their Na^+ concentrations. The concentration of Mg_i^{2+} will be indicated in the parenthesis following the names of intracellular so-

Composition mM	$50Na(0)$ mM	$70Na(0)$ mM	$110Na(0)$ mM
NaCl	40	60	100
$CoCl_2$	5	5	5
$CaCl_2$	2	2	2
HEPES-NaOH	10	10	10

Table 2.2:

Extracellular solutions.

The osmolarities of solutions are adjusted with *d*-glucose to 310 mOsm.

lutions. For example, 110Na/30Na(30) indicates that the extracellular solution contains 110 mM Na^+, corresponding to the fourth column of table 2.2, the intracellular solution, on the other hand, contains 30 mM Na^+ and 30 mM Mg_i^{2+}, corresponding to the fifth column of table 2.1. As a summary, the extracellular/intracellular solutions which have been used in all experiments of this thesis are following:

- 110Na/15Na(0) in Chapter 3.
- 110Na/15Na(0–7), 110Na/20Na(0–5), 50Na/30Na(0–7), 70Na/30Na(0–7) and 110Na/30Na(0–7) in Chapters 4, 6.
- 110Na/15(0–7) and 110Na/30(0–7,30) in Chapter 5.

All experiments were performed at the room temperature (17 to 21°C).

Chapter 3

Characterization of the sodium channel in cultured rat cerebellar granule cells

A rough characterization of the sodium channel in the rat cerebellar granule cell has been attempted in the previous thesis (Lin 1988). The patch clamp equipment and the acquisition system in our laboratory has been greatly improved now, which allowed to make more precise current recording. Also, it is necessary to have more precise description of the sodium channel on the granule cells in order to further study the intracellular Mg_i^{2+} blocking effect of sodium currents. To approach this object, the sodium current was carefully analysed in terms of the original Hodgkin and Huxley equation, in order to characterize the sodium current in such a way that it can be compared with those described in other preparations.

3.1 The Sodium Channel Development With Days In Culture

The dissociated cerebellar granule cells could undergo the similar differentiation and growth processes in culture as *in vivo* (Levi et al. 1984,

Cull–Candy et al 1985, 1986, 1989, Sciancalepore et al 1989 and Galdzicki et al 1990). Since the application of the intracellular perfusion technique is very difficult in the whole–cell configuration in such small granule cells, all of the whole–cell recordings with different experimental solutions were performed on the different cells. All the experimental results are therefore the statistical results. In order to minimize the individual differences between the different cells, the development of sodium channels *in vitro* was first studied by estimating the change of the maximum sodium membrane conductance per unit membrane area with different days in culture. Having the idea of the sodium channel development, the cells bearing more homogenous distributions of sodium channels therefore were chosen for the further using.

Action potentials, the TTX–sensitive sodium current and at least two types of potassium currents were recorded from the 1 day in culture (DIC) cells up to the 30 DIC (Figure 3.1). However, the space–clamp problem (Section 2.1) becomes serious for the current recording on the cells older than 10 DIC due to the neruitic process (see figure 2.1B).

The sodium channel membrane conductances have been estimated on the cells from different DIC. The sodium channel membrane conductance (g_p) was calculated according to the GHK current equation:

$$g_p = I_p \frac{(1 - \exp(\frac{V_m}{RT}))}{V_m(1 - \exp(\frac{(V_m - V_{rev})}{RT}))} \tag{3.1}$$

all parameters in the equation have their usual meanings. In order to compare results obtained from different cells, sodium currents have been scaled by the membrane areas, calculated from the compensation of the capacitance transient of their corresponding cells using the empirical relation: 1 pF / 100 μm^2 (Moran and Conti, 1990).

Unexpected high membrane conductance per unit membrane was found in 1 DIC old cells, which may be due to the contaminant measurement of other kinds of cell (probably due to the similar appearances of 1 DIC cells), or due to the unstability of cells in 1 DIC. It was found that the membrane conductance tends to increase with days in cultures after 2 DIC (Figure 3.2), although the membrane capacities do no change

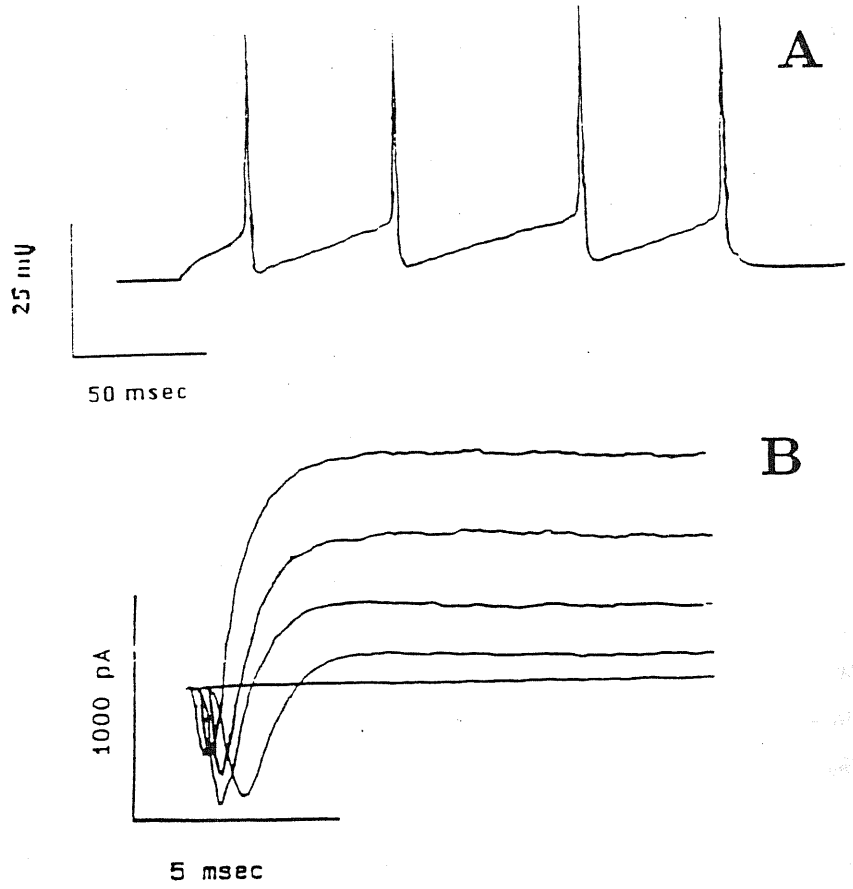

Figure 3.1:
Action potential and total ionic currents recorded from rat cerebellar granule cells. **A** Repetitive action potentials evoked by a current step of 30 pA for 200 msec, resting membrane potential was −65 mV. **B** Total membrane currents recorded in the presence of KCl in the intracellular solution. The holding potential was −60 mV, and the test pulse were from −40 to +40 mV.

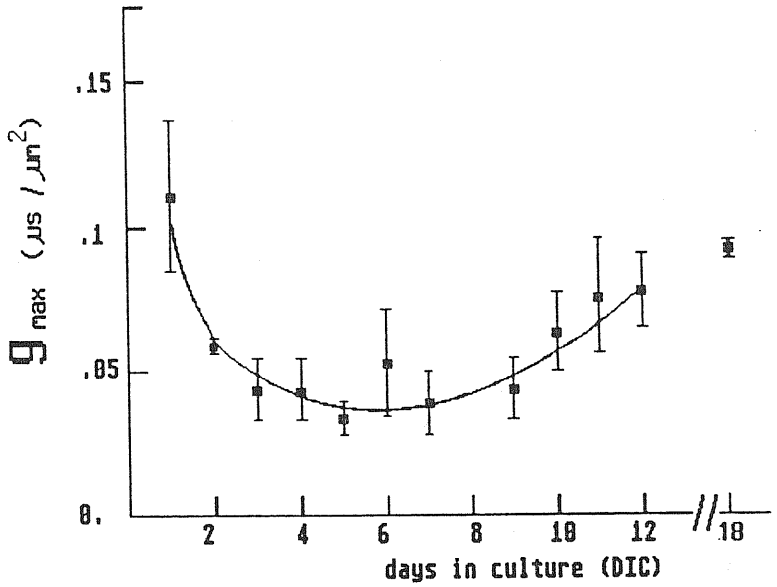

Figure 3.2:
Membrane sodium conductances estimated with different days in culture (DIC). Unexpected high membrane conductance is found in 1 DIC cells. Membrane conductance trends to increase from 2 DIC.

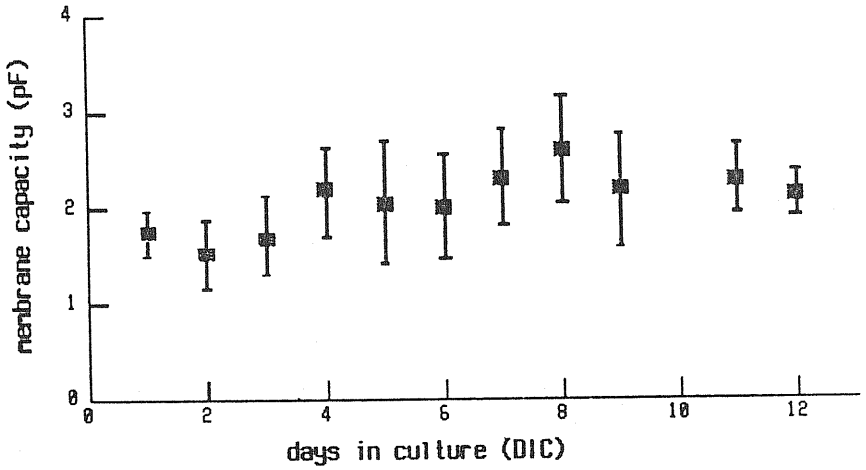

Figure 3.3:
Membrane capacities measured at different days in culture.

significantly (Figure 3.3). The relative homogenous sodium membrane conductances were found between 3 and 7 DIC cells.

As demonstrated above, the most homogenous sodium channel density may be found on the 3 and 7 DIC granule cells. However, in order to diminish the possible space clamp problem caused by the neuritic process, the characterization of sodium channels, as well as the study of intracellular Mg^{2+} effect, will be based on the sodium currents recorded from the cells in the period of 3 to 5 DIC. The membrane capacitance, measured from 63 different 3 to 5 DIC cells, gives a value of 2.2±0.3 pF (mean±SD). This value is consistent with the surface area of the cell body estimated as a sphere of diameter 10 μm. To compare the results obtained from different cells, currents will always be expressed in terms of the current density, i.e. with the correction of membrane area.

3.2 The Characterization of Sodium Channels

Sodium currents have been recorded from different cells by whole–cell configuration of the standard patch–clamp technique (Section 2.2). Figure 3.4A shows a series of sodium current responses, $I(t)$, evoked by the step depolarization to a series of membrane potentials, V, in the range of – 20 to 80 mV. Each trace is the average of 8 original records and has been corrected for the linear leakage and capacitance transients, using the P/4 procedure as described in Section 2.3. The plot of the peak current I_p estimated from the current families shown in figure 3.4A, as a function of the applied voltage V_m, are illustrated in figure 3.4B. I_p was estimated by the method described in Section 2.4.1. The fitting of the linear part of $I_p - V_m$, at the higher membrane potentials illustrates that the sodium reversal potential is 45.7±2.9 mV (n = 9), which is close to the Nernst equilibrium potential for sodium ions ($[Na^+]_o$ = 110 mM, $[Na^+]_i$ = 15 mM). The maximum inward peak current (I_p^{max}) was obtained from a third order polynomial fitting to the inward part of $I_p - V_m$ relationship. The statistical results, obtained from 14 differ-

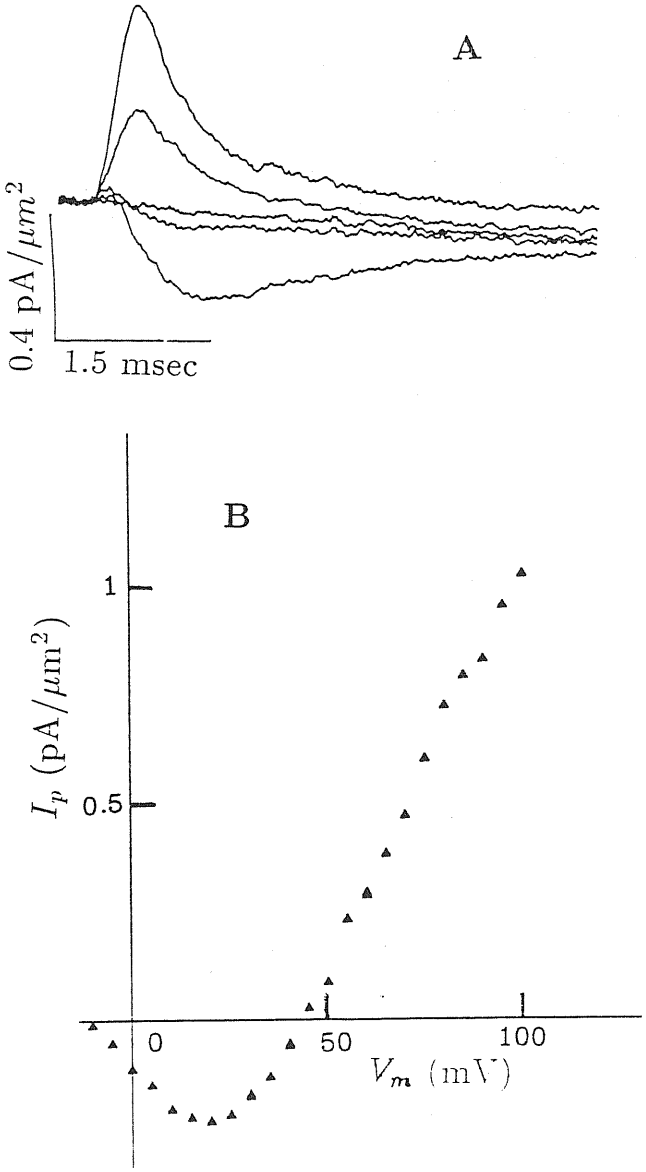

Figure 3.4:

A Sodium currents recorded from the cerebellar granule cell in the whole–cell configuration. The holding potential was –90 mV, and the test pulses were from –10 to +70 mV, in every 20 mV steps. Each trace is an average of 8 records. **B** Peak currents I_p *vs.* membrane potential, V_m relationship. Inward I_p reaches its maximal (0.24 pA/μm^2) around 19 mV and the reversal potential is about 45 mV.

ent patches, gives out that the inward peak current reaches its maximal value 0.21±0.06 pA/μm^2 at membrane potential 16.5±2.8 mV (V_m^p).

$I_p - V_m$ curves were constructed from sodium currents recorded with solutions $110Na/15Na(0)$. There is no significant rectification observed on the outward sodium currents at applied membrane potentials as high as +100 mV. This outward rectification, which has been demonstrated in $I_p - V_m$ relationships obtained in other cell preparations, for example, rat muscle (Pappone 1980), human and rat skeletal muscle (Almers et al. 1984), *Xenopus* oocytes injected with sodium channel mRNA (Stühmer et al. 1987), should be attributed to the presence of magnesium ion in the intracellular solution (Pusch et al. 1989, Pusch 1990a). An outward rectification was indeed observed also in sodium currents on granule cells when currents were recorded in presence of intracellular magnesium ions, which will be detailed in following chapters.

The detail analysis of the voltage–clamp response, recorded from cerebellar granule cells, was made according to the Hodgkin–Huxley model (Hodgkin and Huxley 1952a), with an addition of empirical delay at the onset of the time course of the sodium currents (eq. 2.1), which is significant at low holding potentials (figure 2.6). By fitting the kinetic and steady-state properties of the macroscopic sodium currents with the HH model, it is possible to quantitatively compare the characterization of the sodium channel on the rat cerebellar granule cells with those described in the other preparations. With the analytical method described in Section 2.4.2, the voltage dependence of time constant τ_m and τ_h relations, characterizing the activation and inactivation kinetics respectively, was obtained. Measurements obtained from 9 different cells illustrate the inactivation time constant τ_h in figure 3.5A, and activation time constant τ_m in figure 3.5B. With the holding potential of −90 mV used in our measurements, fitted values of δt ranged typically between 0.2 and 0.5 msec, which began to decrease at pulse potentials higher than −10 mV.

The steady–state activation parameter m_∞ calculated with the relation $m^3 = g/g_{max}$ was plotted as a function of the membrane potential, shown as points in Figure 3.8. The voltage dependent relation,

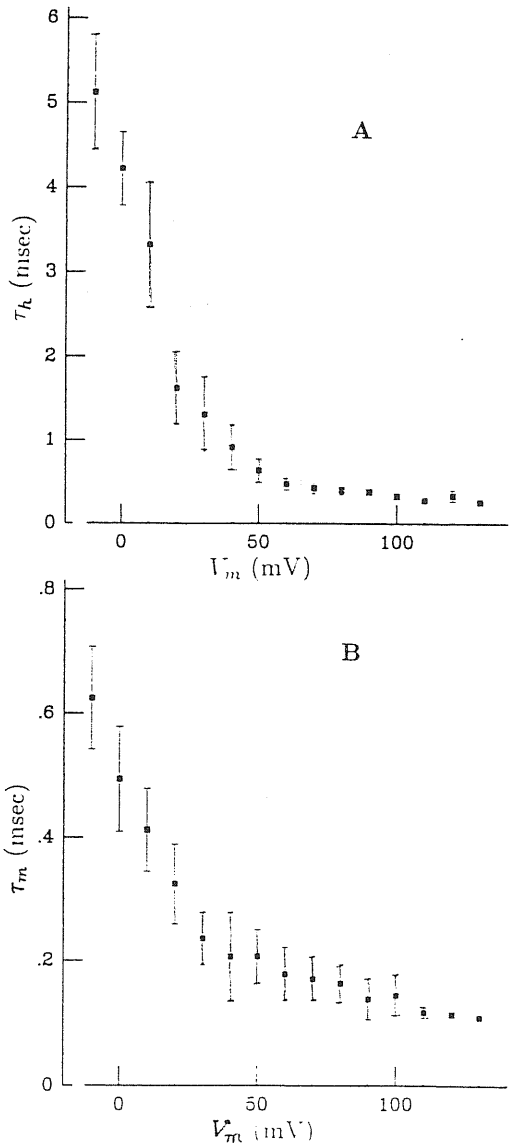

Figure 3.5:

A The voltage dependence of the inactivation time constant τ_h. Data points represent the mean of measurements made from at least 8 different cells and bars represent their standard deviations. τ_h decreases with depolarization to a constant around 0.4 msec. B The voltage dependence of activation time constant τ_m. τ_m decreases with depolarization to a constant around 0.2 msec.

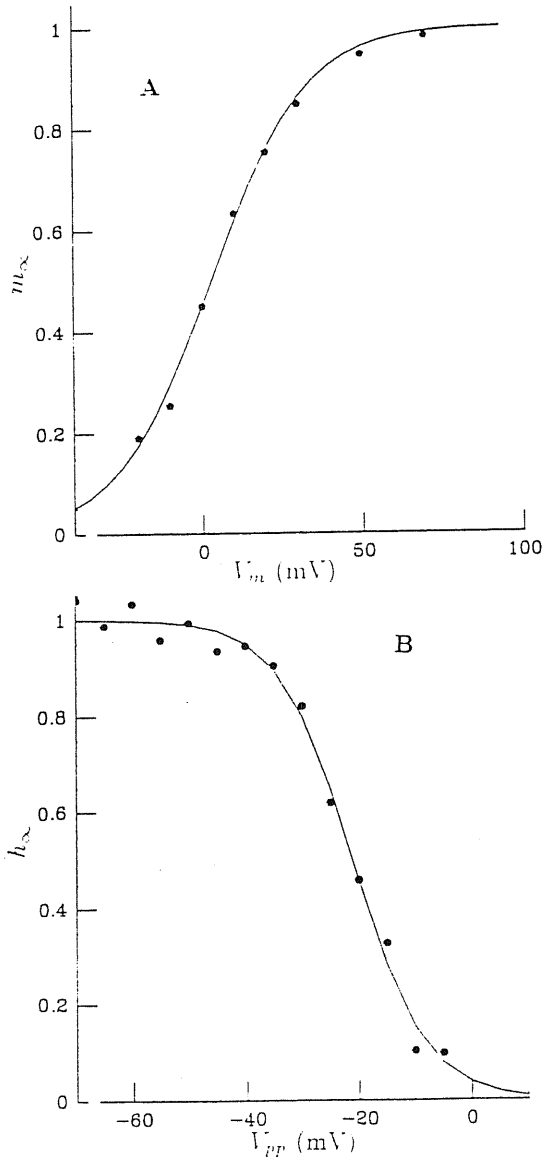

Figure 3.6:

A Steady–state activation parameter m_∞ of sodium currents as a function of test potentials. The smooth line represents the best fit to the data with equation 2.3, with $V_{1/2}^m = 3.0$ mV and $z_m = 1.76$. **B** The voltage dependence of steady–state inactivation parameters h_∞ of sodium currents. Currents were elicited by the double–pulse experiment described in Section 2.3. The normalized peak inward current responses to the test pulse are plotted as a function of prepulse potential. The smooth line is the least-squares fit to data points using equation 2.4, with $V_{1/2}^h = -26.89$ mV and $a_h = 6.73$ mV.

characterized by $V_{1/2}^m$ and the steepness of the potential dependence, was least–square fitted with equation 2.3. The fitting result is shown as the smooth line in figure 3.6A. The values of $V_{1/2}^m$ yielding the best fit in 7 different experiments were 2.8 ± 1.9 mV. The apparent valuence of a single activation process is $z_m = 1.78 \pm 0.16$.

The voltage dependence of the steady–state sodium channel inactivation parameter, h_∞, was determined by applying conditional prepulses of various potentials with 40 msec duration, preceded to a test voltage pulse to –10 mV. Normalized peak currents, plotted against prepulse potentials (V_{pp}) as data points are shown in figure 3.6B. The data were further fitted with equation 2.4 (smooth line). Results obtained from measurements on 6 different cells gave least–square fitting values as $V_{1/2}^h = -25.2 \pm 3.6$ mV, and $a_h = 6.4 \pm 0.8$ mV.

3.3 Comparison of sodium channels from different tissues

Sodium currents on the rat cerebellar granule cells have been recorded from the first days in culture. Although the unexpected large conductance on the first day cultured cells, the maximum membrane sodium conductances tend to increase with days in culture. This increase may correspond to the increase of probability of sodium channels to be activated, or the increase of channel density with days in culture due to the continuouse expression of sodium channels, or both. However, it is difficult to distinguish these two possibilities in the macroscopic current recording. Some noise analysis or single channel recordings, as well as molecular biology studies might be helpful to solve the problem.

Although less directly translatable into molecular mechanisms, the macroscopic analysis provides enough experimental data to fit any reasonable model of the channel gating containing a limited number of parameters. The main purpose of this part of thesis was to characterize the sodium current recorded on the rat cerebellar granule cell, in a more detail way than that was attempted before (Hockberger et al. 1987; Lin

Cells	I_{den} (mA/cm^2)	V_m (mV)	temp.^oC
Squid axon (1)	1.30	−10	5
Bovine chromaffin (2)	0.06	−20	20
Snail neuron (3)	0.5	−6	13.5
mouse neuroblastoma (4)	0.4	−10	20
Guinea pig DRG (5)	2.5	0	20
Rat dorsal root ganglion neuron (DRG) (6)	0.07	−25	20
Chick DRG (7)	0.2	−10	12
Rat granule cell (8)	0.021±0.006	16.5±2.8	18–21

Table 3.1:

The sodium peak current density I_{den} in the excitable cells

(1) Hodgkin and Huxley (1952), (2) Fenwick et al. (1982), (3) Adams et al. (1979), (4) Moolenar and Spector (1978), (5) Kameyama 1983, (6) Kostyuk et al. (1981), (7) Carbone and Lux (1986), (8) this work (mean±S.D, n = 14).

1988).

Considering the maximum inward peak current per unit membrane area as the sodium current density (I_{den}), it is found that the sodium current density on the rat cerebellar granule cell is relative lower than those obtained from the other preparations (table 3.1). This difference may reflect the intrinsical property of different cells: the excitability of the membrane may be different in the different excitable cells, according to their specific functions. However, it can also be explained by the facts that different $[Na^+]_o$ and $[Ca^{2+}]_o$ are used in the different preparations, since both $[Na^+]_o$ and $[Ca^{2+}]_o$ can influence the inward current amplitude via different mechanisms. The former one has been found in part of my experiments, in which sodium currents were recorded with different $[Na^+]_o$. With the presence of only 50 mM Na_o^+, the inward currents are almost unmeasured. Figure 3.7 gives out the $I_p - V_m$ rela-

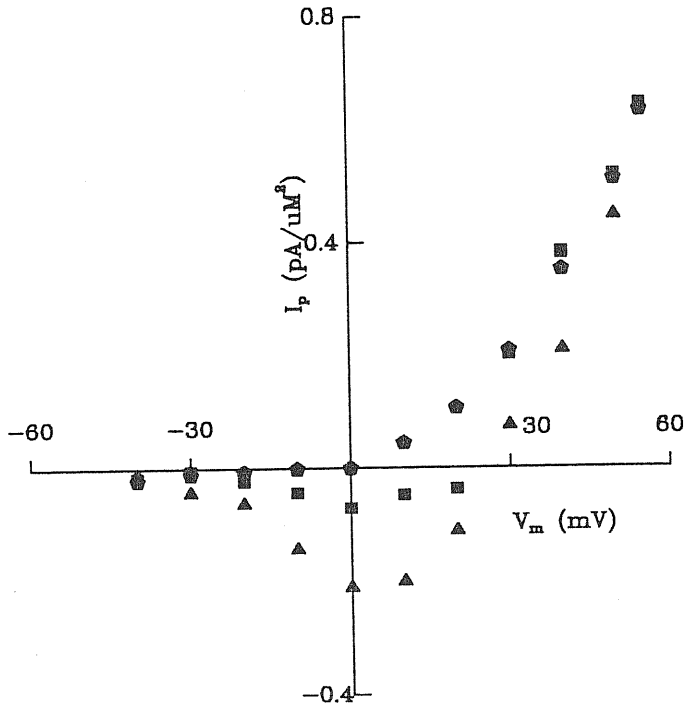

Figure 3.7:
$I_p - V_m$ relationships obtained with the presence of different $[Na^+]_o$. Triangles represent the data obtained with 110 mM Na_o^+, squares obtained with 70 mM Na_o^+ and pentagons obtained with 50 mM Na_o^+.

tionships obtained with the different extracellular Na^+ concentrations. The $[Na^+]_o$ dependence of inward current is clearly shown in this figure. The extracellular Ca^{2+} effect on the inward sodium current has already been studied in the other two preparations (Nilius 1988, Pusch 1990b). The Ca_o^+ blocking effect of the sodium channel is proposed. For example, the increase of $[Ca^{2+}]_o$ from 0.1 to 20 mM leads to the decrease of single–channel conductance of the guinea–pig heart sodium channel from 27 to 14 pS (Nilius 1988). It is also found that 1.8 mM $[Ca^{2+}]_o$ reduces significantly the single–channel amplitudes both wild–type and mutant sodium channel expressed from rat brain sodium channel cDNA (Pusch 1990b).

Time constants of activation and inactivation kinetic processes,

Cells	τ_m (msec)	V_m (mV)	temp.°C
Squid axon (1)	0.51	−40	6
Rat brain Na channel (2)	0.40	−40	20
Rat cerebellar granule cell (3)	0.38±0.05	20	18–21

Table 3.2:

The activate time constant τ_m of the sodium currents in various excitable cells.

(1) Hodgkin and Huxley (1952), (2) Stühmer et al. (1987), (3) the present work (mean±SD, n = 8)

Cells	τ_h (msec)	V_m (mV)	temp.°C
Squid axon (1)	1.50	0	6
Bovine chromaffin (2)	1.2	0	20
mouse neuroblastoma (3)	0.5	−8	20
Rat dorsal root ganglion neuron (DRG) (4)	1.5	0	12
Rat pituitary GH3 (5)	1.1	20	20
Rat cerebellar granule cell (6)	1.18±0.14	20	18–21

Table 3.3:

The inactivation time constants of the sodium currents in different excitable cells.

(1) Hodgkin and Huxley (1952), (2) Fenwick et al. (1982), (3) Moolenar and Spector (1978), (4) Carbone and Lux (1987), (5)Matteson and Armstrong (1984), (6) the present work (mean±SD, n = 8).

Cells	$V^m_{1/2}$ (mV)	z_m
mouse neuroblastoma (1)	−36.9±0.8	1.72±0.22
sodium channels expressed		
from rat brain cDNA (2)	−40.5	2.9
canine ventricular myocytes (3)	−48.6±1.3	
cerebellar granule cell (4)	2.8±1.9	1.78±0.16

Table 3.4:

Parameters of the steady–state activation Na channel gating processes.

(1) Moran and Conti (1990), (2) Stühmer et al. (1987), (3) Berman et al. (1988) (4) this work (mean±SD, n = 7).

however, are comparable with those described in the others cell preparations (table 3.2 and table 3.3). The steady–state activation and inactivation parameters are also compared with those in other preparations (table 3.4 and table 3.5). The half activation and half inactivation potentials of sodium currents in the rat cerebellar granule cells appear to shift to more depolarized membrane potentials, when compared with the other neural preparations. These shifts may correspond to the more negative inner surface potential in the granule cell than in others, since the steepness of the voltage dependence of steady–state activation and inactivation processes behaves the same as those observed in other neurons.

In general, our results confirm the notion that sodium channels on rat cerebellar granule cells behave in a typical manner as those in other neuronal preparations (see the comparison in tables).

Cells	$V_{1/2}^h$	a_h
mouse neuroblastoma (1)	−74.5±3.6	11.1±0.2
neurobalstoma NIE115 (2)	−20.3	8.0
human skeletal muscle (3)	−76.0	5.7
sodium channels expressed		
from rat brain cDNA (4)	−63.9±5.9	10.2±1.2
canine ventricular myocytes(5)	−77.5±3.4	9.37±0.9
human mytoball (6)	−65.9±4.6	5.6±1.0
cerebellar granular cell (7)	−25.2±3.6	6.4±0.8

Table 3.5:

Parameters of the steady–state inactivation Na channel gating processes.

(1) Moran and Conti (1990), (2) Aldrich and Stevens (1983), (3) Almers et al. (1982), (4) Stühmer et al. (1987), (5) Berman et al. 1988, (6) Pröbstle et al. 1988 and (7) this work (mean±SD, n = 6).

Chapter 4

Mg^{2+} blockage of sodium currents

As an important cofactor of many protein kinases, the intracellular Mg^{2+} has been widely studied by the biochemists. Since the middle of 1980's, it has also been found that Mg_i^{2+} may modulate the function of ionic channels, such as the $NMDA$–activated channel, the ATP–sensitive potassium channels etc (see Section 1.3). From the former researchers' studies, it has been found that the half blocking concentrations of Mg^{2+} at the high membrane potentials are all in the range of the physiological intracellular Mg^{2+} concentration (0.4–3.7 mM, Blater and McGuigan 1988, Alvarez–Leefmans et al. 1986). Some ionic channels are very sensitive to the presence of Mg_i^{2+}. For example, the Mg_i^{2+} blocking effect on the inwardly rectifying potassium channels can be detected at $[Mg^{2+}]_i$ as low as 1.7 μM (Matsuda 1988). Therefore, it is possible that the Mg_i^{2+} blockage should also correspond to certain physiological regulation functions of the ionic channels.

The reduction of outward sodium currents in spite of increasing of the driving force has already been observed in several preparations (Pappone 1980, Almers et al. 1984; Stühmer et al. 1987 and Fahlke and Ruppersberg 1988). The reduction on the outward sodium current has been studied in some detail by Pusch and coworkers on rat brain sodium channels expressed in the *Xenopus* oocytes (Pusch et al. 1989,

Pusch 1990a). In these works, it was found that the reduction of the outward sodium currents at the higher membrane potentials is due to the presence of Mg_i^{2+}. No attempt up to now, however, has been done on the sodium channel of neuron cells. Since the sodium channel plays an important role in the generation of the action potential (Section 1.1), it will be interesting to investigate if Mg^{2+} can also lead to the blockage effect in the neuronal sodium channels. On the other hand, the physiological environment of oocytes might be quite different from the native neurons (for example, the degree of phosphorylation of the membrane proteins may be quite different), which may also lead to additional effects on the Mg_i^{2+} blockage. Hence, it is necessary to have the knowledge if such a Mg_i^{2+} effect could also happen in neurons abd how it happens. These knowledges will be helpful to understand its physiological function and its reaction mechanism. Furthermore, in their work about the Mg^{2+} effect on the cloned sodium channels, the mechanism of the Mg^{2+} effect has not studied in detail (Section 1.3). Therefore, it is another object of this thesis to undertake a series of theoretical attempts to explain the possible Mg^{2+} blocking effect in a more molecular terms. The understanding of the Mg^{2+} blockage of sodium currents may also provide a clue to understand the blocking mechanism of other "Mg^{2+}–like" divalent ions, such as Co_i^{2+} effect on ionic channels (Ascher and Nowak 1988).

In this chapter, it will be demonstrated that Mg_i^{2+} does introduce significant blocking effect on the sodium channel in central mammalian neurons. Then, there will be more experiments results shown in order to characterize the Mg^{2+} blocking effect of sodium currents.

4.1 Experimental protocol

All the current records shown here, were recorded with the whole–cell configuration of the standard patch clamp technique, with one–pulse protocols described in Section 2.3.1. The whole–cell currents have been recorded with different experimental solutions by varying the intracel-

lular Mg^{2+} and Na^+ concentrations, as well as the extracellular Na^+ concentrations. The recording solutions used here are described in Section 2.5. In order to compare the results obtained from different cells, all the results shown below have been scaled by the corresponding membrane areas, i.e. the current densities is used (see Section 3.1).

4.2 Mg_i^{2+} blocking effect is an increasing function of $[Mg^{2+}]_i$ and membrane potential

The macroscopic Na^+ current families, evoked by a series of voltage pulses from –40 to 130 mV, were recorded with $[Mg^{2+}]_i$ varying from 0 to 7 mM (figure 4.1). The sodium current behaviour illustrates that the Mg_i^{2+} blocking effect of the sodium currents increases upon increasing the $Mg^{2+}{}_i$ concentration. Relationships of the peak current, I_p and the membrane potential, V_m, obtained with different experimental solutions are constructed according to the method described in the Section 2.4.1. Representative I_p–V_m relationships in the presence of 0, 0.5 and 7 mM Mg_i^{2+} are shown in figure 4.2. From $I_p - V_m$ relationships, it is observed that 7 mM Mg_i^{2+} can also reduce somehow the inward sodium currents, which begins at applied membrane potentials higher than 10 mV. However, Mg_i^{2+} blocking effect becomes more striking at membrane potentials higher than the sodium equilibrium potential. The blockage of outward sodium currents presents also in low $[Mg^{2+}]_i$ (0.5 mM) and clearly increases as $[Mg^{2+}]_i$ increases to 7 mM. From observations described above, it can be concluded that the Mg_i^{2+} blocking effect is voltage–, as well as $[Mg^{2+}]_i$–dependent. The obvious reduction of outward sodium currents at the membrane potentials higher than the sodium equilibrium potential represents the rectification observed by the others (Pappone 1980, Almers et al. 1984, Stühmer et al. 1987 and Fahlke and Ruppersberg 1988). These experimental results are consistent with those observed in the sodium channel expressed in *Xenopus*

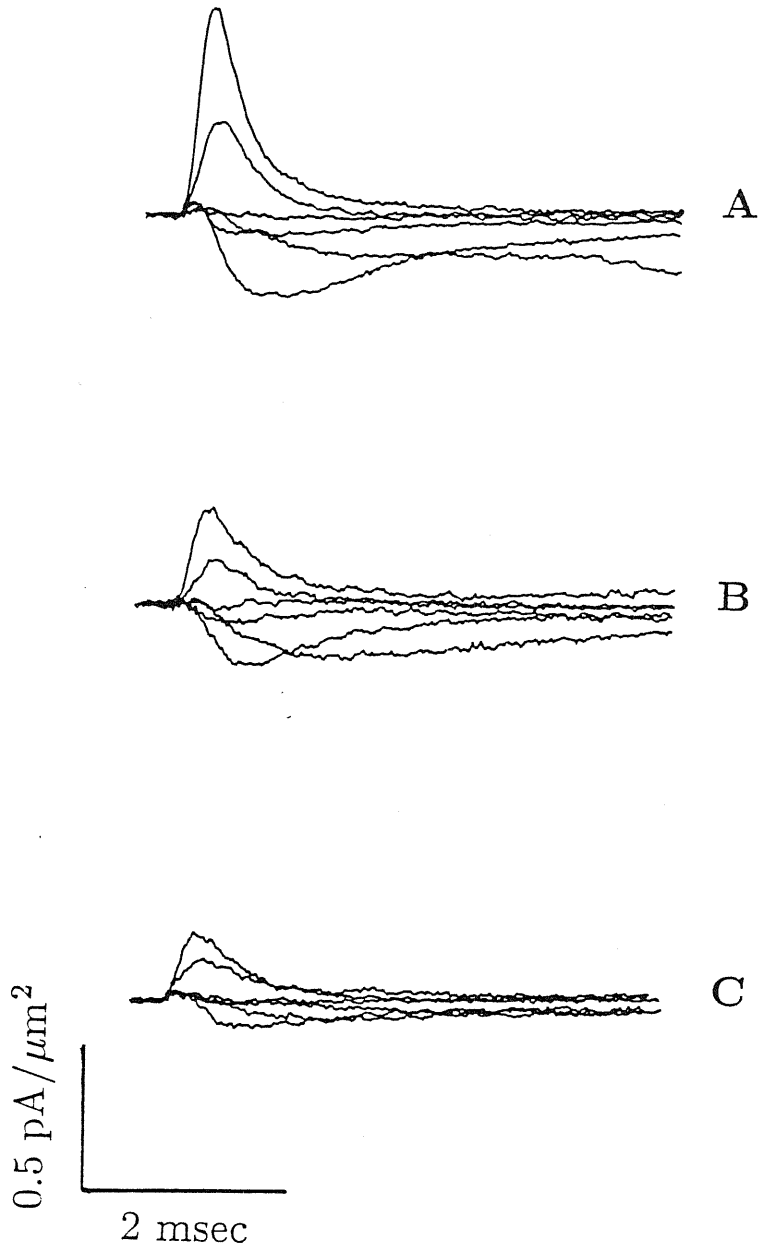

Figure 4.1:

Families of sodium currents elicited from three whole–cell patches. The voltage steps applied compose of a holding potential of –90 mV, –100 mV prepulse with 5 msec duration and the test potentials varying from –20 mV to 80 mV in 20 mV steps. Each trace represents the average of 8 records after the subtraction of linear leakage and capacitive currents. $[Na^+]_i$ = 15 mM, $[Na^+]_o$ = 110 mM. **A** was obtained with 0 mM $[Mg^{2+}]_i$, **B** with 0.5 mM $[Mg^{2+}]_i$ and **C** with 7 mM $[Mg^{2+}]_i$. All the current traces have been corrected by membrane areas.

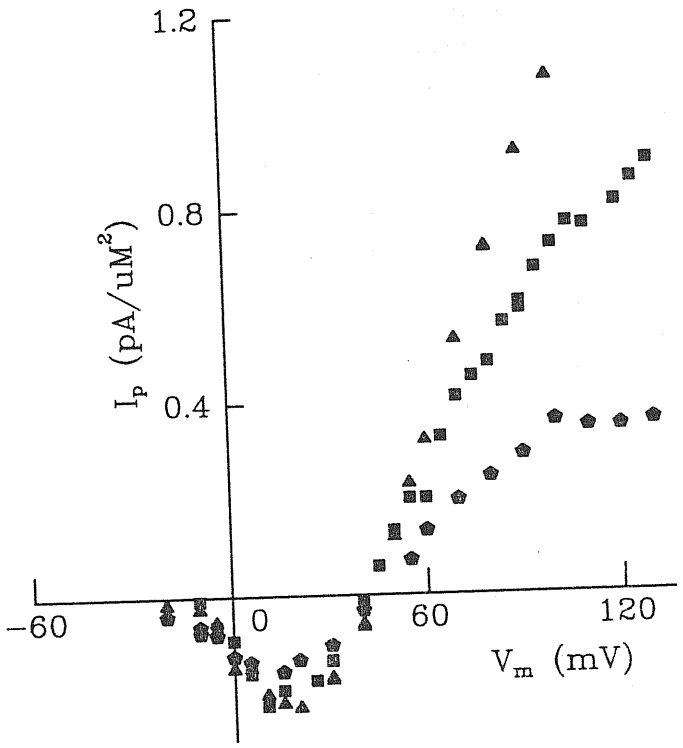

Figure 4.2:

Peak current (I_p)–voltage (V_m) relationships, obtained with $[Na^+]_i$ = 15 mM and $[Na^+]_o$ = 110 mM. Triangles represent data obtained in the absence of Mg_i^{2+}, Squares represent data obtained with 0.5 mM Mg^{2+} and pentagons represent those in the presence of 7 mM Mg_i^{2+}. The decrease of inward peak current at $V_m \geq 10$ mV is also observed in the presence of 7 mM Mg_i^{2+}. However, the blockage of outward current becomes more significant and presents in both $[Mg^{2+}]_i$. Results are obtained from 3 different patches. Peak currents have been scaled by membrane ares.

$[Mg^{2+}]_i$	I_n ($[Na^+]_i$ = 15 mM)	I_n ($[Na^+]_i$ = 30 mM)
0.0	1.00±0.08 (n = 20)	1.00±0.07 (n = 26)
0.5	0.67±0.07 (n = 9)	0.84±0.08 (n = 4)
3.0	0.51±0.09 (n = 9)	0.64±0.04 (n = 3)
7.0	0.35±0.07 (n = 6)	0.47±0.04 (n = 6)

Table 4.1:
Normalized mean peak currents (I_n) obtained at the applied potential of 100 mV, and different $[Na^+]_i$ and $[Mg^{2+}]_i$. Values represent mean ± SD. $[Na^+]_o$ is fixed at 110 mM.

oocytes (Pusch et al. 1989, Pusch 1990a).

4.3 Mg_i^{2+} blocking effect is dependent on $[Na^+]_i$ and $[Na^+]_o$

In order to estimate the interference between Na^+ and Mg^{2+}, further sodium current records have been obtained by varying $[Na^+]_i$, $[Na^+]_o$, in addition of varying the intracellular Mg_i^{2+} concentrations (see Section 2.5).

The voltage–dependent Mg_i^{2+} blocking effect of sodium currents is still clearly observed when $[Na^+]_i$ is raised to 30 mM (shown in figure 4.3). The Mg^{2+} blocking effect of sodium currents, especially on the inward current parts, diminishes upon this increasing of $[Na^+]_i$. Since the outward sodium current is an increasing function of intracellular Na^+ concentration (Hille 1984, Nilius 1988), the Mg^{2+} blocking effect of sodium currents recorded from different $[Na^+]_i$ solutions are evaluated by comparing the normalized peak currents I_n (i.e. $I_n = I_p([Mg^{2+}])/I_p(0)$). In table 4.1, normalized peak currents I_n at 100 mV, obtained in the presence of 15 mM and 30 mM Na_i^+, are compared. It is clear that the Mg_i^{2+} blocking effect increases as the intracellular Mg^{2+} concentrations increases, but decreases as the intracellular Na^+ concen-

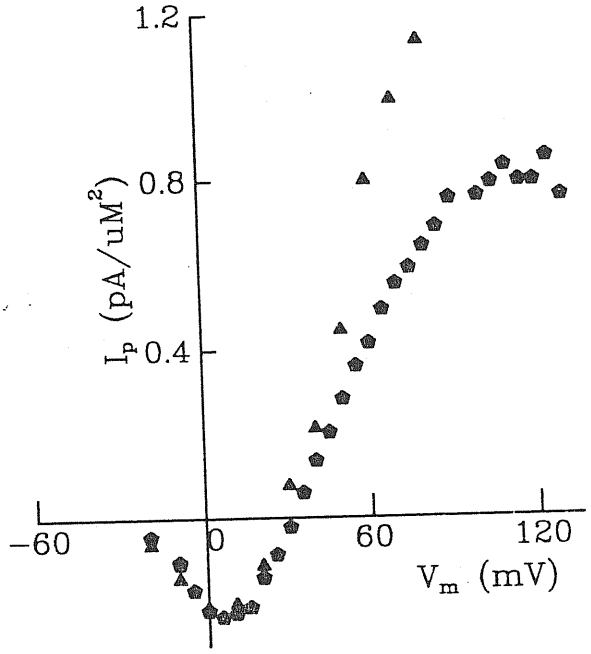

Figure 4.3:
Peak current (I_p)–voltage (V_m) relationships, obtained with 30 mM intracellular Na_i^+ and 110 mM Na_o^+. Triangles present I_p obtained at $[Mg^{2+}]_i = 0$ mM and pentagons at $[Mg^{2+}]_i = 7$ mM. All peak currents have been corrected by membrane areas.

$[Mg^{2+}]_i$	I_n ($[Na^+]_o$ = 50 mM)	I_n ($[Na^+]_o$ = 70 mM)	I_n ($[Na^+]_o$ = 110 mM)
0.0	1.00±0.13 (n = 10)	1.00±0.07 (n = 16)	1.00±0.07 (n = 26)
1.0	0.70±0.10 (n = 8)	0.73±0.05 (n = 10)	0.78±0.09 (n = 4)
3.0	0.56±0.07 (n = 8)	0.60±0.06 (n = 10)	0.64±0.04 (n = 3)
7.0	0.43±0.10 (n = 7)	0.45±0.10 (n = 9)	0.47±0.04 (n = 6)

Table 4.2:
Normalized mean peak currents (I_n) obtained at the applied potential of 100 mV, and different $[Na^+]_o$ and $[Mg^{2+}]_i$. Values represent mean±SD. $[Na^+]_i$ is fixed at 30 mM.

tration increases. The overall comparison of Na_i^{2+} influence on the Mg_i^{2+} effect is shown in figure 4.4. In this figure, the normalized peak currents are compared at all the membrane potentials. The decreasing Mg_i^{2+} blocking effect with the increasing of $[Na^+]_i$ is clear.

The interaction between Na_o^+ and Mg^{2+} has also been tested by recording sodium currents with different extracellular Na^+ concentrations, varying from 50, 70 to 110 mM. In these experiments, the intracellular solutions were fixed as 30Na(0–7). Although the relevance between Mg_i^{2+} and Na_o^+ does not appear as significant as that between Mg_i^{2+} and Na_i^+, the Mg_i^{2+} blocking effect of outward sodium currents increases slightly as $[Na^+]_o$ decreases (table 4.2).

4.4 Discussion

Mg^{2+}, recognized as a cofactor and regulator in the function of certain enzymes, has also been found to be a factor which can modulate many types of channel proteins (see Section 1.3). As early as in the beginning of 1980's, it has been observed that there is a reduction of sodium membrane conductance at the higher membrane potentials ("rectification effect") (Pappone 1980; Almers et al. 1984; Stühmer et al. 1987). Fahlke and Ruppersberg (1988) have studied in detail the decrease of

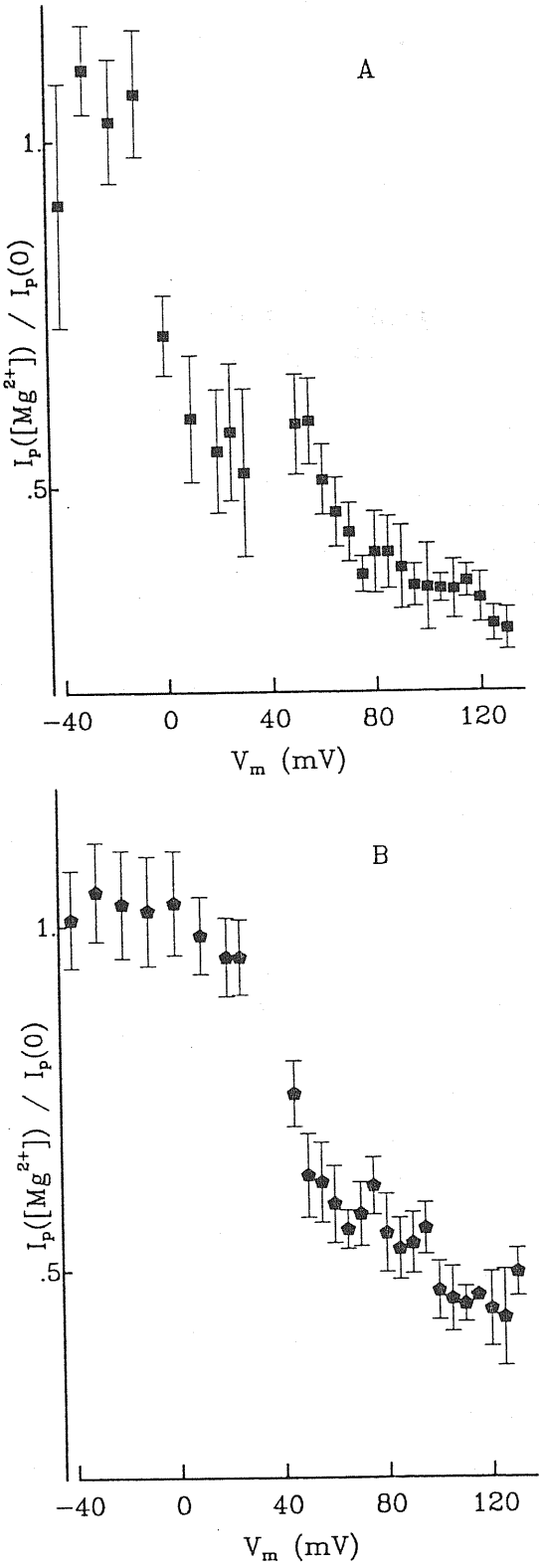

Figure 4.4:

Normalized sodium peak currents I_n evaluated at different membrane potentials V_m. I_n was obtained by dividing the mean of peak currents obtained with 7 mM Mg^{2+} with those obtained in the absence of Mg^{2+}. A is obtained with 15 mM Na_i^+, 110 mM Na_o^+. B is obtained with 30 mM Na_i^+, 110 mM Na_o^+.

sodium outward currents in the human skeletal muscle. They observed that the outward sodium currents decrease despite the larger driving force for Na^+. They attributed their results to a conformational change of the sodium channel at the high voltages. Their intracellular solution, however, contained 1.5 mM Mg^{2+}. This makes it likely that the decrease of the currents, they observed, is due to the voltage–dependent Mg_i^{2+}. blockage.

the intracellular Mg^{2+} blocking on the outward Na^+ currents have been found in cloned sodium channels and endogenous sodium channels in chromaffin cells (Pusch et al. 1989 and Pusch 1990a). It is also found in our studies that Mg_i^{2+} can lead to the reduction of sodium channel membrane conductance on the rat cerebellar granule cell. Macroscopic sodium currents have been recorded with the different experimental solutions by the whole–cell patch clamp configuration. The Mg_i^{2+} blockage of the sodium current was found to be voltage dependent, that is, the stronger blockage was found at the higher membrane potential. The reduction of the outward sodium currents has been observed in the presence of low intracellular Mg^{2+} concentration as 0.5 mM. The blockage increases as Mg_i^{2+} concentration increases. This finding is consistent with those described by Pusch et al. (1989) and Pusch (1990a).

The interactions between Mg_i^{2+} and Na_i^+, Na_o^+ have also been studied in this thesis. It is found that Mg^{2+} blocking effect is slightly influenced by the extracellular Na^+ concentration, but is strongly influenced by the concentration of Na_i^+. The blocking effect increases as $[Na^+]_i$ decreases. However, this $[Na^+]_i$–dependence contrasts with that observed by Pusch (1990a). To understand this contrary, two significant differences existing in both experimental solutions should be considered. First one is that Na_i^+ was replaced by K_i^+ in order to decrease $[Na^+]_i$ in Pusch's intracellular solutions, while Cs^+ was used to replace $[Na^+]_i$ in my case. It cannot easily be gotten rid that there is certain interactions between K^+ and Na^+, or K^+ and Mg^{2+}. Also we have to consider that the permeability of alkali cations through the sodium channel follows the sequence of $Li^+ \simeq Na^+ > K^+ > Rb^+ > Cs^+$ (Chandler and Meves 1965). The second difference, which may be more serious one, is that

the varying range of sodium concentrations used is quite different. This difference is important, specially considering that Danko et al. (1986) reported that the blocking effect of divalent guanidinium analogues of the sodium channels in squid axon bears the similar $[Na^+]_i$ dependence to that observed by Pusch (1990a). In the experiments described in theis thesis, the concentrations of Na_i^+ were varied from 15, 20 to 30 mM. In Pusch's experiments, however, $[Na^+]_i$ was changed from 30 to 125 mM. In Danko and coworker's work, $[Na^+]_i$ was changed from 50 to 200 mM. The big difference of $[Na^+]_i$ may trigger certain different intrinsic mechanism of sodium channels. For example, the sodium channels may behave as an one–ion pore, i.e. one ion hold by sodium channels at a time at the physiological $[Na^+]_i$, but behave as a multi–ion pore at the unusual high $[Na^+]_i$. The presence of multi ions inside the sodium channel may bring about some specific effects. This change is possible, since there is already some arguments that there are more than one binding sites inside the sodium channel (Hille 1975, Begenisich and Cahalan 1980a, b). To confirm this possibility, it is useful to make some experiments in which $[Na^+]_i$ should be changed gradually. If the second hypothesis proposed above is correct, a turning point of $[Na^+]_i$–dependence of Mg_i^{2+} blockage is expected.

As a simply summary, the intracellular Mg^{2+} blocking effect of the sodium current observed in granule cells is dependent on the membrane potential, $[Mg^{2+}]_i$, as well as Na^+ concentrations from both sides.

Chapter 5

The influence of Mg_i^{2+} on the sodium channel gating

From the previous pharmacological studies, the drug effects of ionic channels on excitable cells can be classified as the channel blocking and the gating modification (Hille 1984). One of the most well known sodium channel blockers is tetrodotoxin (TTX), which blocks sodium channels in nanomolar concentrations. TTX blocks the sodium channels by competing with Na^+ for a common site on channels and binding the site with a high affinity (see Section 1.2.2). The gating process modification of the sodium channels by drugs mainly includes (1) The prevention of inactivation. Some of this kind of modifications involve irreversible cleavage of covalent bonds. Many of the cleavages slow the rate of inactivation. For example, the internal perfusion with pronase, which is a mixture of proteolytic enzymes-endopeptidases, can destroy the inactivation, but leave the activation process and the peak current amplitude untouch (Bezanilla and Armstrong 1977). The single–channel conductance measured by fluctuations is also not changed (Conti et al. 1976b). (2) The promotion of activation at rest, e.g the external applied aconitine leads to –50 mV shift of activation process (Mozhayeva et al. 1977). Several kinds of drug receptors of the sodium channels have been illustrated in figure 1.9B. and (3) Shifts of the voltage dependence of all gating processes. This modification is mainly due to specific ionic conditions of

the recording solutions, such as the existance of the external divalent ions (Hille 1968) or the unusual pH values (Woodhull 1973).

Coming back to our case, it has been illustrated in the last chapter that Mg_i^{2+} can influence sodium currents in a voltage dependent way. That is, the outward sodium currents reduce even with the increase of the driving force in the presence of Mg_i^{2+}. The inward sodium current, on the other hand, is less effected by the presence of Mg_i^{2+}. In order to investigate whether the reduction of maximum sodium membrane conductance is due to the Mg_i^{2+} modification of the voltage dependent sodium channel gating mechanism, the gating parameters of sodium currents in the presence of different $[Mg^{2+}]_i$ were analysed. The experimental solutions used in the experiments, described in this chapter, are shown in Section 2.5.

5.1 Sodium channel activation is shift by 30 mM $[Mg^{2+}]_i$

The macroscopic sodium currents were recorded in the presence of different $[Mg^{2+}]_i$. Figure 5.1 shows the families of sodium currents obtained with 0, 7 and 30 mM $[Mg^{2+}]_i$ ($[Na^+]_i$ = 30 mM, $[Na^+]_o$ = 110 mM). It is observed that Mg_i^{2+} blocking effect increases as $[Mg^{2+}]_i$ increases, which is the same as that described in the last chapter. In the presence of 30 mM Mg_i^{2+}, the outward sodium currents are strongly blocked. It is noteworthy however that the inward sodium currents appear at the lower potentials than those obtained with the control patch or with 7 mM Mg_i^{2+} in the patch.

The $I_p - V_m$ relationships of sodium currents shown in figure 5.1 are established in figure 5.2. $I_p - V_m$ relationships of sodium currents constructed in the presence of 0 and 7 mM $[Mg^{2+}]_i$ are compared in figure 5.2A. The reduction on the outward peak currents is clearly shown, while the Mg_i^{2+} effect on inward peak currents is not observable. Figure 5.2B illustrates the difference of $I_p - V_m$ relationships obtained in the presence of 0 and 30 mM $[Mg^{2+}]_i$. Three features can be observed from

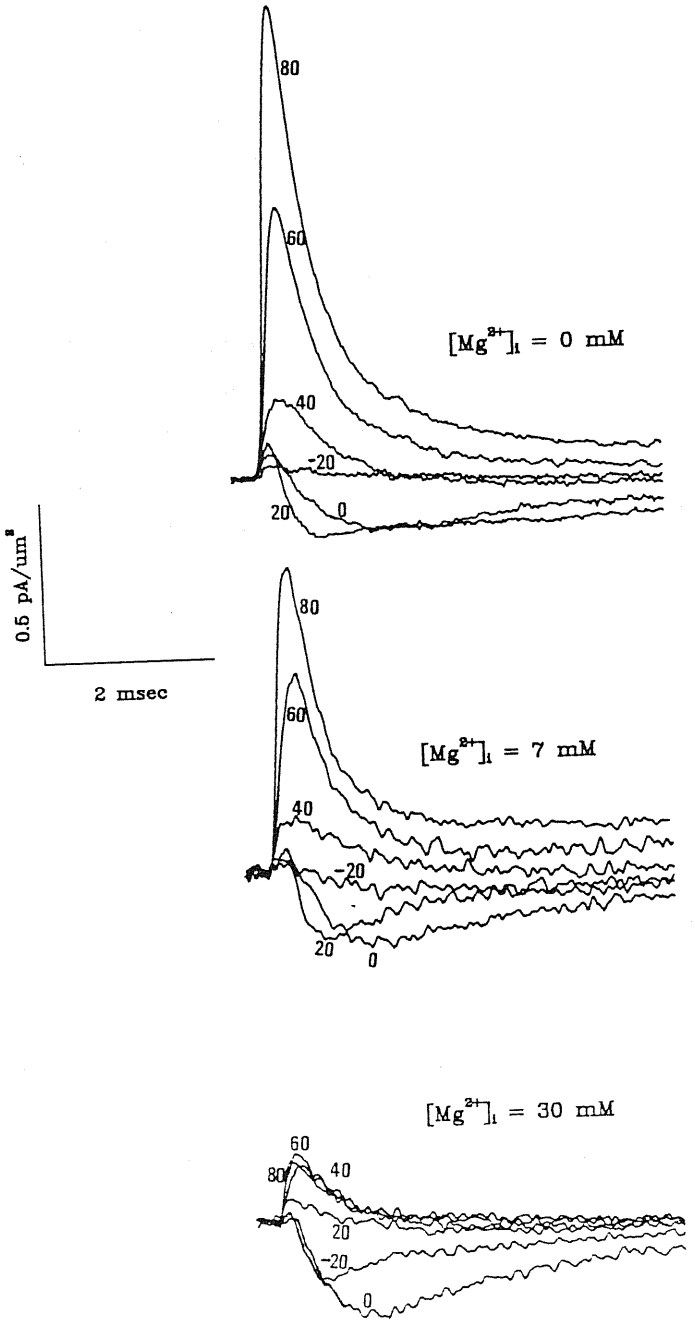

Figure 5.1:

Families of sodium currents elicited from three patches by voltage steps from a holding potential of –90 mV and 5 msec –100 mV prepulse to test potentials from –20 mV to 80 mV in 20 mV steps, at different Mg_i^{2+} concentrations, indicated above the current traces. All currents have been corrected by membrane areas. $[Na^+]_i = 30$ mM and $[Na^+]_o = 110$ mM.

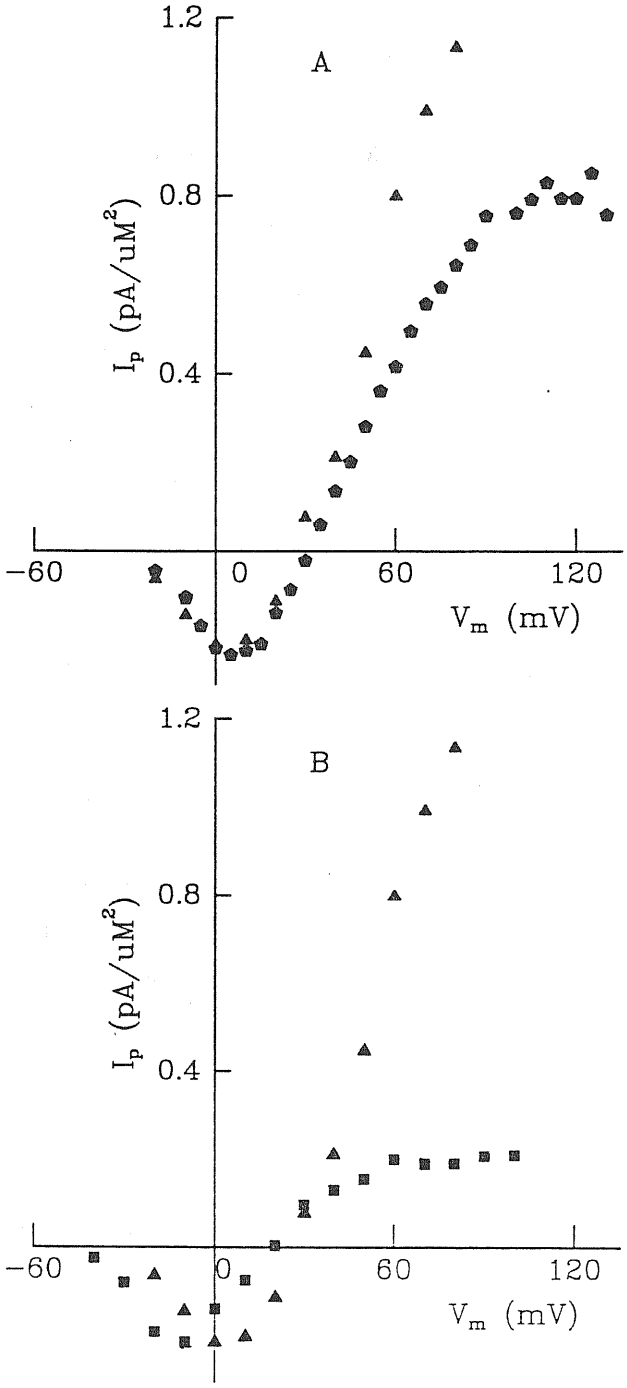

Figure 5.2:

$I_p - V_m$ relationships obtained at $[Mg^{2+}]_i = 0, 7$ mM (A) and $[Mg^{2+}]_i = 0, 30$ mM (B). Triangles present control I_p obtained in absence of $[Mg^{2+}]_i$, squares and pentagons are those obtained in the presence of $[Mg^{2+}]_i$. $[Na^+]_i = 30$ mM and $[Na^+]_o = 110$ mM.

these two figures: (1) The reduction of the outward sodium currents measured in the presence of 30 mM Mg_i^{2+} appears at lower potentials comparing with the potential at 0 and 7 mM Mg^{2+}, i.e. the voltage dependence of Mg_i^{2+} blockage shifts to lower potential. (2) The inward sodium currents appear at lower membrane potentials than those recorded in 0 or 7 mM Mg_i^{2+}. These two observations suggest a negative shift of the activation process of the sodium channels. The maximum inward peak current, I_p^{max}, is similar to that in the absence of Mg_i^{2+}. The value of I_p^{max} from 13 different 30 mM Mg_i^{2+} patches was estimated to be 0.22 ± 0.07 pA/μm^2, which is not statistically different from the value of 0.23 ± 0.07 pA/μm^2 measured from 10 control patches. However, the potential at which the inward peak currents reach their maximum, V_p^{max}, is estimated to be -15.5 ± 2.5 mV. This is lower than the V_p^{max} estimated in the absence of Mg_i^{2+}, which is 8.0 ± 1.9 mV. (3) The sodium reversal potential V_{rev} decreases in the presence of 30 mM Mg^{2+}. In the absence of Mg_i^{2+}, V_{rev} is estimated to be 30.3 ± 2.7 mV (n = 10) and V_{rev} is shifted to 18.4 ± 3.0 mV (n = 14) with $[Mg^{2+}]_i = 30$ mM. This reversal potential shift is most probably due to the Mg^{2+} permeability change of the sodium channel.

The negative potential shift of the activation of sodium currents observed in the presence of 30 mM Mg_i^{2+} suggests that Mg_i^{2+} may influence the voltage dependent gating process of the sodium channel. Therefore, it is necessary to further investigate if Mg^{2+} blockage which is clearly visible at $[Mg^{2+}]_i \leq 7$ mM is also due to its influence on the gating process.

5.2 Approximate methods to estimate Mg_i^{2+} effect on the sodium channel gating processes

An approximate approach to study the sodium channel gating process consists of the comparison of the voltage dependent properties of the

$[Mg^{2+}]_i$ (mM)	10 mV	80 mV	100 mV	N
0.0	1.57±0.17	0.47±0.04	0.47±0.04	15
0.5	1.29±0.19	0.48±0.03	0.45±0.03	4
1.0	1.44±0.41	0.44±0.02	0.42±0.03	5
3.0	1.22±0.19	0.45±0.04	0.40±0.04	9
7.0	1.33±0.20	0.47±0.02	0.44±0.02	5

Table 5.1:
The time to peak (T_p, msec), evaluated at different applied membrane potentials. Values are mean ± SD. Experimental $[Na^+]$ conditions are: $[Na^+]_i = 15$ mM, $[Na^+]_o = 110$ mM.

peak currents in the presence of different $[Mg^{2+}]_i$. Since I_p depends on the kinetics of the activation of the sodium channel, the time to peak, t_p, can be estimated as an approximate value of the activation time constant, τ_m. The invariance of t_p measured at the different applied potentials in the presence of $[Mg^{2+}]_i \leq 7$ mM is presented in table 5.1.

The activation curves were constructed from I_p obtained at different concentrations of Mg_i^{2+} according to the method described by Pröbstle et al. (1988). With this method, the peak currents were further expressed as:

$$I_p = \frac{g_{max}(V_m - V_{rev})}{1 - \exp\left(\frac{V_m - V_h}{a}\right)} \tag{5.1}$$

where V_h is the half activation potential, a is the e–fold voltage dependence of I_p activation. This "I_p–activation" curve can be used as another approximate method to investigate the steady–state activation of sodium channels. However, there is no significant changes of V_h and a found in sodium currents obtained with the experimental soltuions $110Na/15Na(0-7)$ (see table 5.2).

$[Mg^{2+}]_i$ (mM)	V_h (mV)	a (mV)	N
0.0	10.8±2.1	9.9±0.9	13
0.5	10.5±2.1	10.1±1.3	6
1.0	9.2±1.0	9.4±1.2	6
3.0	11.8±1.9	10.1±1.0	5
7.0	10.4±3.0	9.6±1.2	11

Table 5.2:
Half activation potential (V_h) and e–fold voltage dependence of activation (a). Data were obtained from fitting the peak current, estimated at each potential, with equation 5.1. Values are mean±SD. ($[Na^+]_i$ = 15 mM, $[Na^+]_o$ = 110 mM)

5.3 The voltage–dependent gating parameters of sodium channels

A further and more precise analysis of the gating mechanism of the sodium channels in the presence of different Mg_i^{2+} concentrations was performed, using the HH model, as described by Moran and Conti (1990) and in Chapter 3. In this case, the sodium currents measured in the presence of $[Mg^{2+}]_i$ varying from 0 to 30 mM were analysed ($110Na/30Na(0-7,30)$). Experimental protocols compose of one–pulse and double–pulse experiments as described in Section 2.3. The procedure of data analysis has been explained in Section 2.4.

Total sodium current traces elicited by the different membrane potentials were fitted with equation 2.1, which describes the sodium current in terms of a rapid activation process that opens channels during a depolarization and a slower independent inactivation process that closes them during a maintained depolarization. This fitting gives out directly the voltage dependence of the activation and inactivation kinetics constants: τ_m and τ_h. τ_m and τ_h in the presence of different $[Mg^{2+}]_i$,

$[Mg^{2+}]_i$ (mM)	−10 mV	10 mV	60 mV	n
0.0	5.67±0.14	1.93±0.60	0.46±0.06	5
7.0	4.82±0.92	2.12±0.58	0.43±0.06	7
30.0	2.54±0.71	0.98±0.20	0.40±0.04	11

Table 5.3:

The inactivation time constant (τ_h, msec)

Data was estimated at different membrane potentials and with 0, 7 and 30 mM Mg_i^{2+}. Values presented are mean±SD ($[Na^+]_i$ = 15 mM, $[Na^+]_o$ = 30 mM).

$[Mg^{2+}]_i$ (mV)	−10 mV	10 mV	50 mV	n
0.0	0.62±0.14	0.44±0.11	0.20±0.02	5
7.0	0.62±0.08	0.44±0.09	0.27±0.04	7
30.0	0.44±0.03	0.30±0.07	0.19±0.02	11

Table 5.4:

The activation time constant (τ_m, msec)

Data was estimated at different membrane potentials and with 0, 7 and 30 mM Mg_i^{2+}. Values presented are mean±SD ($[Na^+]_i$ = 15 mM, $[Na^+]_o$ = 30 mM).

varying from 0, 1, 3, 7 to 30 mM, have been estimated. The mean values of τ_h and τ_m obtained in different solutions have been compared in table 5.3 and table 5.4. It was found that there is no significant difference in both τ_h and τ_m at $[Mg^{2+}]_i \leq 7$ mM. However, the voltage dependent relations of τ_m and τ_h do significantly shift to the negative potential about −25 mV when $[Mg^{2+}]_i$ is changed from 0 to 30 mM (see table 5.3, and table 5.4, figure 5.3). δt, an empircal time delay at the onset of the sodium current (eq. 2.1), has also be estimated in the different experi-

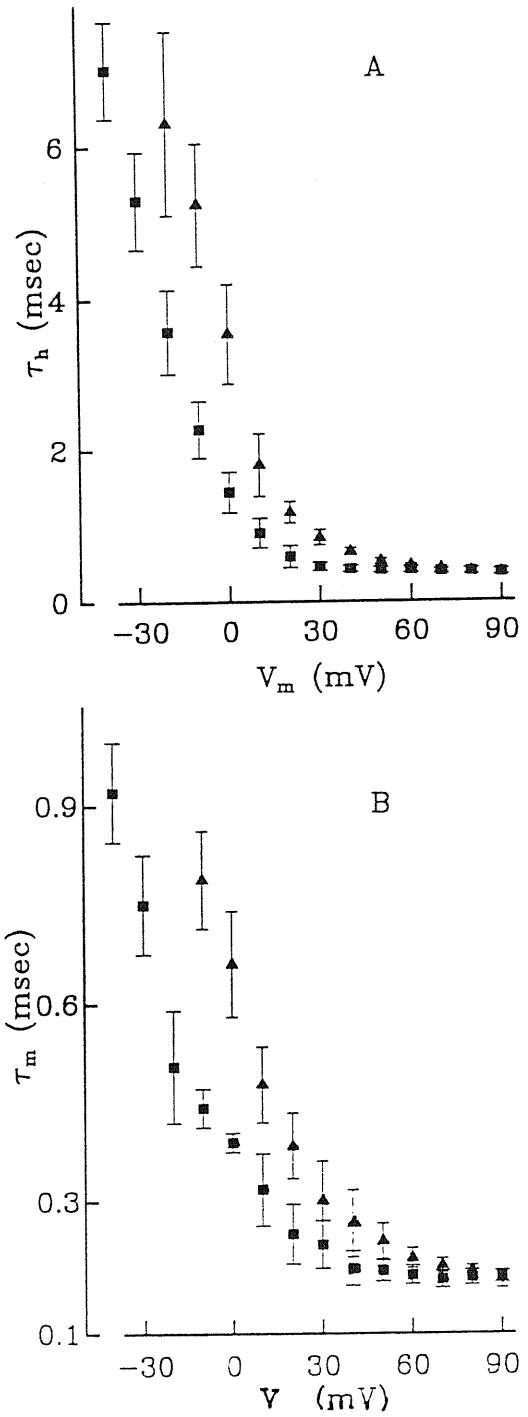

Figure 5.3:

The voltage dependent inactivation (**A**) and activation (**B**) time constants. Triangles are values measured in the absence of Mg_i^{2+}, squares are those with $[Mg^{2+}]_i$ = 30 mM ($[Na^+]_i$ = 30 mM, $[Na^+]_o$ = 110 mM). Each data point represents the mean of measurements with the number indicated in tables 5.3 and 5.4. Bars represent their standard deviations. Voltage shifts in both cases are about −25 mV, when $[Mg^{2+}]_i$ is increased from 0 to 30 mM. Time constants measured in the presence of 7 mM Mg_i^{2+} (not shown) overlay quite well with those obtained at 0 mM Mg_i^{2+}.

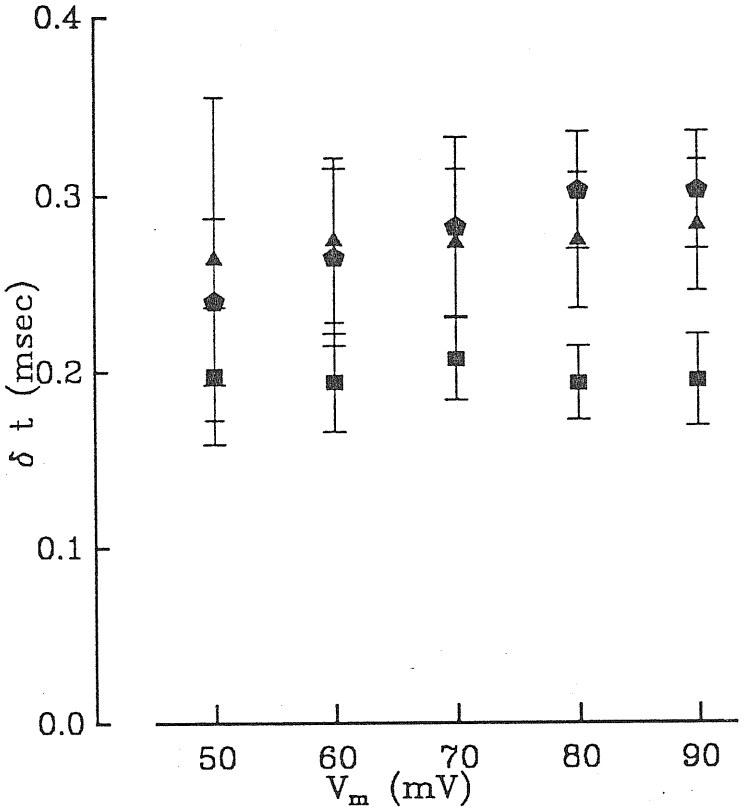

Figure 5.4:

δt measured in the presence of 0, 7 and 30 mM Mg^{2+}. There is no significant difference on δt at lower potential or in the presence of 0 and 7 mM Mg^{2+}. Squares represent δt measured in the presence of 30 Mg_i^{2+}, pentagons are those with $[Mg_i^{2+} = 7$ mM and triangles are those with $[Mg^{2+}]_i = 0$ mM. In all cases, $[Na^+]_i = 30$ mM, $[Na^+]_o = 110$ mM.

mental solutions. There is no significant difference found in the values of δt measured at $[Mg^{2+}]_i \leq 7$ mM, but it appears to decrease at higher membrane potentials in the presence of 30 mM Mg^{2+} (figure 5.4).

The voltage dependence of the steady–state activation parameter m_∞, has been further calculated with the relation: $m_\infty^3 = g/g_{max}$. The half–activation potential, $V_{1/2}^m$, at which the open–state probability for each activation gate is 0.5, and the apparent valence, z_m, of a single activation process (m–gate) obtained from different $[Mg^{2+}]_i$ conditions are compared in table 5.5. These parameters were obtained by fitting equation 2.3 to the experimental data.

The voltage dependence of the steady–state inactivation parameter, h_∞, was obtained by fitting the normalized peak currents obtained from

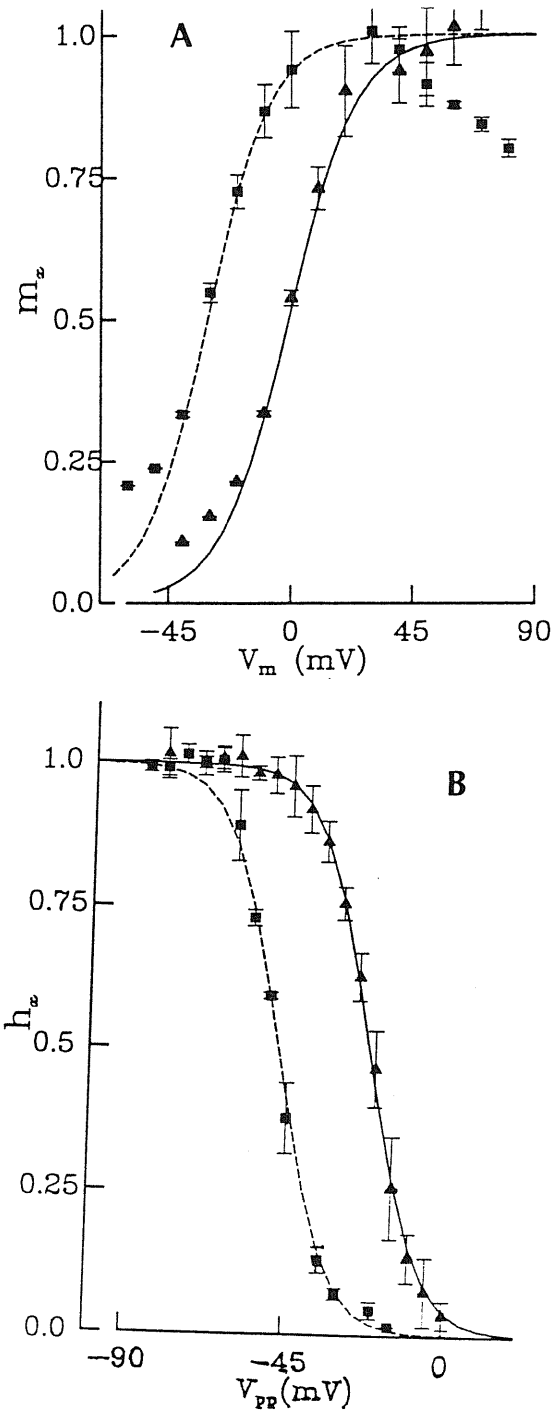

Figure 5.5:

The voltage dependence of steady–state activation (**A**) and inactivation (**B**) gating parameters in the presence of 0 (triangles) and 30 mM (squares) Mg_i^+ ($[Na^+]_i$ = 30 mM, $[Na^+]_o$ = 110 mM). All the data represent mean values, with the number of experiments indicated in table 5.5. Bars are their standard deviation. **A** Smooth lines were obtained by fitting data with equation 2.3. $V^m_{1/2}$ shift is −29.1±0.4 mV. **B** The steady–state inactivation parameter h_∞ as function of prepulse potential. Smooth lines represent the fitting results to equation 2.4. $V^h_{1/2}$ shift is −25.7±7.8 mV.

$[Mg^{2+}]_i$ (mM)	$V^m_{1/2}$ (mV)	z_m	N	$V^h_{1/2}$ (mV)	a_h (mV)	N
0.0	−1.8±0.1	2.1±0.2	7	−21.8±3.9	−6.9±0.6	5
0.5				−19.2	−6.1	1
1.0	−6.5±4.3	2.0±0.4	3	−26.9	−6.7	1
3.0	−1.4	1.9	1			
7.0	−4.3±3.1	2.0±0.2	5	−26.6±4.5	−6.8±2.2	2
30.0	−30.9±0.1	2.2±0.2	6	−47.5±3.9	−6.9±0.3	4

Table 5.5:
Activation ($V^m_{1/2}$, z_m) and inactivation ($V^h_{1/2}$, a_h) parameters, which characterize the voltage dependence of steady state activation and inactivation parameters of the Hodgkin–Huxley model. ($[Na^+]_i$ = 30 mM $[Na^+]_o$ = 110 mM)

the traditional double–pulse experiments against the prepulse potential with equation 2.4. Analogously to m_∞, $V^h_{1/2}$ and a_h characterize the half–inactivation potential and the steepness of the voltage–dependence. $V^h_{1/2}$, a_h obtained with the presence of different $[Mg^{2+}]_i$, have also been compared in table 5.5. All the data do not indicate significant differences at $[Mg^{2+}]_i \leq 7$ mM. However, both $V^m_{1/2}$ and $V^h_{1/2}$ show the negative shifts, which are in range of −25 to −29 mV, but leave the steepness of the activation and inactivation curves unchanged, when $[Mg^{2+}]_i$ was increased from 0 to 30 mM. The voltage dependence of m_∞ and h_∞, obtained in the presence of 0 and 30 mM Mg^{2+}_i, is compared in figure 5.5.

These results suggest that the Mg^{2+}_i effect on the sodium gating processes is nonlinearly dependent on its concentration. A similar shift in range of −25 to −29 mV of the activation and inactivation processes and the unchange of the steepness of the voltage dependent gating processes, with $[Mg^{2+}_i$ changed from 0 to 30 mM, can be explained by the local surface potential change produced by Mg^{2+} on the intracellular membrane surface. Similar interpretations have been proposed by Hille

(1968) and Hahin and Campbell (1983) to explain the effect of extracellular Ca^{2+} on sodium currents.

5.4 Surface potential change caused by Mg_i^{2+}

In this part of the thesis, a series of experiments and analysis have been performed to investigate if Mg_i^{2+} may have effects on the sodium channel gating processes. It is found that the voltage dependence of all the gating parameters of the sodium channel are shifted in a equal range of −25 to −29 mV by 30 mM Mg_i^{2+}. The shift of voltage dependence of gating parameters is insignificant at $[Mg^{2+}]_i \leq 7$ mM.

There are two reasons which may cause the shift of the voltage dependent relation. The first one is due to the ionic strength of the ionic solution used in the experiments. In fact, in the experiments of this thesis, the ionic strength ψ of 30 mM Mg_i^{2+} intracellular solution is different from those of 0 and 7 mM Mg_i^{2+} solutions. The other possibility may be Mg^{2+} screening the negative charges on the inner membrane surface. 30 mM Mg_i^{2+} screening effect may be more significant than that of 7 mM Mg_i^{2+}.

As mentioned in Section 1.2.3, the sodium channel is a transmembrane protein with the polarized pore and linkages exposed to the intracellular or extracellular polarized media. There are some net negative charges on the sodium channel surface or the entrance of the channel which decides the cation selectivity of the sodium channel. Furthermore, the essential components of the biological membrane are phospholipids, which bear a negative charged phosphate–head and two nonpolar fatty acid tails. The phosphate–heads of phospholipids are generally polarized, which leads to the presence of net negative charges existing on the natural membrane surface. The membrane charges can be neutralized by cations in the bulk solutions on both sides of the membrane. Figure 5.6 describes a simplified membrane with a single negative charged surface. A positive potential applied across this membrane is shown. If there were no negative surface charge, a test particle would approach the

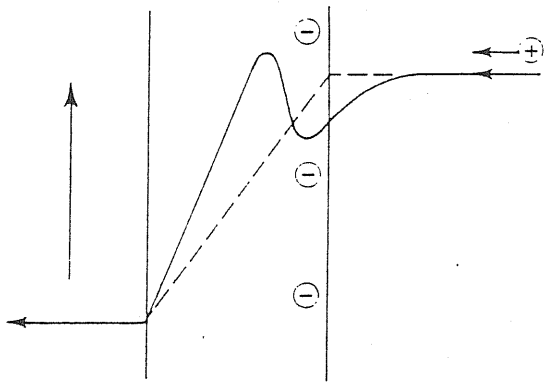

Figure 5.6:
Potential drop for a test charge moving through a membrane. The dotted line is linear potential drop for a homogenous membrane with no embedded charge, and the solid line is potential change for a positive test charge approaching a membrane with imbedded negative surface charge.

surface and its potential would dissipate steadily as it crossed the homogeneous membrane, as shown by the dotted line in the figure. With the negative charges present, the surface will have a lower potential than the solution and the test charge would move to this lower potential. In order to escape from the surface, it would now have to acquire the energy to separate from the negative charge and enter the membrane. If a collision provides sufficient energy to separate it from the negative charge, it will then have a reasonable probability of crossing the membrane. The time required for the test charge to cross the membrane is a very sensitive function of the microscopic structure of the membrane. The potential drop from the solution to the negative charged surface $V_d(x)$ approximately follows the relation given by the Gouy–Chapman theory.

$$V_d(x) = \frac{\sigma}{\varepsilon\kappa}\exp\left(-\kappa(x-a)\right) \tag{5.2}$$

$\varepsilon = \varepsilon_r\varepsilon_o$, in which ε_r and ε_o are dielectric constants of electical medium and vacuum. σ is the total surface charge per unit area. a is the

minimum distance that the bulk cation can approach to the membrane surface. κ determines how rapidly the potential decay occurs. κ^{-1} has the unit of length and is called the Debye length. κ is a function of the ionic strength and defined as:

$$\kappa = \sqrt{\frac{2F^2\psi}{\varepsilon RT}} \tag{5.3}$$

and the ionic strength ψ is defined as

$$\psi = \frac{1}{2}\sum z_i^2 c_i^0 \tag{5.4}$$

c_i^0 is the bulk concentration of the ith ion. z_i is its charge valence. These relations are hold for the calculation of the potential drops $V_o(x)$ and $V_i(x)$ caused by the extracellular and intracellular membrane surface charges. With the consideration of the surface charge effect, the membrane potential which are actually felt by the voltage–sensor of the ionic channel should be

$$V = V_m - (V_i(x) - V_o(x)) \tag{5.5}$$

With equation 5.2 the ratio of the potential drop caused by 7 mM Mg_i^{2+} $V_7(x)$, to that caused by the 30 mM Mg_i^{2+} $V_{30}(x)$, can be calculated and considered as the membrane potential drop by the different intracellular solutions, since the cell bath solutions are the same in both cases and all the other conditions i.e. ε, σ ad $x - a$ are assumed to be the same from cells to cells. Therefore, $V_7(x)/V_{30}(x)$ is

$$\frac{V_7(x)}{V_{30}(x)} = \frac{\kappa_{30}}{\kappa_7}\exp\left(\kappa_{30} - \kappa_7\right) = 1.27 \tag{5.6}$$

Analogously, $V_0(x)/V_7(x) = 1.23$ and $V_0(x)/V_{30}(x) = 1.43$. These ratio however, can not account for the voltage dependence shift described above completely, since the shift caused by 30 mM Mg_i^{2+} is in the range of –25 to –29 mV, which is much larger than that caused by 7 mM Mg_i^{2+}. There is no significant difference in fact in the latter case, compared to that measured in the presence of 0 Mg_i^{2+}. Therefore, the significant shift caused by 30 mM Mg_i^{2+} should be mainly due to the Mg^{2+} screening the

negative surface charge, i.e. Mg_i^{2+} binding to the negative charged membrane sites and leads to the local potential change. The concentration of unbound surface binding sites on the membrane can be calculated in terms of the electrochemical potential of Mg_i^{2+} as:

$$\sigma = \frac{\sigma_{total}}{1 + K[Mg^{2+}]_i \exp\left(\frac{-zFV_i(0)}{RT}\right)} \tag{5.7}$$

where K is the equilibrium constant of Mg^{2+} binding with the negative surface charges. From this equation, it is clear that the potential drop caused by the membrane charge decreases as $[Mg^{2+}]_i$ increases, which may account for the significant shift caused by the 30 mM Mg_i^{2+}.

The ionic screening effects have already been studied in the different ionic systems. One of the best studied examples is the shifts the voltage-dependent sodium channel gating process by the external Ca^{2+}. This phenomena was first found by Frankenhaeuser and Hodgkin (1957). They found that the calcium concentration changes shift the voltage dependence of sodium and potassium gating processes as if a bias is added to the membrane potential. The shift of the voltage dependence of the gating process was found also by the other divalent cations, see figure 5.7. One popular used explanation for this phenomena is the surface potential theory, which has been discussed above. That is, the local electric fields set up by charges near the membrane-solution interface can bias voltage-sensors within the membrane. Cations in solutions may screen the negative charges on the membrane, which leads to the change of the local electrical fields. In some cases, however, there are more effects on the gating modification than the equal potential shift. For example, in frog nerve, Ni^{2+} slow activation and inactivation processes of sodium channels, as if the temperature had been lowered, in addition of shift the voltage dependence (Dodge 1961, Hille 1968, Conti et al. 1976b). In squid axon, Zn^{2+} slows inactivation but not deactivation (Gilly and Armstrong 1982). In frog muscle, Ca^{2+} shift all the sodium channel gating parameters equally, but low pH does not (Hahin and Campbell 1983, Campbell and Hahin 1984). Therefore, ionic effects fall into a pattern. When cations are added, such as Zn^{2+}, Ni^{2+} and H^+, primarily

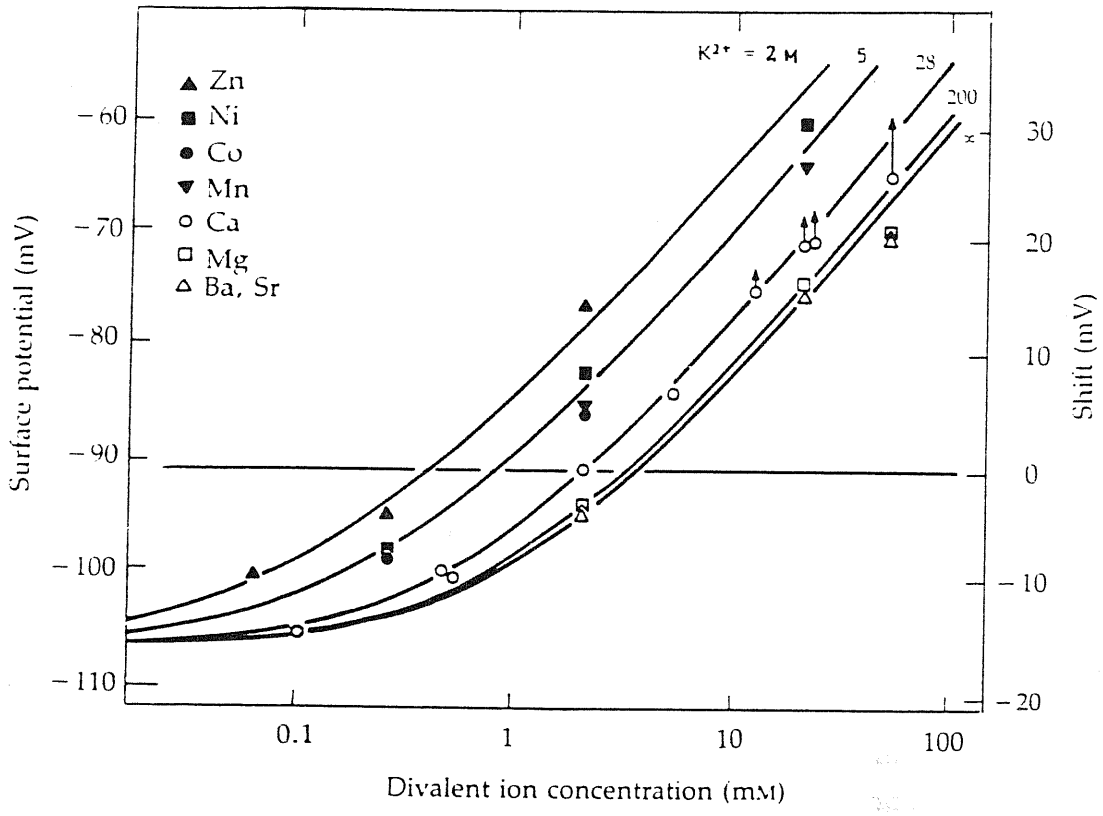

Figure 5.7:

Voltage shifts with different divalent ions. Shift of Na inactivation (right scale) in frog nodes of Ranvier are plotted against concentrations of added divalent ion, with the horizontal line marking the control value for 2 mM Ca^{2+}. Solutions contain only one kind of divalent ion at a time. Curves and the left scales are surface potentials calculated from a Gouy–Chapman–Stern model of surface potentials. (Hille et al 1975).

by binding to the specific site of the sodium channel (see figure 1.9B), rather than just screening, it causes more effects on the gating process than a simple shift of the voltage dependence of the gating process.

The aim of this chapter is to investigate if Mg_i^{2+} blocking effect is due to its modification on the sodium channel gating process. From present studies, it is found that the voltage dependence of all gating parameters of the sodium channel can be shifted to negative potential by 30 mM Mg_i^{2+} in a equal range of –25 to –29 mV. However, the steepness of the voltage dependence of steady–state activation and inactivation does not change with the increasing of $[Mg^{2+}]_i$ to 30 mM. Furthermore, the shift of the voltage dependence of gating parameters is insignificant at $[Mg^{2+}]_i \leq 7$ mM. From these observations, it can be concluded that the high concentrated intracellular Mg^{2+} (30 mM) may screen the negative charge on the inner surface of the sodium channel protein and lead to an equal shift of the voltage dependence of sodium channel gating parameters. The screening of the negative surface charges by Mg_i^{2+} may enhance the Mg^{2+} blocking effect by reducing the actual Na^+ concentration near the internal mouth of sodium channel. However, it is unable to explain the strong blockage happening at the low Mg^{2+} concentrations such as 0.5 mM to 7 mM, at which the Mg_i^{2+} screening effect is insignificant. Furthermore, it is also insufficient to explain the other characterizations of Mg^{2+} blockage as its strong dependence on $[Na^+]_i$, since the screening ability of the monovalent cation is much less than that of the divalent one. In fact, to screen the same amount of negative surface charges, the monovalent ionic concentration needed is much higher than the divalent ionic concentration needed. The ratio of the divalent cation concentration needed to the monovalent cation concentration needed can be approximately calculated with the Grahame equation as (Starzak 1984):

$$c_{divalent} = (\frac{c_{mono}}{272\sigma})^2. \tag{5.8}$$

To explain well the blockage, Mg^{2+} must have more effect on the sodium channel other than the simple screening negative surface charges on the inner membrane surface. As we have demonstrated, Mg_i^{2+} can interfere

with Na^+ not only from the intracellular side, but from the extracellular side as well. The only place where the intracellular and extracellular ions may meet is inside the channel. Therefore, it is most probable that Mg_i^{2+} enters the sodium channel during the sodium permeation (i.e open–channel state). The entrance of Mg_i^{2+} may interrupt the normal accommodation of sodium channels to Na^+ and lead to the Mg^{2+} blocking effect of sodium currents observed.

Chapter 6

Kinetic model for Mg^{2+} blockage

In the last chapter, it has been demonstrated that the high concentrated Mg_i^{2+} (30 mM) can screen the negative charge on the inner cell surface and lead to the local electric field change. This surface potential change results in the equal shift of the voltage dependent gating parameters. The negative shifts of the steady state inactivation parameter h_∞ and the inactivation time constants may decrease somehow the peak currents. Furthermore, the decrease of the negative charges on the inner surface of the sodium channels may decrease the local $[Na^+]_i$ near the inner entrance of sodium channels, which may also lead to the decrease of sodium currents. But this shift is insufficient to explain the obvious Mg^{2+} blockage caused by the low intracellular Mg^{2+} concentrations, such as 0.5 mM. In the low $[Mg^{2+}]_i$ condition ($[Mg^{2+}]_i \leq 7$ mM), no gating parameters are significantly affected by Mg_i^{2+} (Chapter 5). Therefore, it can be concluded that the Mg^{2+} blockage mainly results from the interference of Mg^{2+} with the sodium permeation through an open channel.

In Chapter 4, it was demonstrated that Mg^{2+} blockage is not only significantly enhanced with the decreasing of $[Na^+]_i$, but also slightly increases as $[Na^+]_o$ decreases. This phenomenon actually is a common characterization of the enzymatic competitive reaction. The only place

where Na^+ from the outside and Mg^{2+} from the inside might meet should be the sodium channel pore itself. Hence the competitive blocking effect of Mg^{2+} can be explained as Mg_i^{2+} competing with Na^+ for occupying the sodium channel. The occupancy of sodium channels by Mg^{2+} would interfere the normal accommodation of the sodium channel to Na^+ and leads to the blockage of the sodium permeation.

In order to account for the dependence of Mg_i^{2+} blockage on Na_i^+ and Na_o^+, a sodium permeation model was investigated based on the Michaelis–Menten kinetics in enzymatic reactions. With this model, the blockage of Mg^{2+} can be explained quite well.

6.1 Data preparation

The peak currents obtained at the different membrane potentials, as well as with different ionic concentrations described in Section 2.5 have been used to quantitatively analyse the kinetic model proposed below. In most of the data analysis, the mean of the normalized peak currents from two experimental ionic conditions (e.g. $I_p([Mg^+]_i)/I_p(0)$) was used. Means of peak currents were obtained from 4 patches up to 26 patches at each ionic concentrations. The mean of normalized peak currents was obtained as following.

Assuming a normalized function R defined as $R = P(i)/Q(j)$, with $i = 1, N$ and $j = 1, M$, the mean of R, $< R >$, is given as:

$$< R >= \frac{1}{NM}\sum_i^N\sum_j^M \frac{P(i)}{Q(j)} = \frac{1}{NM}\sum_i^N\sum_j^M R_{ij} \tag{6.1}$$

and its standard deviation is given as:

$$\sigma_R = \sqrt{\frac{\sum_i^N\sum_j^M (R_{ij} - < R >)^2}{NM(NM-1)}} \tag{6.2}$$

6.2 Sodium ion permeation

The ionic flux through the ionic channels has been explained by saturating pore models, which were first introduced to biology by Hodgkin

and Keynes (1955) and developed by Heckmann (1965a, b, 1968, 1972) and Läuger (1973). In these models, it was assumed that (1) ions must bind to certain sites in the pore as part of the permeation process, and (2) a site can bind only one ion at a time. These assumptions are fully analogous to those in the derivation of the enzyme kinetics. Ionic channels can generally be distinguished as two classes of saturating models: one–ion pores and multi–ion pores. The former may have several internal sites, be permeable to several types of ions, but can contain only one ion at a time in the pore. The ionic permeation through this kinds of channels can be described by a very simple saturable system, as:

$$S_{1,2,3} + X_i \rightleftharpoons S_1X \rightleftharpoons S_2X \rightleftharpoons S_3X \rightleftharpoons S_{1,2,3} + X_o$$

In which, $S_{1,2,3}$ represents that there are three binding sites inside an one–ion pore. The permeation of intracellular ion X_i through such a pore consists of three steps of binding–unbinding processes.

Multi–ion pores may contain more than one ion in the pore simultaneously, which may induce conductance g and reversal potential V_{rev} as a function of the ratio of ionic concentrations (i.e. concentration–dependent permeability ratios). Many ionic channels, in fact, belong to the this class. The conductance–concentration relation of the multi-ion channels is very complex and the simple saturation pore model proposed above, which is suitable for one–ion pore, might not be directly applied. But to see all these details, the concentration has to be varied over many orders of magnitude. In practical experiments, limited to concentration changes of only one or two order of magnitude, the conductance might appear to obey the simple one–ion saturation (Hille 1984). This theory is also applicable in our situation that the sodium channel can be considered as a simple one-ion channel with the presence of the low permeable ionic concentraions.

There are already some arguments that there are more than one binding sites inside sodium channels (Hille 1975, Begenisich and Cahalan 1980a, b). However, a further simplified one binding site kinetic model can be applied to describe the sodium permeation, based on the assumption that the ionic flux is mainly determined by the rate limiting

binding–unbinding step of ions with the channel. Therefore, the sodium permeation can be described with the simplified one–ion pore saturable model described as the following scheme:

$$S + Na_i^+ \underset{k_{-1}}{\overset{k_1[\mathrm{Na}^+]_i}{\rightleftharpoons}} SNa^+ \underset{k_{-2}[\mathrm{Na}^+]_o}{\overset{k_2}{\rightleftharpoons}} S + Na_o^+$$

where S represents the sodium channel. $S\mathrm{Na}^+$ is the binding state of Na^+ with the channel. Different k represents the rate constant of the reaction to different direction. Rate constants have dimensions either $\mathrm{s}^{-1}\mathrm{M}^{-1}$ for k_1 and k_{-2} or s^{-1} for k_{-1} and k_2. All the rate constants are the functions of the membrane potential. They also depend on the chemical potential associated to their relative reactions. The binding of Na^+ with its rate–limiting sites can be characterized by the voltage dependent Michaelis constants K_{Nai} for Na_i^+ and K_{Nao} for Na_o^+. The Michaelis constants are defined as:

$$K_{Nai}(V_m) = \frac{k_{-1} + k_2}{k_1} \tag{6.3}$$

and

$$K_{Nao}(V_m) = \frac{k_{-1} + k_2}{k_{-2}}. \tag{6.4}$$

These two constant reflect the interdependence of Na_i^+ and Na_o^+ during the sodium permeation.

6.3 Kinetic model of Mg^{2+} blockage

In the presence of a competitive blocker, Mg_i^{2+}, the permeation through the sodium channel described above may be modified as:

$$\begin{array}{ccccc} & k_1[\mathrm{Na}^+]_i & & k_2 & \\ S + Na_i^+ & \rightleftharpoons & SNa^+ & \rightleftharpoons & S + Na_o^+ \\ & k_{-1} & & k_{-2}[\mathrm{Na}^+]_o & \end{array}$$

$$+$$

$$Mg_i^{2+}$$

$$k_{-3} \uparrow\downarrow k_3[\mathrm{Mg}^{2+}]_i$$

$$SMg^{2+} \qquad \textbf{** Blocked State}$$

where $S\mathrm{Mg}^{2+}$ is the combination form of Mg_i^{2+} with the sodium channel. Because no Mg_i^{2+} exists in the extracellular membrane side, the binding ability Mg^{2+} with the sodium channel can be directly characterized by the dissociation constant $K_{Mg}(V_m)$, which is a function of membrane potential. It is defined as

$$K_{Mg}(V_m) = \frac{k_{-3}}{k_3}. \tag{6.5}$$

6.3.1 The steady state sodium flux in presence of Mg^{2+}

The sodium ionic flux, which is directly measured at the steady state, can be described as:

$$J = [S][Na^+]_i k_1 + [SNa^+]k_2 - [S][Na^+]_o k_{-2} - [SNa^+]k_{-1} \tag{6.6}$$

The sodium channel S has three existing forms:

$$[S]_{tot} = [S] + [SNa^+] + [SMg^{2+}]. \tag{6.7}$$

Since at the steady–state, $d[SNa^+]/dt = 0$ and $d[SMg^{2+}]/dt = 0$, another two equations can be obtained. From the former condition, we have:

$$[SNa^+](k_2 + k_{-1}) - [S](k_1[Na^+]_i + k_{-2}[Na^+]_o) = 0. \tag{6.8}$$

From the latter one, we get:

$$[SMg^{2+}] = \frac{[S][Mg^{2+}]}{K_{Mg}}. \tag{6.9}$$

Introducing eq. (6.9) into eq. (6.7), we further get:

$$[SNa^+] = [S]_{tot} - [S]\left(1 + \frac{[Mg^{2+}]}{K_{Mg}}\right). \tag{6.10}$$

Combine eq. (6.10) and eq. (6.8), the expression of $[S]$ in terms of $[S]_{tot}$ can be obtained:

$$[S] = \frac{[S]_{tot}}{1 + \frac{[Mg^{2+}]}{K_{Mg}} + A}, \tag{6.11}$$

in which,

$$A \equiv \frac{k_1[Na^+]_i + k_{-2}[Na^+]_o}{k_2 + k_{-1}} = \frac{[Na^+]_i}{K_{Nai}} + \frac{[Na^+]_o}{K_{Nao}}.$$

Introducing equation (6.11) into equation (6.8):

$$[SNa^+] = \frac{[S]_{tot}}{1 + (1 + \frac{[Mg^{2+}]}{K_{Mg}})\frac{1}{A}}. \tag{6.12}$$

Introducing eqs. (6.11), (6.12) into eq. (6.6)/$[S]_{tot}$, together with the relation between the flux and current as $I = zFJ$, the sodium current in the presence of Mg_i^{2+} is given as:

$$I = \frac{I^*}{1 + (1 + \frac{[Mg^{2+}]}{K_{Mg}})\frac{1}{A}} \tag{6.13}$$

where, I^* corresponds to the theoretical maximum sodium current, which could be reached when all the channels are conductive and Mg_i^{2+} is absent. It is defined as:

$$I^* = 2\frac{k_1k_2[Na^+]_i - k_{-1}k_{-2}[Na^+]_o}{k_1[Na^+]_i + k_{-2}[Na^+]_o}[S]_{tot}$$

It is also equivalent to

$$I^* = \bar{I}(1 + \frac{1}{A}).$$

where $\bar{I}$ is the sodium current directly measured in the absence of Mg_i^{2+}.

The sodium current in the presence of Mg_i^{2+}, expressed by equation (6.13), is a function time t, membrane potential V, ionic concentrations of intracellular and extracellular Na^+, as well as that of intracellular Mg^{2+}. Full expression is shown as equation (6.14):

$$I(t, V_m, [Na^+]_i, [Na^+]_o, [Mg^{2+}]_i) = \frac{I^*(t, V_m, [Na^+]_i, [Na^+]_o)}{1 + (1 + \frac{[Mg^{2+}]_i}{K_{Mg}(V_m)})\frac{1}{A}} \quad (6.14)$$

This equation, however, makes the quantitative analysis almost impossible due to the presence of the time variable t. In order to supersede t in the actual data analysis, the peak sodium current was applied in the data analysis. Peak current, I_p, is defined as :

$$I_p(V_m, [Na^+]_i, [Na^+]_o, [Mg^{2+}]_i) =$$

$$I'_p(V_m, [Na^+]_i, [Na^+]_o, [Mg^{2+}]_i) P_o(V_m, [Na^+]_i, [Na^+]_o, [Mg^{2+}]_i) \quad (6.15)$$

where I_p is the peak current which can be measured directly at an applied membrane potential V_m. I'_p is the theoretical peak current when all the sodium channels are conductive and P_o is the probability of the channel to be in the conductive state.

The peak currents are normalized as (I_n):

$$I_n(V_m, [Na^+]_i, [Na^+]_o, [Mg^{2+}]_i) = \frac{I_p(V_m, [Na^+]_i, [Na^+]_o, [Mg^{2+}]_i)}{I_p(V_m, [Na^+]_i, [Na^+]_o, 0)} \quad (6.16)$$

equation (6.14) can be simplified to:

$$I_n(V_m, [Na^+]_i, [Na^+]_o, [Mg^{2+}]_i) = \frac{1}{1 + \frac{[Mg^{2+}]_i}{K_{Mg}^{app}(V_m, [Na^+]_i, [Na^+]_o)}}, \quad (6.17)$$

where the apparent binding constant K_{Mg}^{app} is defined as:

$$K_{Mg}^{app}(V_m, [Na^+]_i, [Na^+]_o) = K_{Mg}(V_m)(1+A)$$
$$= K_{Mg}(V_m)(1 + \frac{[Na^+]_i}{K_{Nai}(V_m)} + \frac{[Na^+]_o}{K_{Nao}(V_m)}) \quad (6.18)$$

6.3.2 Fitting theoretical model with experimental data

The steady state sodium current expression derived in the last section provides us a directly method to quantitatively analyse the Mg^{2+} blockage in terms of the Mg^{2+} dissociation constant of $K_{Mg}(V_m)$ and the Michaelis constants of Na^+, $K_{Nai}(V_m)$ and $K_{Nao}(V_m)$ with the sodium channel. It is noteworthy however, that the peak current analysis method, proposed above, can be applied only if the gating mechanism of sodium channel is not significatively influenced by Mg_i^{2+}. That is, P_o in the equation (6.15) is not significantly influenced by the presence of Mg_i^{2+}. This condition is satisfied when $[Mg^{2+}]_i \leq 7$ mM, which has been demonstrated in the Chapter 5 (see tables 5.1 to table 5.5). If this is the case, I_n should be expected to approach to a constant, at least in a range where I_p' is not significantly influenced by Mg_i^{2+}. Figure 6.1 illustrates this behavior of I_n. In this figure, the values of I_n were obtained by normalizing the mean peak currents, $< I_p >$, obtained with 7 mM Mg_i^{2+} in patches by those obtained in the absence of Mg_i^{2+}. It is shown that I_n is quite constant at membrane potentials lower than the equilibrium potential of sodium channels, and then decreases in a voltage dependent way as potential increases.

Values of K_{Mg}^{app} have been calculated from equation 6.17 by least–square fitting I_n, as a function of $[Mg^{2+}]_i$. I_n were measured at a given membrane potential V_m, ionic concentrations $[Na^+]_i$ and $[Na^+]_o$ respectively. Fitting results illustrate the voltage–, $[Na^+]_i$– and $[Na^+]_o$–dependence of K_{Mg}^{app} behaviors. K_{Mg}^{app} estimated from the different experimental conditions (i.e. V_m, $[Na^+]_i$ and $[Na^+]_o$) are shown as the data points in figure 6.2. It is observable that the dependence of K_{Mg}^{app} on

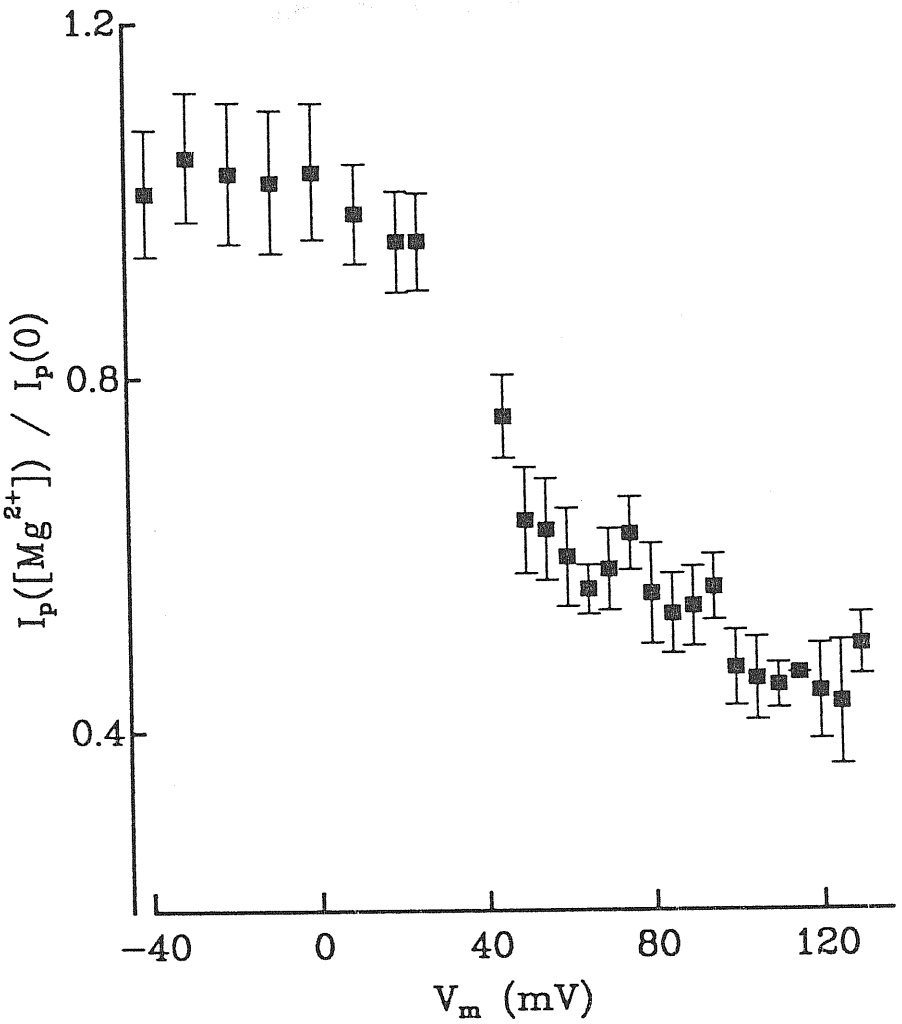

Figure 6.1:

Normalized sodium peak currents I_n evaluated at different membrane potentials V_m. Data points I_n were obtained by normalizing $I_p([Mg_i^{2+}])$ obtained with 7 mM Mg_i^{2+} by I_p obtained in absence of Mg_i^{2+}. Bars represent their standard deviations after such normalization. Normalized data points were from 23 control patches and 8 Mg_i^{2+} patches. Sodium equilibrium potentials are 30.8±2.7 mV (0 mM Mg_i^{2+}) and 31.3±3.7 mV (7 mM Mg_i^{2+}). $[Na^+]_i$ = 30 mM and $[Na^+]_o$ = 110 mM. I_n fluctuates around 1 when membrane potential is lower than the sodium equilibrium potential, which suggests there is no significant influence of Mg_i^{2+} on the gating mechanism of the sodium channel. The decrease of I_n at membrane potentials higher than the sodium equilibrium potential indicates the voltage dependent blockage of sodium currents by Mg_i^{2+}.

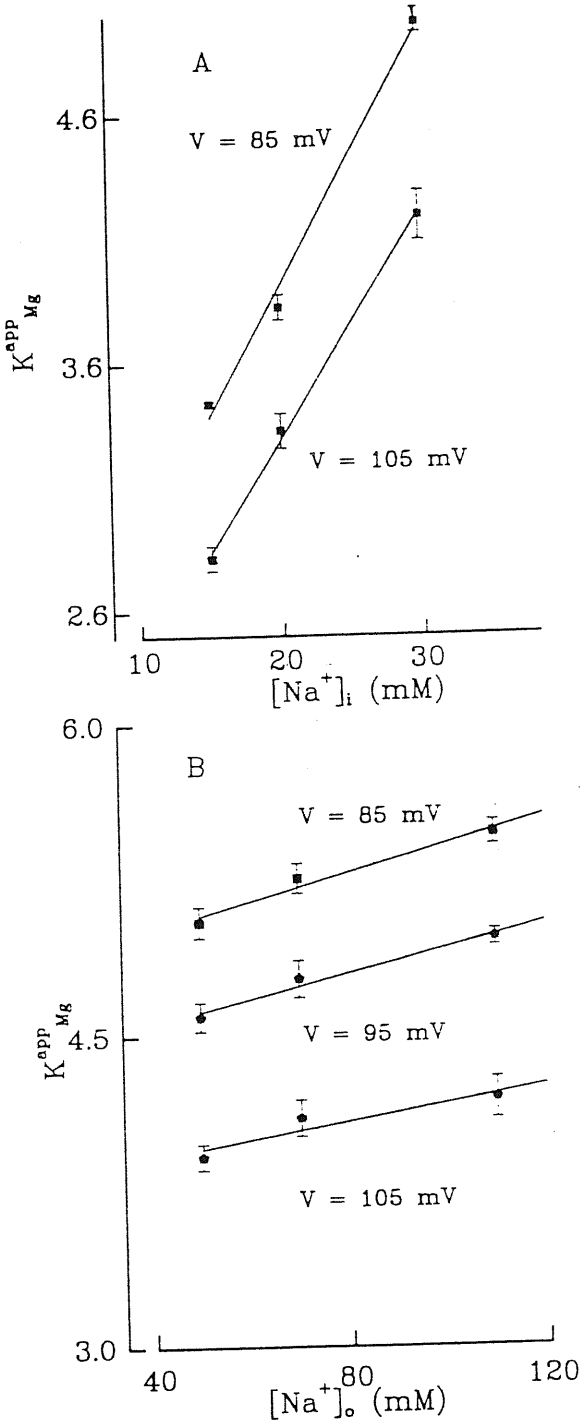

Figure 6.2:

Apparent binding constant K_{Mg}^{app} as function of $[Na^+]_i$ (**A**) and $[Na^+]_o$ (**B**). K_{Mg}^{app} were obtained from equation 6.17, at different membrane potentials V_m and different ionic concentrations $[Na^+]_i$ and $[Na^+]_o$. K_{Mg}^{app} were plotted as data points in figures, bars represent their standard deviations. K_{Mg}^{app} were further fitted with equation 6.18 against $[Na^+]_i$ with $[Na^+]_o$ fixed at 110 mM (**A**), or against $[Na^+]_o$ with $[Na^+]_i$ fixed at 30 mM (**B**). Fitting results were represents as smooth lines in figures.

$[Na^+]_o$ is less than its dependence on $[Na^+]_i$.

Values of K_{Mg}^{app} were further fitted as functions of $[Na^+]_i$ and $[Na^+]_o$ respectively, as described by equation (6.18). Fixed $[Na^+]_o$ at 110 mM, two voltage dependent constants A1 and B1 were obtained, by fitting $K_{Mg}^{app}(V_m)$ as function of $[Na^+]_i$ with equation (6.18)

$$A1 = K_{Mg}(V_m)(1 + \frac{110}{K_{Nao}(V_m)})$$

$$B1 = \frac{K_{Mg}(V_m)}{K_{Nai}(V_m)}. \tag{6.19}$$

Fixed $[Na^+]_i$ at 30 mM, A2 and B2 at the different membrane potential V_m. were obtained by fitting $K_{Mg}^{app}(V_m)$ as a function of $[Na^+]_o$:

$$A2 = K_{Mg}(V_m)(1 + \frac{30}{K_{Nai}(V_m)})$$

$$B2 = \frac{K_{Mg}(V_m)}{K_{Nao}(V_m)} \tag{6.20}$$

Combining these four expressions, one can get expressions (equation 6.21) of dissociation constant K_{Mg} and Michaelis constants K_{Nai} and K_{Nao} at the different membrane potentials (V_m) as following:

$$K_{Nai}(V_m) = \frac{110 - 30\frac{A1}{A2}\frac{B1}{B2}}{(\frac{A1}{A2} - 1)\frac{B1}{B2}}$$

$$K_{Mg}(V_m) = K_{Nai}(V_m)B1$$

$$K_{Nao}(V_m) = \frac{K_{Mg}(V_m)}{B2} \tag{6.21}$$

Up to now, the interaction between Mg^{2+} and Na^+ has been separated. The Mg^{2+} binding affinity with the sodium channel can be calculated as an only function of the membrane potential. Values of K_{Mg}, K_{Nao} and K_{Nai}, calculated from 9 different membrane potentials, have been shown as data points in figure 6.3. The behavior of K_{Mg} at the different potentials shows that the dissociation constant of Mg^{2+} with the sodium channel is a decreasing function of the membrane potential, that is, the affinity increases with the depolarization of the membrane.

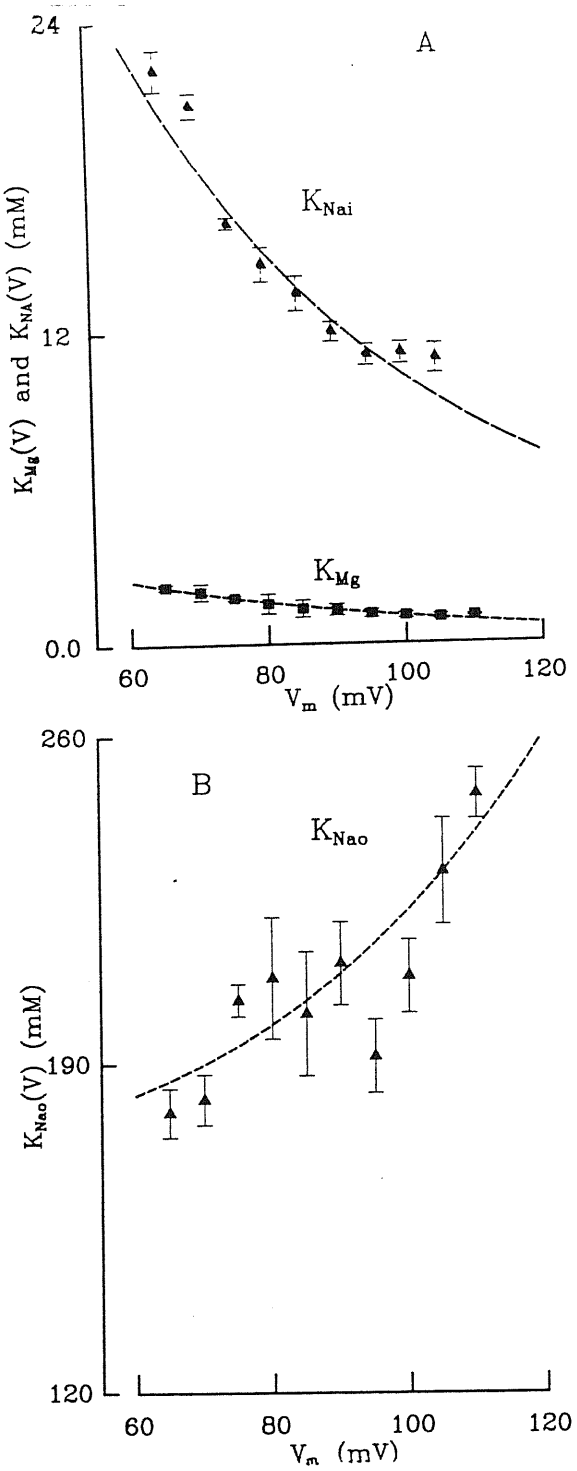

Figure 6.3:

The voltage dependence of dissociation constants $K_{Mg}(V_m)$ (squares) and Michaelis constants $K_{Nai}(V_m)$ (triangles) are illustrated in **A**. The voltage dependence of Michaelis constant $K_{Nao}(V_m)$ is shown in **B**. Each data point was obtained by fitting $K^{app}_{Mg}(V_m, [Na^+]_i, [Na^+]_o)$ as function of $[Na^+]_i$ and $[Na^+]_o$ respectively, using the equation 6.18. Bars are the standard deviations obtained from calculations. Smooth lines were obtained by fitting $K_{Mg}(V_m)$ to the equation 6.27 and $K_{Nai}(V_m)$, $K_{Nao}(V_m)$ to equations 6.28 and 6.29. Fitting results are detailed in the text.

The kinetic constants K_{Nai} and K_{Nao} reflect the steady state concentration relation between the different substrates of the binding site of the channel. From the definitions of these two constants (eqs (6.3), (6.4)), it can been seen that the increase of K_{Nao} values with the depolarization reflects the smaller backward (i.e. inward) Na^+ flux compared with the forward one. On the other hand, the decrease of K_{Nai} with the depolarization reflects the forward Na^+ flux due to Na_i^+ rushing into the channel to be dominant at the higher membrane potentials.

In order to further explain the voltage dependence of K_{Mg}, K_{Nai} and K_{Nao}, the binding–unbinding processes of the Mg_i^{2+} and Na^+ with the sodium channel are further studied.

6.4 The free energy of the reaction

For a reaction indicated in the kinetic scheme for the sodium permeation shown in section 6.2, the general process of the ionic binding–unbinding reaction can be described conveniently in terms of tunneling through barriers induced by thermal fluctuations (see figure 6.4). The corresponding partition function is the sum over all the possible configurations of the reaction with the appropriate Boltzmann factors. In terms of the path–integral formalism, the partition function is given by

$$\Xi = \frac{1}{N}\int \mathcal{D}\phi \exp\left(-\frac{G[\phi]}{k_B T}\right), \tag{6.22}$$

where, ϕ is a general configuration of the reaction, $G[\phi]$ is the free energy functional, k_B is the Boltzmann constant, T is the absolute temperature and N is a normalization factor.

Specifically to the Mg_i^{2+} unbinding reaction, the unbinding rate constant, k_{-3}, can be correspondingly expressed as

$$k_{-3} = \int \mathcal{D}\phi \; 2\pi\omega[\phi] \; \exp\left(-\frac{G[\phi]}{k_B T}\right), \tag{6.23}$$

in which, $2\pi\omega[\phi]$ is the reaction rate at a given configuration ϕ. In the case of heavy ions, e.g. Mg^{2+} and Na^+, the fluctuation effects can be ignored and a saddle point approximation is valid. In this approximation,

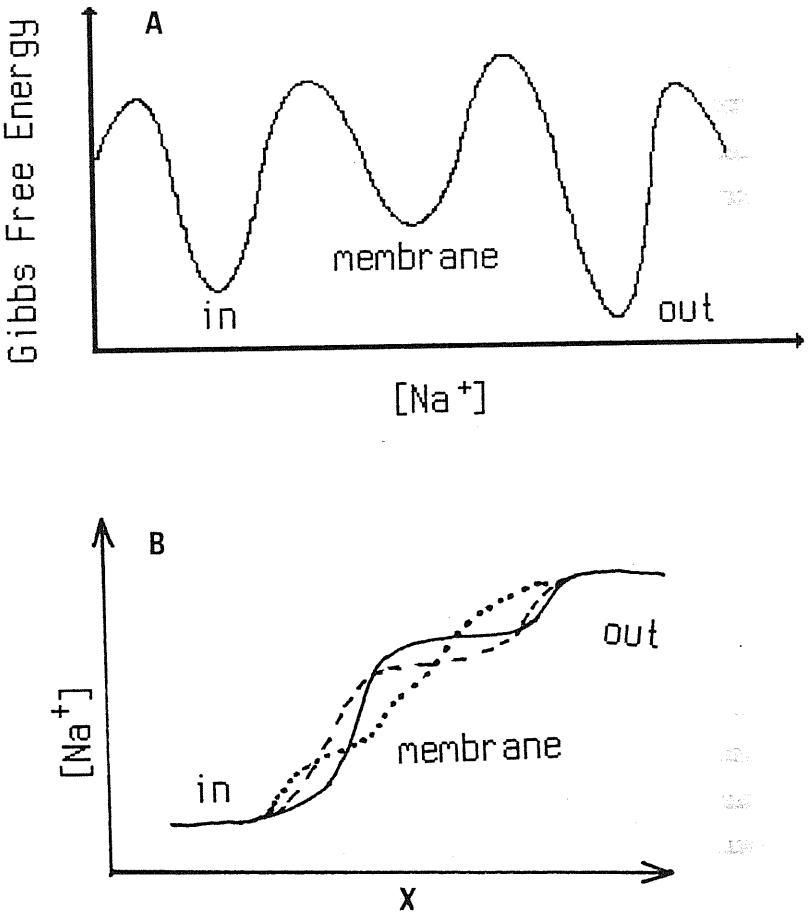

Figure 6.4:
For a simple ionic binding and unbinding reaction, its general process can be described in terms of tunneling through barriers and wells. **A** Gibbs free energy density at the absence of external electrical field. **B** Two possible configurations of $[Na^+]$ in the absence of external electrical field.

we have

$$k_{-3} = 2\pi\omega_{-3} \exp\left(-\frac{G^-_{Mg}}{k_B T}\right), \tag{6.24}$$

where, G^-_{Mg} is the free energy associated to the most probable configuration of the Mg^{2+} unbinding reaction, and $2\pi\omega_{-3}$ is the corresponding reaction rate. It can be further expressed in terms of the thermal energy $k_B T$, i.e. $2\pi\omega_{-3} = k_B T/h$, where h is the Planck constant.

Analogously, the rate constant of Mg^{2+} binding process can be expressed as

$$k_3 = \rho \frac{k_B T}{h} \exp\left(-\frac{G^+_{Mg}}{k_B T}\right) \tag{6.25}$$

where G^+_{Mg} is the free energy of the Mg^{2+} binding reaction. ρ is a constant with the dimension of M^{-1}, to be fixed by the zero-free energy level of the reaction.

Similarly, the binding and unbinding rate constants for Na^+_i and Na^+_o are expressed as

$$\begin{aligned}
k_1 &= \rho_i \frac{k_B T}{h} \exp\left(-\frac{G^+_i}{k_B T}\right) \\
k_{-1} &= \frac{k_B T}{h} \exp\left(-\frac{G^-_i}{k_B T}\right) \\
k_{-2} &= \rho_o \frac{k_B T}{h} \exp\left(-\frac{G^+_o}{k_B T}\right) \\
k_2 &= \frac{k_B T}{h} \exp\left(-\frac{G^-_o}{k_B T}\right)
\end{aligned} \tag{6.26}$$

in which, the subscripts of G, 'i' and 'o', refer to the reactions of Na^+_i and Na^+_o respectively. '+' and '–' refer the binding and unbinding processes. ρ_i and ρ_o are the constants to be fixed by the zero–free energy levels for the reactions of Na^+_i and Na^+_o.

In the presence of the applied membrane potential V_m, the additional Eyring rate factors (Eyring 1935, Glasstone et al. 1941, Moore and Pearson 1981) have to be included in the equations (6.24), (6.25)

and (6.26), in order to take into account the electrical field effect introduced. Therefore, the dissociation constant of Mg^{2+} is given as:

$$K_{Mg}(V_m) \equiv \frac{k_{-3}}{k_3} = K_{Mg}(0)\exp(-2BV_m\delta'). \tag{6.27}$$

Analogously, the voltage–dependent Michaelis constants, $K_{Nai}(V_m)$ and $K_{Nao}(V_m)$, are expressed as:

$$\begin{aligned} K_{Nai}(V_m) &\equiv \frac{k_{-1}+k_2}{k_1} \\ &= K_i(0)\exp\left(-BV_m\delta\right) + K_i'\exp\left(\frac{BV_m}{2}\right)\exp\left(-BV_m\delta\right) \end{aligned} \tag{6.28}$$

$$\begin{aligned} K_{Nao}(V_m) &\equiv \frac{k_{-1}+k_2}{k_{-2}} \\ &= K_o(0)\exp\left(BV_m(1-\delta)\right) + K_o'\exp\left(-\frac{BV_m}{2}\right)\exp\left(BV_m(1-\delta)\right) \end{aligned} \tag{6.29}$$

in which, B is defined as F/RT. δ' and δ represent the fraction of total electrical potential drop, between the inner surface of the membrane and Mg^{2+} and Na^+ binding sites respectively (the total electrical potential drop across the membrane is assumed to be 1). For simplification, the potential drops δ detected by Na^+ or Mg^{2+} will be called as the electrical distance from the inner membrane surface to the binding sites. K_i' and K_o' represent the outward and inward sodium flux probabilities respectively. They are defined as:

$$K_i' \equiv \frac{1}{\rho_i}\exp(-\frac{G_o^- - G_i^+}{k_BT})$$

and

$$K_o' \equiv \frac{1}{\rho_o}\exp(-\frac{G_i^- - G_o^+}{k_BT}).$$

$K_{Mg}(0)$, $K_i(0)$ and $K_o(0)$ are the dissociation constants of Mg^{2+}, Na_i^+ and Na_o^+ with the sodium channel at the zero membrane potential respectively. They are defined as

$$K_{Mg}(0) = \frac{1}{\rho} \exp\left(-\frac{\Delta G_{Mg}}{k_B T}\right) \tag{6.30}$$

$$K_i(0) = \frac{1}{\rho_i} \exp\left(-\frac{\Delta G_i}{k_B T}\right) \tag{6.31}$$

and

$$K_o(0) = \frac{1}{\rho_o} \exp\left(-\frac{\Delta G_o}{k_B T}\right). \tag{6.32}$$

where ΔG represents the different ionic binding-unbinding reaction free energies at the zero membrane potential, with the subscripts related to Mg^{2+}, Na_i^+ and Na_o^+ respectively.

Fixing the zero-free energy level at $\rho = 1$, which corresponds to dissociation constants to be 1 M, i.e. fixing the zero–free energy levels at equilibrium states at $V = 0$ mV, the reaction free energies of Mg^{2+}, Na_i^+ and Na_o^+ systems can be calculated as:

$$\Delta G_{Mg} = -k_B T \ln K_{Mg}(0) \tag{6.33}$$

$$\Delta G_i = -k_B T \ln K_i(0) \tag{6.34}$$

$$\Delta G_o = -k_B T \ln K_o(0) \tag{6.35}$$

The values of K_{Mg}(V), K_{Nai}(V) and K_{Nao}(V), obtained at the different membrane potentials, have been calculated from equations 6.21 with two sets constants A1, A2, B1 and B2. The values of these three parameters are shown as the data points in figure 6.3. The equation (6.27), which can be easily transformed as a linear equation, has been used to fit K_{Mg}(V), in order to locate the binding site of Mg^{2+} and to calculate the free energy of the binding–unbinding process of Mg^{2+} system. Equations (6.28) and (6.29), on the other hand, are comparably difficult to handle. The method used to solve such a complicated nonlinear equation is illustrated in the Appendix. The results of fitting the voltage–dependent $K_{Nai}(V_m)$, $K_{Nao}(V_m)$ and $K_{Mg}(V_m)$ with equations (6.27), (6.28) and (6.29) are shown as smooth lines in the figure 6.3. From these fittings, the dissociation constants of Mg^{2+}, Na_i^+ and Na_o^+ with their binding sites inside the sodium channel at $V_m = 0$ mV have been estimated. For Mg^{2+}, $K_{Mg}(0)$ was estimated to be 8.65±1.51 mM, which

corresponds to the reaction free energy of 4.75±0.17 k_BT. The location of the Mg^{2+} binding site inside the sodium channel is 0.26±0.03 electrical distance from the inner membrane surface. The zero membrane potential dissociation constant for Na_i^+, $K_i(0)$, is estimated to be 83.76±7.60 mM, corresponding to $\Delta G = 2.48\pm0.09\ k_BT$, which is smaller than that of Mg^{2+} and reflects the energy–favorite binding–unbinding of Na^+ with the sodium channel. The location of the Na_i^+ binding site is at 0.75±0.23 electrical distance from the inner membrane surface. Finally, for the extracellular Na^+, the dissociation constant $K_o(0)$ is 20.86±1.49 mM with $\delta = 0.58\pm0.05$ electrical distance from the inner membrane surface. Hence, the different voltage dependence of Mg^{2+} dissociation constant, as well as the Michaelis constants can be explained by the different fractions of the total electrical potential drop by Mg^{2+} and Na^+, i.e. so–called the different ionic locations inside the sodium channel discussed above. The free energy of Na_o^+ binding–unbinding process is calculated to be 3.87±0.07 k_BT unit, which is smaller than that for Na_i^+. This difference between Na_i^+ and Na_o^+ reaction free energies reflect that the chemical potential differences between Na^+ on the both sides of the membrane. This difference should lead to the unlike favorite reaction directions for Na_i^+ and Na_o^+.

6.5 Discussion

A kinetic model to describe the sodium flux in the presence of Mg^{2+} was proposed in this chapter, which is analogous to those used to describe the enzyme kinetics. The possible influence of ionic the concentrations, as well as the interaction between the different kinds of ions (Mg^{2+} and Na^+) on the ionic affinities with the sodium channel have been considered in the model. This consideration benefits as the possible calculation of the dissociation constant K_{Mg} and the Michaelis constants K_{Nai} and K_{Nao} only as functions of the membrane potentials. The dissociation constant of Mg^{2+} is found to be a decrease function of the membrane potential. Michaelis constants K_{Nai} and K_{Nao} have been

found to have the opposite voltage dependence (figure 6.3). These two parameters reflect that the influence of Na_i^+ and Na_o^+ on the steady state sodium flux are different at the different applied membrane potentials.

The rate constants of the different ionic binding–unbinding reactions have been expressed in terms of the free energy of their individual reactions, with an additive Eyring rate factor to account for the effect of the external applied membrane potential. These expressions provide an easy way to locate the binding site of Na^+ and Mg^{2+} inside the sodium channel. It was found that the rate–limiting binding site of Na_o^+ and Na_i^+ appears to be the same, which locates in the range of 0.58±0.05 to 0.75±0.23 electrical distance from the inner membrane surface. This location of the Na^+ binding site, δ, is in the agreement with those calculated by the others: $1-\delta$ =0.36 in the guinea–pig heart sodium channel (Nilius 1988), $1-\delta = 0.37\pm0.2$ in the neuroblastoma (Yamamoto et al. 1984). On the other hand, the rate–limiting binding site of Mg^{2+} inside the sodium channel appears to be different from that of Na^+, since $\delta' = 0.26 \pm 0.03$. The Mg_i^{2+} binding site calculated however is consistent with that calculated by Pusch (1990a), which is 0.25±0.02 (30 mM Na_i^+). The difference of the Na^+ and Mg^{2+} binding sites is consistent with the argument that there may be more than one binding side inside the sodium channel (Hille 1975, Begenisich and Cahalan 1980a, b). However, independently on how many binding sites are necessary to accurately describe the sodium current, which would lead to different transient states of Na^+, i.e. NaS_1, NaS_2 etc., in the sodium permeation scheme, the kinetic model for Mg_i^{2+} blockage proposed above is still efficient, unless one binding site can bind more than one ion at a time. Mg^{2+} is probably not permeating but prevents the Na^+ permeation by competitive binding to a site located at an electrical distance of 0.26±0.03 from the internal surface of the membrane.

With the voltage dependent relations of the dissociation constants $K_{Mg}(V_m)$ and Michaelis constants $K_{Nai}(V_m)$ and $K_{Nao}(V_m)$, it is possible to calculate the dissociation constants of Mg^{2+} and Na^+ with the sodium channel at the zero membrane potential, $K_{Mg}(0)$, $K_i(0)$ and $K_o(0)$. The value of $K_{Mg}(0)$ is much smaller than that of $K_i(0)$, which reflects the

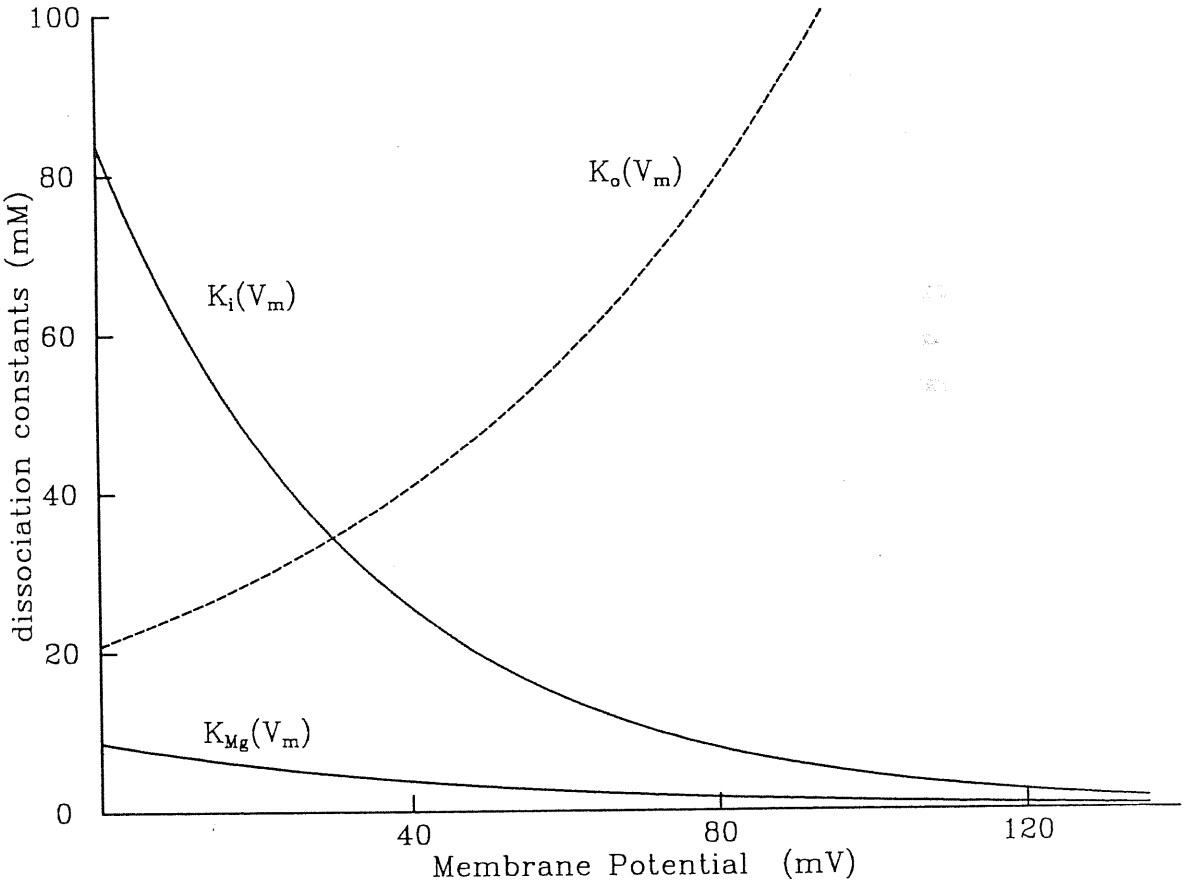

Figure 6.5:
The voltage dependent dissociation constants K_{Mg}, $K_i(V)$ and $K_o(V)$ are constructed from equation 6.27 and equations 6.36 and 6.37 with the fitting results of equations 6.27, 6.28 and 6.29. For $K_{Mg}(V_m)$, $\delta = 0.26$ and $K_{Mg}(0) = 8.66$ mM. For $K_i(V_m)$, $\delta = 0.75$ and $K_i(0) = 83.65$ mM. For $K_o(V_m)$, $\delta = 0.58$ and $K_o(0) = 20.89$ mM.

high affinity of Mg^{2+} with the sodium channel. In fact, the reaction free energies of both reactions calculated reflects that the binding–unbinding of Mg^{2+} with the sodium channel is less energy–favorable than that of Na_i^+. Since $\Delta G_{Mg} = 4.75 \pm 0.17$ and $\Delta G_i = 2.48 \pm 0.09\ k_BT$. The dissociation constants of Na_i^+ and Na_o^+ also appear to be different, which reflect the reaction free energy differences of Na_i^+ and Na_o^+, which leads to the different effect on the sodium permeation by Na_i^+ and Na_o^+.

The voltage dependence of the dissociation constants of Mg_i^{2+},

Na_i^+ and Na_o^+ are constructed with the dissociation constants of Mg^{2+} and Na^+ with the sodium channel at the zero membrane potential, as well as the binding site distance δ, of different ions, using equations 6.27 and

$$K_i(V_m) = K_i(0)\exp(-BV_m\delta) \tag{6.36}$$

$$K_o(V_m) = K_o(0)\exp(BV_m(1-\delta)). \tag{6.37}$$

The results are shown in figure 6.5. From this figure, two distinguished features can be observed. The first one is what has been discussed above. That is, the dissociation constant of K_{Mg} at the any membrane potential is lower than those of both Na_i^+ and Na_o^+. This feature is consistent with the argument above that Mg_i^+ has higher affinity with the sodium channel. This high affinity should be one of the main reasons for the Mg^{2+} blockage. The second feature is that the voltage dependent behavior of K_i is just opposite to that of K_o, which reflects the fact that the outward sodium current is dominant at higher membrane potentials and inward sodium current is dominant one at lower potentials. The cross point of $K_i(V_m)$ and $K_o(V_m)$ should correspond to the state that sodium currents from both directions reach the equilibrium. The potential of this point corresponds to the reversal potential of the system.

Except the high affinity of Mg^{2+} with the sodium channel, Mg^{2+} blocking effect of the sodium channel may be enhance by some other reasons. The selectivity of sodium channels may be one of important factors may enhance Mg^{2+} blockage effect. Mg^{2+} enters the sodium channel and binds to a site during membrane depolarization. Because of the selectivity of the pore (the permeability ratio of Mg^{2+} to Na^+ through sodium channel is less than 0.1 (Hille, 1972)), Mg^{2+} is not further permeable and may come back to the intracellular side due to the unbinding reaction of Mg^{2+}. The permeability ratio of Na^+ to Mg^{2+} of the sodium channels may be approximated calculated from the sodium reversal potential according to the Goldman–Hodgkin–Katz equation.

$$\frac{P_{Na}}{P_{Mg}} = \frac{4[Mg^{2+}]_i}{1+\exp\left(-\frac{V_{rev}F}{RT}\right)} \frac{1-\exp\left(-\frac{V_{rev}F}{RT}\right)}{[Na^+]_o \exp\left(-\frac{V_{rev}F}{RT}\right) - [Na^+]_i}$$

In the presence of 110 mM Na_o^+, 30 mM Na_i^+ and 7 mM Mg_i^{2+}, P_{Na}/P_{Mg} is estimated to be to be 14.45±0.38. This values is in the same magnitude as that calculate by Hille (1972). Most probably, the sodium channel selectivity and the high affinity of Mg^{2+} may coexist and influence each other, which may lead to the entrance of Mg^{2+} into the channel several times during the depolarization, giving out a high frequence of flickering at single channel level. The flicker caused by Mg^{2+} may produce an apparent single channel conductance decrease. In fact, the flickering effect of Mg^{2+} has been observed in single channel measurements of mutant sodium channel expressed in *Xenopus* oocytes (Pusch 1990a). However, the complete explanation of Mg^{2+} may need our further understanding of the sodium channel structure.

Chapter 7

Discussion

7.1 Sodium current on rat cerebellar granule cells

Despite constituting by far the largest population of neurons in the mammalian brain, little was known about the membrane properties of cerebellar granule cells until recently (Cull–Candy and Ogden 1985, Hirano et al 1986, Hockberger et al. 1987), since they are too small to readily accommodate microelectrodes. Large members of the granule cells can be obtained in relatively pure cultures by the mechanical or enzymatic dispersal of the rat cerebellum (Levi et al. 1984). This has led to a number of biochemical, electrophysiological and cell development studies on the granule cells. The first one includes the measurement of $^{22}Na^{+}$ flux (Beale et al. 1980), the uptake and release of glutamate (Levi and Gallo 1986), the turnover of inositol phospholipids (Nicoletti et al 1986) and the intracellular calcium measurement using Fura–2 (Connor et al 1987). The latter two include the characterization or the development studies of ionic channels linked to the amino acid receptors in the granule cells (Cull–Candy et al. 1988, Sciancalepore et al. 1989, 1990) and the potassium channels (Cull–Candy et al. 1989, Robello et al. 1989 and Galdzicki et al. 1990). However, the characterization of the sodium channels has not been carefully studied up to now. The detail study of

sodium channels should be very helpful to understand the overall physiological function of the granule cells. Based on this points, I completed my previous work (Lin 1988) and further performed a series of experiments to record the whole–cell sodium currents and analysed them in terms of the original Hodgkin and Huxley Model (Chapter 3). From these studies, the voltage–dependent gating process of sodium channels in the granule cells, such as the kinetic time constants τ_m, τ_h and the steepness of the activation and inactivation processes, has been found bearing the similar behavior as those characterized in the other preparations (Section 3.3). However, the voltage dependence of the activation and inactivation processes shifts to more positive potential, comparing with the other cells. This difference may reflect that the more negative surface potential on the granule cells membrane. Since the cerebellar granule cells are normally subjected to a continued depolarization in the physiological conditions due to their intrinsic synapses inputs (Levi et al. 1984), this relative negative membrane potential may correspond to certain physiological meaning as permitting granule cells to maintain their excitability. In fact, it is observed that the good culture condition is found in the presence of the high KCl concentration (25 mM) in the culture medium (Levi et al. 1984, Galdzicki 1990).

7.2 Mg_i^{2+} blocking effect on the sodium channel: characterization and explanation

As discussion above and in Chapter 3, the cerebellar granule cell in culture has been recognized as an excellent model for studying the electrophysiological properties of neurons, due to its maintained morphological and functional properties as native neurons. Recording with the experimental solution as 110Na/15Na(0), no significant rectification phenomenon was observed on the outward sodium current. This observation is consistent with Pusch's conclusion (1990a) that the rec-

tification effect described by Pappone (1980) and others (Chapter 4) is due to the presence of Mg^{2+} inside their intracellular solutions.

In order to study Mg^{2+} interference of the sodium permeation, a series of experiments were designed to characterize the Mg^{2+} blocking effect (Section 4.1). It is found that Mg_i^{2+} blocking effect of the sodium channel is voltage and $[Mg^{2+}]_i$ dependent (Section 4.2), which agrees with the observation of Pusch (1990a). The interactions between Mg_i^{2+} and Na_i^+, Na_o^+ has also been studied. It is found that the Mg^{2+} effect can be slightly influenced by the extracellular Na^+ concentrations, but is strongly influenced by the concentration of Na_i^+. The blocking effect increases as $[Na^+]_i$ decreases (Section 4.3). However, the $[Na^+]_i$—dependence of Mg^{2+} blockage contrasts with that observed by Pusch (1990a). The possible explanation for this opposite effect is that there might be other ionic interactions or sodium channels may hold more than one ions at a time in the presence of high $[Na^+]_i$, such as 125 mM (see Section 4.4).

The finding that the high concentrated Mg_i^{2+} (30 mM) shifts the peak current *vs.* membrane potential relationships to more negative potential leads to the study of the possible Mg_i^{2+} influence on the voltage dependent sodium channel gating processe (Section 5.1). The sodium channel gating mechanism was carefully studied in terms of the Hodgkin and Huxley model (Section 5.3). All the voltage dependent gating parameters, obtained from the different experimental solutions, were compared. Two results were found. First of all, the voltage dependence of the sodium channel gating process may be strongly shifted to the more negative potentials in a range of –25 to –29 mV by 30 mM Mg_i^{2+}, but leaves the steepness of the voltage dependent activation and inactivation untouched. These gating behavior provides the evidence that the sodium channel gating process itself does not modified by Mg^{2+}. Mg_i^{2+} change the local membrane potential drop by screening the negative charges on the inner membrane surface (Section 5.4). The other finding of the gating mechanism studies is that the influence on the gating process is nonlinearly dependent on $[Mg^{2+}]_i$, since the voltage shift is still insignificant with $[Mg^{2+}]_i$ up to 7 mM. This nonlinear relation between

the potential shift and Mg^{2+} concentration may also be explained from the Mg_i^{2+} screening theory, since the Mg_i^{2+} concentration nonlinearly affects the surface charge density via the equation (5.7) (Section 5.4).

The screening of the fixed negative surface charges by Mg_i^{2+} may enhance the Mg^{2+} blocking effect by reducing the actual Na^+ concentration near the internal mouth of sodium channel. However, it is unable to explain the strong blockage which has happened at the low Mg^{2+} concentration ($[Mg^{2+}]_i \leq 7$ mM), at which the screening is insignificant. Furthermore, it is also insufficient to explain the other characterizations of the Mg^{2+} blockage described above and in Chapter 4 (Section 5.4). Mg^{2+} must have more effect on the sodium channel other than the simple screening negative surface charges. Since Mg^{2+} can interfere with the Na^+ from both intracellular and extracellular sides, it is proposed that the explanation for the Mg^{2+} blockage should be that Mg^{2+} competes with Na^+ for occupying the sodium channels.

7.3 Mg_i^{2+} blockage can be described with a kinetic model

The sodium permeation can be described as a binding process, i.e. Na^+ has to bind to sites inside the sodium channel during its passing through the membrane (Section 6.2). The rate constants of the ionic binding and unbinding with the sodium channel are voltage dependent and also dependent on the chemical potential of the system. For simplifying the quantitative analysis of this model, an one–binding site approximation is applied, i.e the sodium channel is considered as an integrity. The introduction of this approximation is based on the assumptions that the ionic currents is mainly determined by the ionic binding to its rate–limiting site, and one site can bind only one ion at a time (Section 6.2). In the presence of a competitive blocker Mg_i^{2+}, Mg_i^{2+} blocks the channel by occupying one of binding sites of Na^+, and preventing the further binding (or entering) of Na^+ to Mg_i^{2+} occupying sites (channels). The sodium permeation with the presence of Mg_i^{2+}, therefore, has been de-

scribed as the voltage dependent binding–unbinding process, based on the Michaelis–Menten reaction kinetics (Section 6.3).

The normalized peak sodium current, I_n, has been introduced to describe quantitatively the Mg_i^{2+} blockage model (Section 6.3), with the condition that there is no significative influence of Mg^{2+} on the gating mechanism of sodium currents (Sections 5.2, 5.3, 6.3.2). The model provides a straight way to calculate the voltage dependence of the dissociation constant of Mg^{2+} with sodium channels, as well as the Michaelis constants for the intracellular and extracellular Na^+ with the channel (Section 6.3). The former directly illustrates the blocking capability of Mg^{2+}. The latter two constants illustrate the influence of Na^+ from different sides on the steady–state sodium flux as functions of membrane potential, as well as the interdependence between Na_i^+ and Na_o^+ in the sodium permeation.

Relations between the dissociation constant $K_{Mg}(V_m)$, Michaelis constants $K_{Nai}(V_m)$, $K_{Nao}(V_m)$ and membrane potential V_m have been further described in terms of the reaction free energy (Section 6.4). These expressions provide an easy method to locate the binding site of Na^+ and Mg^{2+} within the sodium channel. It was found that the rate–limiting binding site of Na_o^+ and Na_i^+ appears to be the same. But the Na^+ binding site is different from that of Mg^{2+} binding site (Sections 6.4 and 6.5). This difference is consistent with the argument that there may be more than one binding side inside the membrane (Hille 1975, Begenisich and Cahalan 1980a,b). However, independently on how many binding sites are necessary to accurately describe the sodium current, the kinetic model of Mg_i^{2+} blockage proposed is still efficient to describe the ionic flux through one–ion pore (Section 6.5).

With the voltage dependent relations of the dissociation constant and the Michaelis constants, the dissociation constants of Mg^{2+} and Na^+ with the sodium channel at the zero membrane potential, $K_{Mg}(0)$, $K_i(0)$ and $K_o(0)$ have been calculated (Section 6.4). The value of $K_{Mg}(0)$ is smaller than those of $K_i(0)$ and $K_o(0)$, which reflects the high affinity of Mg^{2+} with the sodium channel. At zero membrane potential, the ionic affinities with the sodium channels follow the relation as: $Na_i^+ < Na_o^+ <$

Mg_i^{2+}. The calculation of the free energy of the ionic binding–unbinding processes also give out an energy–unfavorable binding of Mg_i^{2+} with the sodium channel (Sections 6.4, 6.5).

7.4 Evaluation of data analysis

7.4.1 Data analysis

The whole–cell sodium current recordings have provided a very explicit way to characterize Mg^{2+} blockage on the sodium channels comparing with the single channel recording of sodium currents. This method, however, has its own inconvenience due to the difficulty of the intracellular perfusion on such a small cell as the cerebellar granule cell. Avoiding this problem, all the experiments were performed with different patches and the statistical analysis was applied with the assumption of the even distribution and properties of sodium channels per unit area of the cell membrane. Since the experimental conditions for the different patches may suffer the unexpected changes (individual cell conditions, culture conditions, temperature, real applied potential etc), the good qualified experiments chosen for the data analysis and as more as possible experiments are expected in order to minimize the individual difference. Furthermore, a reliable data analysis should include all the standard deviations in every step of the data analysis, which increases the amount of work. These factors have been considered in my data analysis. The standard deviations of the indirect experimental data e.g. K_{Mg}^{app}, K_{Mg} etc are obtained by introducing the direct experimental errors (e.g. the error generated during the data normalization) as the weights in the fitting (Standard–Chi–Squares fit, Press 1989).

Another inconvenience which may be introduced from the whole–cell sodium current recording is on the quantitative analysis of the Mg^{2+} blockage kinetic model proposed in Section 6.3.1. As discussed before (Section 6.3), the simplified quantitative analysis of the kinetic model is to supersede the time variable, which was done by introducing the peak current in the data analysis. The application of the peak current,

however, needs the prerequisite condition that there is no significant Mg^{2+} influence on the gating process of the sodium current (eq. (6.15)). The studies of the possible Mg^{2+} influence on the gating process, either approximatedly or accurately (methods see Sections 5.2 5.3), therefore is necessary before this simplified analysis method is used. On the other hand, this step of analysis is helpful to get an overall understanding of Mg^{2+} blockage. Anyhow, this inconvenience can be easily avoided in the single–channel current analysis, or the analysis of those types of ionic currents whose peak currents are not sensitive to the gating process.

7.4.2 Kinetic model for sodium permeation

Coming to the Mg^{2+} blockage kinetic model itself (Section 6.3.1), there may be two possible factors which will be interesting to further consider. One factor is the application limitation of the model. The model itself has a wide application specially in describing the ionic flux in one–ion pore, since there is no critical limitation for the establishing of the model (see Section 6.3.1). It does explain the Mg^{2+} blockage effect quite well (Chapter 6). However, the contrary $[Na^+]_i$–dependence of Mg^{2+} blocking effect observed in the experiments described in this thesis with that observed by Pusch (1990a) calls my attention, since it suggests that there might be more than one possible Mg^{2+} blockage mechanism. Despite the possible interactions between the Na^+ and K^+, K^+ and Mg^{2+} discussed in the Section 4.4, it might also be possible that the sodium channels behaves as a multi–ion pore at the presence of such high $[Na^+]_i$ as 125 mM (Pusch 1990a) or 200 mM (Danko et al. 1986). There is another possibility to explain this contrary, although it appears to be quite impossible. That is, one binding site in the sodium channel may hold more than one ion at a time. This possibility is plausible because most of the binding sites might be occupied by Na^+ due to its high concentration. Specially, the Mg^{2+} binding site is found to move to 0.50 ± 0.02 when $[Na^+]_i$ increases to 125 mM (Pusch 1990a). In this case, the kinetic model for Mg^{2+} blockage is modified as:

$$S + Na_i^+ \quad \rightleftharpoons \quad SNa^+ \quad \rightleftharpoons \quad S + Na_o^+$$

$$+$$

$$Mg_i^{2+}$$

$$\Vert$$

$$NaSMg^{2+} \qquad \textbf{** Blocked State}$$

However, this possibility is also hard to believe, considering the possible geometrical space limitation of the sodium channel. No matter which possibility should account for the contrary observations of mine and Pusch's, one caution should be taken is that the blockage effect should be characterized before the model is applied. The Mg^{2+} blockage kinetic model proposed in this thesis is only suitable to explain the competitive blockage.

The other interesting factor is how accuracy the sodium current can be described by this simple kinetic model. In order to simplify the quantitative calculation, an approximation was used, i.e. only the rate–limiting step is considered in the description of the sodium permeation (Section 6.2). With this approximation, the sodium channel is considered as an integrity. This assumption may introduce some deviations in the exact quantitative description of the sodium permeation. The most obvious one is the finding that the location of Mg^{2+} is different from that of Na^+, which means that the sodium channel is not an integrity as I assumed. This deviation on the other hand may be one of the advantages of this simple model. Since the approximation of the channel as an integrity greatly simplifies the quantitative analysis, but the approximation does not cover the intrinsic properties of the channel that there may be more than one binding site inside the sodium channel.

Nevertheless, with all the possible deficiency the model may have, there are two general informations which can be directly obtained from

the simple kinetic model of the sodium permeation proposed in this thesis: (1) The permeation of sodium ions through the channel can be described as a series of voltage dependent binding–unbinding processes. These binding–unbinding processes contribute a series of sodium channels' own characterizations, such as channel selectivity, voltage dependence and channel modulation and so on. (2) The competitive blockage of Mg^{2+} can be described as its occupancy of one of necessary sites of Na^+ passing. The occupancy of this site interferes the steady state sodium flux in both directions. The affinity of Mg^{2+} with this site is voltage dependent, due to the presence of external electrical field. The affinity of Mg^{2+} with sodium channels at all membrane potential is much higher than that for Na_i^+, which leads to the widely observed reduction of the sodium channel membrane conductance. Despite these results, the significance of this model proposed in Chapter 6 might be the consideration of Na^+ effects from the both sides of the membrane. This kinetic analysis method first time provides an approach to directly and quantitatively separate the different ionic effects. With this method, it is possible to calculate the real dissociation constant of Mg^{2+} with the sodium channel, which is not a function of $[Na^+]_i$ anymore and can be used as an instinctive parameter to characterize the Mg^{2+} blockage. This result makes this simple model distinguish from all the analysis methods used by the former researchers. In fact, the finding that $K_d(0)$ as a function of $[Na^+]_i$ by Pusch (1990a) may suggest that $K_d(0)$ actually corresponds to $K_{Mg}^{app}(0)$ in my work.

As a generalization, It is believed that this simple kinetic model and the experiment protocol designed in this thesis can be also used to investigate the blocking effect of the other divalent of the ionic channels. For example, the blocking effect of Co^{2+} on the $NMDA$–activated ionic channel has a similar effect as Mgh_i^{2+} (Ascher and Nowak 1988). It could also be extended to check the extracellular ionic effects, such as Ca_o^{2+} effect on the sodium currents observed by Nilius (1989) and Pusch (1990b).

7.5 Physiology function of Mg_i^{2+} blockage

The inhibitory effects of the internal Mg^{2+} have been demonstrated for a variety of ion channels. The Mg^{2+} block described by Horie et al. (1987) for ATP–sensitive K^+ channels in guinea–pig ventricular cells and that for inwardly rectifying K^+ channels (Matsuda et al. 1987; Ishihara et al. 1989) and the muscarinic potassium channels (Horie and Irisawa 1987) are similar to the sodium channel blockage described in this thesis. The free $[Mg^{2+}]_i$ varies between 0.4 and 3.7 mM for muscle tissue (Blatter and McGuigan 1988), or 1.7 mM (Alvarez–Leefmans et al. 1986). Changes in the free $[Mg^{2+}]_i$ due to ATP hydrolysis may reach the millimolar range during the excess energy consumption. Hence, it is possible that the Mg^{2+} effect of ionic currents may correspond to certain self–control function of cells. Pusch (1990a) has examined the effect on action–potential firing when sodium channels are blocked by Mg_i^{2+}, based on the Hodgkin–Huxley model. From this simulation, he found that the amplitude of the action potential can be reduced 15 mV with a delay of 0.6 ms in the presence of 5 mM Mg^{2+}. He concluded that an increase of the intracellular free Mg^{2+} by the large rates of ATP hydrolysis, apart from the known effects on the other channel types, might significantly alter the excitability properties of a cell simply because of the voltage–dependent block of sodium channels. However, the definite physiological function of Mg_i^{2+} has to be confirmed by the measurement of the action potentials in nerves in the presence of Mg^{2+} (Pusch 1990a).

From results presented in this thesis, the half blocking concentration of Mg_i^{2+} is shown to be a decreasing function of the applied membrane potential: K_{Mg} is 8.65±1.51 mM at 0 mV; 1.37±0.33 mM at 85 mV and 0.99±0.10 mM at 105 mV. The dissociation constants obtained at the high membrane potentials are comparable with the physiological intracellular Mg^{2+} concentration. This data suggest that the physiological Mg_i^{2+} concentration is effective enough to block the sodium channels significantly when cells are exposed to the considerable depolarization. This effect may correspond to a physiological regulation mechanism of sodium channels.

Conclusions

1. Sodium channels on the rat cerebellar granule cells can be described in terms of the HH model. The behavior of the voltage dependent sodium channel gating process bears the common features as those described in the other cell preparations.
2. Sodium currents on the rat cerebellar granule cells can be blocked by the intracellular Mg^{2+}. The blocking effect of the intracellular Mg^{2+} is Voltage–, $[Na^+]_i$–, $[Na^+]_o$– and $[Mg^{2+}]_i$–dependent.
3. The voltage–dependent sodium channel gating mechanism is nonlinearly influenced by $[Mg^{2+}]_i$. There is not significant gating mechanism influence observed at $[Mg^{2+}]_i \leq 7$ mM. However, the voltage dependence of sodium currents is shift to more negative potential by 30 mM Mg_i^{2+}.
4. The unvarying of the steepness of the voltage dependence of the sodium channel gating process by 30 mM Mg^{2+} suggests that the shift is due to Mg_i^{2+} screening the negative surface charges.
5. The nonlinear influence of Mg_i^{2+} on the gating mechanism of sodium currents can not explain the Mg_i^{2+} blockage at low $[Mg^{2+}]_i$, such as 0.5 and 1 mM. Mg^{2+} must have more effect than just screening.
6. The sodium permeation can be described with a simple saturable model, in which Na^+ has to bind to certain sites in

the pore as part of the permeation process.

7. Mg^{2+} blocking effect may be explained by a competitive kinetic binding model, in which Mg^{2+} competes with Na^+ for occupying sodium channels. The occupying of Mg_i^{2+} interferes the normal accommodation of sodium channels to Na^+.

8. The rate constants of ionic binding–unbinding processes are voltage dependent, which should correspond to the voltage dependence of Mg^{2+} blockage, as well as part of the voltage dependent behavior of the sodium currents.

9. The dissociation constant of Mg_i^{2+} and the Michaelis constants for Na^+ can be further expressed in terms of the free energy of the ionic binding–unbinding reaction.

10. Binding sites for Na_o^+ and Na_i^+ are calculated to be 0.58 ± 0.05 and 0.75 ± 0.23 electrical distance from the inner membrane surface respectively. The insignificant difference may correspond to the same binding site of Na_i^+ and Na_o^+. This location is in agreement with those calculated from the other preparations.

11. The fraction of the total applied electrical potential drop between the inner membrane surface and the Mg^{2+} binding site is 0.26 ± 0.05, which directly relates to the voltage dependence of Mg^{2+}.

12. The dissociation constant of ions with the sodium channel at the zero membrane potential is 8.65 ± 1.51 mM for Mg_i^{2+}; 83.76 ± 7.6 mM for Na_i^+ and 20.86 ± 1.49 mM for Na_o^+. The high affinity of Mg^{2+} should be one of the major reasons of Mg_i^{2+} blockage.

13. The voltage dependence of the dissociation constants of Na_i^+ and Na_o^+ displays the opposite behavior of dissociation constants of Na_i^+ and Na_o^+. This explains the free energy difference of Na_i^+ and Na_o^+ at the zero membrane potential.

14. The low half dissociation concentrations of Mg^{2+} at the higher

membrane potentials are in the same magnitude as the free $[Mg^{2+}]$ measured in cells, which may correspond to certain self–control functions of cells.

Appendix Nonlinear Fitting

Consider a non–linear model as following equation:

$$y = ae^{-cx} + be^{-cx}e^{\mu x}. \tag{.1}$$

To fit this non-linear equation, we separate the fitting problem into a linear sub-problem and a non-linear sub-problem. More specifically, we first fix the non-linear parameter c, and optimize locally the linear parameters a and b. Then, by varying the parameter c, and looking for the global minimum of Chi-square (χ^2)

$$\chi^2 = \sum_{n=1}^{N} \frac{\left(y_n - ae^{-cx_n} - be^{-cx_n}e^{\mu x_n}\right)^2}{\sigma_n^2}, \tag{.2}$$

we obtain the global optimization of the parameters a,b and c.

The detail procedure is following. Given c, the local minimum of χ^2 is determined by two conditions of stationarity of χ^2 respect to a and b: from $\partial\chi^2/\partial a = 0$, we get

$$\sum_{n=1}^{N} \frac{2\left(y_n - ae^{-cx_n} - be^{-\eta x_n}\right)e^{-cx_n}}{\sigma_n^2} = 0; \tag{.3}$$

and from $\partial\chi^2/\partial b = 0$, we get

$$\sum_{n=1}^{N} \frac{2\left(y_n - ae^{-cx_n} - be^{-\eta x_n}\right)e^{-\eta x_n}}{\sigma_n^2} = 0 \tag{.4}$$

where, $\eta = c - \mu$.

From these two conditions, we can get a system with two linear equations:

$$a\sum_{n=1}^{N} \frac{e^{-2cx_n}}{\sigma_n^2} + b\sum_{n=1}^{N} \frac{e^{-(c+\eta)x_n}}{\sigma_n^2} = \sum_{n=1}^{N} \frac{y_n e^{-cx_n}}{\sigma_n^2} \tag{.5}$$

$$a\sum_{n=1}^{N} \frac{e^{-(c+\eta)x_n}}{\sigma_n^2} + b\sum_{n=1}^{N} \frac{e^{-2\eta x_n}}{\sigma_n^2} = \sum_{n=1}^{N} \frac{y_n e^{-\eta x_n}}{\sigma_n^2} \tag{.6}$$

More conveniently, we defined three parameters A, B, C:

$$A \equiv \sum_{n=1}^{N} \frac{y_n e^{-cx_n}}{\sigma_n^2} \sum_{n=1}^{N} \frac{e^{-2\eta x_n}}{\sigma_n^2} - \sum_{n=1}^{N} \frac{y_n e^{-\eta x_n}}{\sigma_n^2} \sum_{n=1}^{N} \frac{e^{-(c+\eta)x_n}}{\sigma_n^2}; \tag{.7}$$

$$B \equiv \sum_{n=1}^{N} \frac{y_n e^{-\eta x_n}}{\sigma_n^2} \sum_{n=1}^{N} \frac{e^{-2cx_n}}{\sigma_n^2} - \sum_{n=1}^{N} \frac{y_n e^{-cx_n}}{\sigma_n^2} \sum_{n=1}^{N} \frac{e^{-(c+\eta)x_n}}{\sigma_n^2}; \tag{.8}$$

$$D \equiv \sum_{n=1}^{N} \frac{e^{-2cx_n}}{\sigma_n^2} \sum_{n=1}^{N} \frac{e^{-2\eta x_n}}{\sigma_n^2} - \left(\sum_{n=1}^{N} \frac{e^{-(c+\eta)x_n}}{\sigma_n^2} \right)^2. \tag{.9}$$

in terms of which we get parameters a and b from equations:

$$a = \frac{A}{D} \tag{.10}$$

$$b = \frac{B}{D} \tag{.11}$$

By varying different c, we therefore can get a series of constant a and b. The global minimization of χ^2 allows us to get the best fit a, b and c.

Standard deviations of a, b, and c are calculated as:

$$\sigma_a = \sqrt{\sum_{n}^{N} \sigma_n^2 \left(\frac{\partial a}{\partial y_n} \right)^2 + \left(\frac{\partial a}{\partial c} \right)^2} \tag{.12}$$

$$\sigma_b = \sqrt{\sum_{n}^{N} \sigma_n^2 \left(\frac{\partial b}{\partial y_n} \right)^2 + \left(\frac{\partial b}{\partial c} \right)^2} \tag{.13}$$

$$\sigma_c = \sqrt{\left(\frac{\partial^2 \chi^2}{\partial c^2} \right)^{-1}} \tag{.14}$$

Bibliography

[1] Adams DJ and Gage PW (1979) Characteristics of sodium and calcium conductance changes produced by membrane depolarization in an *Aplysia* neurone. J. Physiol. (London) 289:143

[2] Alberts B, Brey D, Lewis J, Raff M, Roberts K and Watson JD (1983) Molecular Biology of the Cell. Garland Publishing Inc, New York, USA.

[3] Aldrich RW (1989) Mutating and gating. Nature (London) 339:578–579.

[4] Aldrich RW and Stevens CF (1983) Inactivation of open and closed sodium channels determined separately. Cold Spring Harbor Symp. Quant. Biol. 48:147–154

[5] Aldrich RW, Corey DP and Stevens CF (1983) A reinterpretation of mammalian sodium channel gating based on single channel recording. Nature (London) 306:436–441

[6] Almers W, Roberts WM and Ruff RL (1984) Voltage clamp of rat and human skeletal muscle: measurements with an improved loose–patch technique. J. Physiol. (London) 347:751–768.

[7] Altura BM and Altura BT (1985) New perspectives on the role of magnesium in the pathophysiology of the cardiovascular system. Magnesium 4:245–271

[8] Alvarez-Leefmans FJ, Gamino SM, Giraldez F and Gonzales-Serratos H (1986) Intracellular free magnesium in frog skele-

tal muscle fibers measured with ion-selective micro-electrodes. J. Physiol (London) 378:461–483

[9] Anderson CR and Stevens CF (1973) Voltage clamp analysis of acetylcholine produced end–plate current fluctuations at frog neuromuscular junction. J. Physiol. (London) 235:655–691.

[10] Armstrong CM (1966) Time course of TEA^+–induced anomalous rectification in squid giant axons. J. Gen. Physiol. 50, 491–503

[11] Armstrong CM and Bezanilla F (1973) Currents related to movement of the gating particles of the sodium channels. Nature (London) 242:459–461.

[12] Armstrong CM and Bezanilla F (1974) Charge movement associated with the opening and closing of activation gates of the Na channels. J. Gen. Physiol. 63:533–552.

[13] Armstrong CM and Bezanilla F (1977) Inactivation of the sodium channel. II. Gating current experiments. J. Gen. Physiol. 70:567–590.

[14] Ascher P and Nowak L (1988) The role of divalent cations in the *N*–methyl–D–Aspartate responses of mouse central neurons in culture. J. Physiol. (London) 399:247–266

[15] Auld VJ, Goldin AL, Krafte DS, Catterall WA, Lester HA, Davidson N and Dunn RJ (1990) Proc. Natl. Acad. Sci. USA 87:323–327

[16] Barbon H, Jover E, Courand F and Rochat H (1983) Photoaffinity labelling of α– and β– scorpion toxin receptors associated with rat brain sodium channel. Biochem. Biophys. Res. Com. 115:415–422.

[17] Beale R, Dutton GR and Currie DN (1980) An ionic flux study of action potential sodium channels in neuron– and glia–enriched cultures of cells dissociated from rat cerebellum. Brain Res. 183:241–246.

[18] Begenisich TB and Cahalan MD (1980a) Sodium channel permeation in squid axon I: reversal potential measurements. J. Physiol. (London) 307:217–242

[19] Begenisich TB and Cahalan MD (1980b) Sodium channel permeation in squid axon II: non–independence and current–voltage relations J. Physiol. (London) 307:243–257

[20] Berman MF, Camardo JS, Robinson RB and Siegelbaum SA (1988) Single sodium channels from canine ventricular myocytes: voltage dependence and relative rates of activation and inactivation. J. Physiol. (London) 415:503–531.

[21] Bezanilla F and Armstrong M (1977) Inactivation of sodium channel. I Sodium current experiments. J. Gen. Physiol. 70:567–590

[22] Blatter LA, McGuigan AS (1988) Estimation of upper limit of the free magnesium concentration measured with Mg–sensitive microelectrodes in ferret ventricular muscle: (1) Use of the Nicolsky–Eisenman equation and (2) in calibrating solutions of the appropriate concentration. Magnesium 7:154:165.

[23] Brown AM, Murimoto K, Tsua Y and Wilson DL, (1981) Calcium current–dependent and voltage–dependent inactivation of calcium channel in *Helix aspersa.* J. Physiol. (London) 320:193–218

[24] Campbell DT and Hahin R (1984) Altered sodium and gating current kinetics in frog skeletal muscle caused by low external pH. J. Gen. Physiol. 84:771–788.

[25] Carbone E and Lux HD (1984) A low voltage activated, fully inactivated Ca channel in sensory neurons. Nature (London) 310:501–502

[26] Carbone E and Lux HD (1984) A low voltage activated, fully inactivated Ca channels in sensory neurons. J. Physiol. (London) 213:1–19.

[27] Carbone E And Lux HD (1986) Sodium channels in chick dorsal root ganglion neurons. Eur. Biophys. J. 13:259–271

[28] Catterall WA (1980) Neurotoxins that acts on voltage–sensitive sodium channels in excitable membranes. Ann. Rev. Pharmacol. Toxicol. 20:15–43.

[29] Chanlder WK and Meves H (1965) Voltage clamp experiments on internally perfused giant axons. J. Physiol. (London) 180, 788–820

[30] Cole KS (1949) Dynamic electrical characteristics of the squid axon membrane. Arch. Sci. Physiol. 3:253–258.

[31] Connor JA, Tseng HY and Hockberger PE (1987) Depolarization–and transmitter–induced changes in intracellular Ca^{2+} of rat cerebellar granule cells in explant cultures. J. Neurosci. 5:1384–1400.

[32] Conti F, Hille B, Neumcke B, Nonner W and Stämpfli R (1976a) Measurement of the conductance of the sodium channel from current fluctuatons at the node of Ranvier. J. Physiol. (London) 262:729–742.

[33] Conti F, Hille B, Neumcke B, Nonner W and Stämpfli R (1976b) Conductance of the sodium channel in myelinated nerve fibers with modified sodium inactivation. J. Physiol. (London) 262:729–742.

[34] Conti F and Stühmer W (1989) Quantal charge redistributions accompanying the structure transitions of sodium channel. Eur. Biophys. J. 17:53–59

[35] Cull–Candy SG, Dilger P, Odgen DC and temple S (1985) Patch–clamp of rat cerebellar neurones in tissue culture. J. Physiol. 362:45p

[36] Cull–Candy SG, Dilger P, Marshall CG and Odgen DC (1986) Voltage–activated currents in freshly dispersed granule cells from neonatal rat cerebellum. J. Physiol. 381:114p.

[37] Cull–Candy SG, Howe JR. and Odgen DC (1988) Voltage–activated currents in freshly dispersed granule cells from neonatal rat cerebellum. J. Physiol. 381:114p

[38] Cull–Candy SG, Marshall CG and Odgen D (1989) Voltage–activated membrane currents in rat cerebellar granule neurones. J. Physiol. 414:179–199.

[39] Cull–Candy SG and Odgen D (1985) Ionic channels activated by L–glutamate and GABA in cultured cerebellar neurones of rat. Proceeding of the Royal Society B. 224:367–373.

[40] Danko M, Simth-Maxwell C, McKinney L and Begenisich T (1986) Block of sodium channels by internal mono- and divalent guanidinium analogues. Biophys. J. 49:509–519.

[41] Dodge FA (1961) Ionic permeability changes underlying nerve excitation. In *Biophysics of Physiological and Pharmacological Actions*, American Association for the Advancement of Science, Washington, D.C., 119–143.

[42] Dunlap K and Fischbach GD (1981) Neurotransmitters decrease the calcium conductance activated by depolarization of embryonic chick sensory neurons. J. Physiol. (London) 317:519.

[43] Eyring H (1935) The activated complex in chemical reactions. J. Chem. Phys. 3:107–115

[44] Fahlke C and Ruppersberg JP (1988) Saturation effects and rectifier properties of sodium channels in human skeletal muscle. Eur. Biophys. J. 16:307:312.

[45] Fenwick EM, Marty A and Neher E (1982) Sodium and calcium channels in bovine chromaffin cells. J. Physiol. (London) 331:599.

[46] Frankenhaeuser B and Hodgkin AL (1957) The activation of calcium on the electrical properties of squid axons. J. Physiol. (London) 137:218–244.

[47] Galdzicki Z, Lin F, Moran O, Novelli A, Puia G and Sciancalepore M (1990) Development of Voltage Dependent Ionic Currents in Rat Cerebellar Granule Cells Grown in Primary Culture. Int. J. of Neurosci. (in press)

[48] Gilly WF, and Armstrong CM (1982) Slowing of sodium channel opening kinetics in squid axon by extracellular zinc. J. Gen. Physiol. 79:935–964.

[49] Glasstone S, Laidler KJ and Eyring H (1941) The Theory of rate processes. McGraw–Hill, New York, 611p

[50] Goldman DE (1943) Potential, impedance, and rectification in membranes. J. Gen. Physiol. 27:37–60.

[51] Guy HR and Conti F (1990) Pursuing the structure and function of voltage–gate channels. TINS 13:201–206

[52] Hahin R and Campbell DT (1983) Simple shift in the voltage dependence of sodium channel gating caused by divalent cations. J. Gen. Physiol. 82:785–802.

[53] Halstead BW (1978) Poisonous and Venomous Marine Animals of the World. Darwin Press, Princeton, N.J. 283 pp.

[54] Hamill OP, Marty A, Neher E, Sakmann B and Sigworth FJ (1981) Improved patch-clamp techniques for high resolution current recording from cells and cell-free membrane patches. Pflügers Arch. 391:85–100

[55] Heckmann K (1965a) Zur Theorie der "Single File"-Diffusion I. Z. Phys. Chem. 44:184–203.

[56] Heckmann K (1965b) Zur Theorie der "Single File"-Diffusion II. Z. Phys. Chem. 46:1–25.

[57] Heckmann K (1968) Zur Theorie der "Single File"-Diffusion III. Sigmoid Konzentrationsabhängigkeit unidirectionaler Flüsse bei "single file" Diffusion. Z. Phys. Chem. 58:201–219.

[58] Heckmann K (1972) Single-file diffusion. In *Biomembrane*, Vol.3: *passive Permeability of Cell Membranes*, F.Kreuzer and J.F.G. Slegers (eds.). Plenum Press, New York, 127–153.

[59] Hille B (1968) Charges and potentials at the nerve surface: Divalent ions and pH. J. Gen. Physiol. 51:221–236.

[60] Hille B (1972) The permeability of sodium channel to metal cations in myelinated nerves. J. Gen. Physiol. 51:199–219.

[61] Hille B (1975) Ionic selectivity, saturation, and block in sodium channels. A four–barrier model. J. Gen. Physiol. 66:535–560.

[62] Hille B (1977) Ionic basis of resting and action potentials. In Handbook of Physiology. The Nervous system 1. Brookhart JM, Mountcastle VB, Kandel ER and Geiger SR (eds). American Physiological Society. Washington DC 99–130pp.

[63] Hille B (1984) Ionic Channels of Excitable Membrane. Sinauer Associates Inc. Publisher, Sunderland.

[64] Hille B, Woodhull AM and Shapio BI (1975) Negative surface charge near sodium channels of nerve: Divalent ions, monovalent ions, and pH. Phil. Trans. R. Soc. Lond. B 270:301–318.

[65] Hirano T, Kubo Y and Wu MM (1986) Cerebellar granule cells in culture: monosynaptic connection with Purkinje cells and ionic currents. Prot. Nat. Acad. Sci. USA. 83:4957–4961.

[66] Hockberger PE, Tseng HY and Connor JA (1987) Immunochemical and electrophysiological differentiation of rat cerebellar granule cells in explant cultures. J. Neurosci. 7:1370–1383.

[67] Hodgkin AL and Huxley AF (1952a) A quantitative description of membrane current and its application to conduction and excitation in nerve. J. Physiol. (London) 117:500–544.

[68] Hodgkin AL and Huxley AF (1952b) Currents carried by sodium and potassium ions through the membrane of the giant axon of *Loligo*. J. Physiol. (London) 116:449–472

[69] Hodgkin AL and Huxley AF (1952c) The dual effect of membrane potential on sodium conductance in the giant axon of *Loligo*. J. Physiol. (London) 116:497–506

[70] Hodgkin AL and Huxley AF (1952d) The components of membrane conductance in the giant axon of *Loligo*. J. Physiol. 116:473–496

[71] Hodgkin AL, Huxley AF and Katz B(1949) Ionic currents underlying activity in giant axon of the squid. Arch. Sci. Physiol. 3:129–150

[72] Hodgkin AL, Huxley AF and Katz B (1952) Measurements of current-voltage relations in the membrane of giant axon of *Loglio*. J. Physiol. (London) 116:424–448

[73] Hodgkin AL and Katz B (1949) The effect of sodium ions on the electrical activity of the giant axon of the squid. J. Physiol. (London) 108:37–77

[74] Hodgkin AL and Keynes RD (1955) The potassium permeability of a giant nerve fibre. J. Physiol. (London) 128:61–88.

[75] Horie M, Irisawa H (1987) Rectification of muscarinic K^+ current by magnesium ion in guinea pig atrial cells. American J Physiol. 253:H210-H214.

[76] Horie M, Irisawa H, Noma A (1987) Voltage–dependent Magnesium block of adenosine–triphosphate–sensitive potassium channel in guinea–pig ventricular cells. J. Physiol. (London) 387:251-271.

[77] Huang LM, Moran N and Ehrenstein G (1982) Batrachotoxin modifies the gating kinetics of sodium channels in internally per-

fused neuroblastoma cells. Proc. Natl. Acad. Sci. USA 79:1082–2085.

[78] Johnson and Ascher P (1990) Voltage–dependent block by intracellular Mg^{2+} of *N*–methyl–D–aspartate–activated channels. Biophys. J. 57:1085–1090

[79] Jover E, Courand F and Rochat H 91980) Two types of scorpion neurotoxins characterized by their binding to two separated receptor sites on rat brain synaptosomes. Biochem. Biophys. Res. Com. 95, 1607–1614.

[80] Kameyama M (1983) Ionic currents in cultured dorsal root ganglion cells from adult guinea pigs. J. Membr. Biol. 72:195.

[81] Katz B (1949) Les constantes électriques de la membrane du muscle. Arch. Sci., Physiol. 3, 285–299

[82] Katz B and Miledi (1970) Membrane noise produced by acetycholine. Nature (London) 226:962–963.

[83] Katz B and Miledi (1971) Further observations on acetylcholine noise. Nature (london) 232:124–126.

[84] Keynes RD and Rojas E (1974) Kinetics and steady–state properties of the charged system controlling sodium conductance in the squid giant axon. J. Physiol. (London) 239:393–434.

[85] Keynes RD and Rojas E (1976) The temporal and steady-state relationships between activation of the sodium conductance and movement of the gating particles in the squid giant axon. J. Physiol. (London) 255:157–189.

[86] Keynes RD and Kimura JE (1983) Kinetics of activation of the sodium conductance in the squid giant axon. J. Physiol. (London) 336:621–634.

[87] Kostyuk PG, Veselovsky NS and Fedulova SA (1981) Ionic currents in the somatic membrane of rat dorsal root ganglion neurons. Neuroscience 6:2431.

[88] Kuffler SW, Nicholis JG and Martin AR (1984) From neuron to brain. Second Edition. Sinauer Associates Inc. Publishers, Sunderland, Massachusetts.

[89] Läuger P (1973) Ion transport through pores: A rate–theory analysis. Biochim. Biophys. Acta 311:423–441

[90] Levi G, Aloisi F, Ciotti MT and Gallo V (1984) Autoradiographic localization and depolarization–induced release of acidic amino acids in differentiation granule cell cultures. Brain Res. 290:77–86.

[91] Levi G and Gallo V (1986) Release studies related to the neurotransmitter role of glutamate in the cerebellum, an overview. Neurosci. Res. II 1627–1642.

[92] Lin F (1988) Sodium currents on the rat cerebellum granule cells. Master thesis, International School for Advanced Studies Trieste, Italy.

[93] Lin F and Moran O (1989) Sodium currents in long–term rat cerebellar granule cell cultures. Eur. J. Neurosci. supp 2:154.

[94] Machetti C, Carignani C and Robello M. (1990) A voltage–dependent calcium current in cultured rat cerebellar granule cells. Abstract in IX congresso of Societá Italiana di Biofisica Pura ed Applicata.

[95] Marmont G. Studies on the axon membrane. I. A new method. J. Cell. Comp. Physiol. 34:351–382.

[96] Marty A and Neher E (1983) Tight–seal whole–cell recording. In: Single channel recording, edited by Sakmann B, Neher E. Plenum Press, New York, London 107–122pp.

[97] Matsuda H (1988) Open–state substructure of inwardly rectifying potassium channels revealed by magnesium block in guinea–pig heart cells. J. Physiol. (London) 397:237–258.

[98] Matsuda H, Saigusa A and Irisawa H (1987) Ohmic conductance through the inwardly rectifying K channel and blocking by internal Mg^{2+}. Nature (London) 325:156–159.

[99] Matteson DR and Armstrong CM (1984) Na and Ca channels in a transformed line of anterior pituitary cells. J. Gen. Physiol. 83:371.

[100] Mayer ML, Westbrook GL, Guthrie PB (1984) Voltage–dependent block by Mg^{2+} of NMDA response in spinal cord neurons. Nature 309:261–263.

[101] Meves H (1984) Hodgkin–Huxley: Thirty years after. In Current topics in membranes and transport. vol 22: The Squid axon edited by Kleinzeller A and Baker PF. Academic press inc. 279–329pp.

[102] Moolenar WH and Spector I (1977) Membrane currents examined under voltage-clamp in cultured neuroblastoma cells. Science 196:331–333.

[103] Moolenar WH and Spector I (1978) Ionic currents in cultured mouse neuroblastoma cells under voltage-clamp conditions. J. Physiol. (London) 278:265.

[104] Moore JW and Pearson RG (1981) Kinetics and Mechanism. 3rd edition, John Wiley, New York, 455pp.

[105] Moran O and Conti F (1990) Sodium ionic and gating currents in mammalian cells. Eur. Biophys. J. 18:25–32

[106] Mozhayeva GN, Naumov AP, Negalyaev YA and Nosyreva ED (1977) Permeability of aconitine–modified sodium channels to univalent cations in myelinated nerves. Biochim. Biophys. ACTA 466:461–473.

[107] Narahashi T, Moore JW and Scott WR (1964) Tetrodotoxin blockage of sodium conductance increase in lobster giant axons. J. Gen. Physiol. 47:965–974.

[108] Narahashi T, Haas HG and Therrien EF (1967) Saxitoxin and tetrodotoxin: Comparison of nerve blocking mechanism. Science 157:1441–1442.

[109] Neher E., and Sakmann B. (1976) Single–channel currents recorded from membrane of denervated frog muscle fibers. Nature (London) 260:779–802

[110] Neumcke B and Stämpfli R (1982) Sodium currents and sodium current fluctuations in rat myelinated nerve fibers. J. Physiol. (London) 329:163–184.

[111] Nicoletti F, Wrobleski JT and Costa E (1987) Magnesium ions inhibit the stimulation of inositol phospholipid hydrolysis by endogeneous excitatory aminoacids in primary cultures of cerebellar granule cells. J. Neurochem. 48:967–973

[112] Nilius B (1988) Calcium block of guinea–pig heart sodium channels with and without modification by the piperazinylindole DPI 201-106. J. Physiol. (London) 399:537–558

[113] Noda M, Shimizu S, Tanabe T, Takai T, Kayano T, Ikeda T, Takahashi H, Nakayama H, Kanaoka Y, Minamino N, Kangawa K, Matsui H, Raftery M, Hirose T, Inayama S, Hayashida H, Miyata T and Numa S (1984) Primary structure of *Electrophorus electricus* sodium channel deduced from cDNA sequence. Nature (London) 312:121–127.

[114] Noda M, Ikeda T, Kayano T, Suzuki H, Takeshima H, Kurasaki M, Takahashi H and Numa S (1986) Existence of distinct sodium channel messenger RNAs in rat brain. Nature (London) 320:188–192.

[115] Nowak L, Bregestovski P, Asher P, Herbet A and Prochiantz A (1984) Magnesium gates glutamate–activated channels in mouse central neurones. Nature (London) 307:462–465.

[116] Pappone PA (1980) Voltage–clamp experiments in normal and denervated mammalian skeletal muscle fibers. J. Physiol. (London) 306:377-410.

[117] Patlak J and Horn R (1982) Effect of N–bromoacetamide on single sodium channel currents in excised membrane patches. J. Gen. Physiol. **79**:333–351

[118] Press WH, Flannery BP, Teukolsky SA and Vetterling WT (1989) Numerical recipes "FORTRAN version". Cambridge University Press, Cambridge.

[119] Pröbstle T, Rüdel R, Ruppersberg JP, (1988) Hodgkin–Huxley parameters of sodium channels in human myoballs. Pflügers Arch 412:264–269.

[120] Pusch M, Conti F, and Stühmer W (1989) Intracellular magnesium blocks sodium outward currents in a voltage and dose dependent manner. Biophys. J. 55:1267–1271.

[121] Pusch M (1990a) Open–channel block of Na^+ channels by intracellular Mg^{2+}. Eur. Biophys. J. 18:317–326

[122] Pusch M (1990b) Divalent cations as probes for structure–function relationships of cloned voltage–dependent sodium channels. Eur. Biophys. J. 18:327–333.

[123] Robello M, Carignani C, and Machetti C, (1989) A transient voltage–dependent outward current in cultured cerebellar granules. Biosci. Rep. 9:451–457.

[124] Schneider MF and Chandler WK (1973) Voltage–dependent charge movement in skeketal muscle: A possible step in excitation–contraction coupling. Nature (London) 242:244–246.

[125] Sciancalepore M, Forti L and Moran O (1989) Changes of *N*–methyl–*d*–aspartate activated channels of cerebellar granule cells with days in culture. Biochem. Biophys. Res. Comm. 165:481–487.

[126] Sciancalepore M, Galdzicki Z, Zheng X and Moran O (1990) Kinate activated single channel currents revealed by Domoic acid. Eur. Biophys. J. (in press).

[127] Sigworth FJ (1980) The conductance of sodium channels under conditions of reduced current at the node of Ranvier. J. Physiol. (London) 307:97–129.

[128] Sigworth FJ and Neher E (1980) Single Na^+ channel currents observed in cultured rat muscle cells. Nature (London) 287:447–449

[129] Starzak ME (1984) The physical chemistry of membranes. Chapter 8. Academic press Inc. Orlando.

[130] Strata P, Benedetti F (1988) Aspetti di fisiologia del magnesio. EMI, Pavia.

[131] Stryer L (1988) Biochemistry. W.H. Freeman and Company. New York.

[132] Stühmer W, Methfessel C, Sakmann B, Noda M and Numa S (1987) Patch clamp characterization of sodium channels expressed from rat brain cDNA. Eur. Biophys. J. 14:131–138.

[133] Stühmer W, Conti F, Suzuki H, Wang W, Noda M, Yahagi N, Kubo H, and Numa S (1989) Structural parts involved in activation and inactivation of the sodium channel. Nature (London) 339:597–603.

[134] Taylor RE and Bezanilla F (1983) Sodium and gating current time shifts resulting from changes in initial conditions. J. Gen. Physiol. 81:773–784.

[135] Vanderberg CA (1987) Inward rectification of a potassium channel in cardiac ventricular cells depends on internal magnesium ions. Proc. Natl. Acad. Sci. USA, 84, 2560–2564

[136] Vidair C and Rubin H (1981) J. Cell. Physiol. 108, 317–325

[137] White R, Hartzell HC (1988) Effects of intracellular free magnesium on calcium current in isolated cardiac myocytes. Science 239:778–780.

[138] Wood JM and Anderton BH (1981) Monoclonal antibodies to mammalian neurofilaments. Biosci. Rep. 1:263–268.

[139] Woodbury JW (1971) Eyring rate theory model of the current–voltage relationships of ion channels in excitable membranes. In *Chemical Dynamics: Papers in Honor of Henry Eyring.* Edited by Hirschfelder JO. John, Wiley and Sons. pp. 601–607.

[140] Woodhull AM (1973) Ionic blockage of sodium channels in nerve. J. Gen. Physiol. 61:687–708

[141] Yamamoto D, Yeh JZ, Narahashi T, (1984) Voltage–dependent block of normal and tetramethrin–modified single sodium channels. Biophys. J. 45:337–344.

[142] Zheng X (1989) Domoic acid activated channels in central nervous system neurones. Master thesis, International School for Advanced Studies, Trieste, Italy.